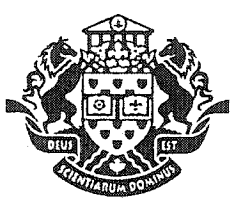

Université d'Ottawa · University of Ottawa

Université d'Ottawa · University of Ottawa

FACULTÉ DES ÉTUDES SUPÉRIEURES ET POSTDOCTORALES

FACULTY OF GRADUATE AND POSTDOCTORAL STUDIES

BATTYE, Nicholas John

AUTEUR DE LA THÈSE - AUTHOR OF THESIS

M.Sc. (Earth Sciences)

GRADE - DEGREE

Earth Sciences

FACULTÉ, ÉCOLE, DÉPARTEMENT - FACULTY, SCHOOL, DEPARTMENT

TITRE DE LA THÈSE - TITLE OF THE THESIS

Noble Gases in Canadian Shield Groundwaters from the Con Mine, Yellowknife, N.W.T.

I. Clark

DIRECTEUR DE LA THÈSE - THESIS SUPERVISOR

EXAMINATEURS DE LA THÈSE - THESIS EXAMINERS

K. Hattori

F. Michel

J.-M. De Koninck, Ph.D.

LE DOYEN DE LA FACULTÉ DES ÉTUDES SUPÉRIEURES ET POSTDOCTORALES

SIGNATURE

DEAN OF THE FACULTY OF GRADUATE AND POSTDOCTORAL STUDIES

Noble Gases in Canadian Shield Groundwaters from the Con Mine, Yellowknife, N.W.T.

By

Nicholas John Battye

A thesis submitted to the Faculty of Graduate and Postdoctoral Studies in partial fulfillment of the requirements for the degree of M.Sc. in Earth Sciences

Ottawa-Carleton Geoscience Centre
and the
University of Ottawa

Your file Votre référence
ISBN: 0-612-92440-8
Our file Notre référence
ISBN: 0-612-92440-8

I have not failed 700 times. I have not failed once. I have succeeded in proving that those 700 ways will not work. When I have eliminated the ways that will not work, I will find the way that will work.

-Thomas Edison

ABSTRACT

Dissolved noble gas concentrations in Canadian Shield groundwaters from various depths of the Miramar Con Mine, Yellowknife, were examined for paleotemperature information and isotopic ratios. A high-vacuum stainless steel line with reactive gas gettering, isotope spike dilution and quadrupole mass spectrometer was constructed, tested and calibrated prior to sample analysis. In addition to noble gases, groundwater flow rates and formational pressures, as well as the major ions, stable isotopes and tritium values, were also measured.

Data collected on flow rates and formational pressures was compared to that published by Intera Consultants Ltd. (1997). Trends indicate an almost universal decline in both parameters over the four year period, reflective of changing mine conditions.

The major ions in solution are represented primarily by Ca, Na, Cl, SO_4, and HCO_3, at shallow depths. In the deep subsurface, Ca, Na, and Cl become the dominant species, forming a Ca-Na/Cl brine characteristic of the Canadian Shield that reaches a TDS of 304 g/L.

Stable isotope results vary between –21‰ and –14‰ for $\delta^{18}O$, and –162‰ and –73‰ for δD. These values, in part, have been used by Clark et al. (2000) to add a glacial meltwater component onto the existing modern meteoric and brine components to increase the complexity of mixing dynamics in the mine.

Tritium was detected at all locations, ranging from 26 to 0.9 TU. This would suggest that no area of the mine, with the possible exception of the 5300' level, has been left undisturbed by modern meteoric groundwater influxes.

Only one paleotemperature estimate was possible due to extreme over-pressurization of noble gases and reduced variability of solubility with temperature that is inherent in groundwater containing brine fractions. Sample B-8906 (3500' level, brine free) provided a temperature estimate of 5°C.

The over-pressuring of noble gases was normalized to the brine component. He concentrations were found to be 851 000x atmospheric for the 4900' level. Ar concentrations were 57x and 136x atmospheric for the 4900' and 5300' levels respectively. Kr levels are within atmospheric range, +/- 5, subject to instrument limitations. Xe exhibits 35x and 17x over-pressuring for the 4900' and 5300' levels. Current theories explaining the additions of He and Ar are the natural radioactive decay processes of U/Th and K bearing minerals, as well as a mass element flux originating from the Precambrian basement. Xe ratios appear to be atmospheric in origin, and as of yet, remain unexplained.

Using He as a means of groundwater dating provides an estimate of 230 +/- 50% Ma. Although radiogenic in origin, 40Ar*, and subsequently Ar ratios (up to 3450), cannot be

used as a qualitative dating tool. They are however, some of the highest ratios measured in crustal fluids and insinuate a subsurface residence time on the order of millions of years.

ACKNOWLEDGEMENTS

As with all scientific works, there exists a host of people who have helped make this final product possible. Although a listing of all the helpful people would be rather lengthy and difficult to amass, I would like to take this opportunity to acknowledge certain individuals that made a decisive impact on both myself and this project.

I would first and foremost like to thank my supervisor at the University of Ottawa, Dr. Ian Clark, who accepted me when no one else would. His guidance and support was endless, as was his patience and time. His upbeat nature and optimism was always refreshing and desperately needed when things went wrong (as they frequently did). He also provided the financial support necessary to sustain me throughout the duration of this project.

I would also like to thank my co-supervisor, Dr. Tom Kotzer (CLSI), who, even after my blowing-out both of his ultra-low level mass spectrometer filaments back to back in less than a minute during my first month of work, managed a jolly laugh and refrained from exiling me from his lab forever. His wisdom and good humour knew no bounds. Best wishes to you in Saskatoon.

Thanks are due to Dr. Dennis Bottomley and the CNSC for their financial backing of this project. Specifically, his patience and flexibility in the face of unavoidable delays was much appreciated, as was his direction and uncanny ability to whip up the perfect reference at the perfect times.

Many thanks to the Isotope Laboratory Crew at the University who ran isotope results and tolerated my seemingly constant interruption. Specifically I would like to thank Paul Middlestead who never failed to provide the clutch piece of equipment in my time of need. Though in the end I believe I emptied his entire back-up stock of everything, he was always accommodating and full of good advise.

Thanks to Helene De Gouffe for her always prompt processing of travel claims, and Rob Renaud who went before me and helped pave the way.

Finally, I would like to my family for their steadfast support. Their constant asking of the question, "When will you be done? When will you be done?", kept me ploughing ahead. Special thanks to my mom who always knew things would work out in the end and who aptly described the project as a 'character-building' experience...

TABLE OF CONTENTS

LIST OF FIGURES

LIST OF TABLES

1. INTRODUCTION

1.1 Terms of Reference

The origin and history of groundwaters in the crystalline environment of the Canadian Shield have safety-relevant implications for the burial of radioactive waste, and are of interest to The Canadian Nuclear Safety Commission (CNSC). Of particular interest is to determine whether the noble gas concentrations in deep Shield brines hold information that could discriminate between an origin as hyper-evaporated Paleozoic seawater or brines created by refreezing of seawater in a Pleistocene periglacial setting. This report summarizes the methodology and results of a noble gas research study carried out by the University of Ottawa, financed by a research contract with the CNSC (Contract no. 99-172). The research program involved the design and building of a noble gas extraction line with quadrupole mass spectrometer analyser. The analysis design includes the addition of isotope spikes for isotope dilution calculations of noble gas concentrations.

1.2 Background to Noble Gas Paleothermometry

Noble gases dissolved in groundwater have been used extensively for paleotemperature estimation (Andrews and Lee, 1979; Youngman, 1989; Stute and Schlosser, 1992, etc.). These estimations are based on the assumption that the solubilities of each noble gas are temperature dependent. Under this assumption, the concentrations of dissolved noble gases in the near-surface aquifer will represent markers that define the temperature at the time of recharge. The noble gases, which include helium, neon, argon, krypton and xenon, as well as their isotopes, have different atmospheric concentrations (Table 1). Dissolution into groundwater occurs mainly in the unsaturated zone where pore spaces are only partially filled with water. Non-equilibrium concentration dynamics drive diffusion (near the ground surface) and depend on the ambient ground temperature at the time of transfer into the water column. The variation of solubility with temperature increases along with the mass of the noble gas (Figure 1) (Stute and Schlosser, 1992). Assuming that the recharge temperature is a fairly accurate reflection of the mean annual

air temperature, then the concentrations of the different noble gases should preserve a record of recharge temperature that can be used as a paleoclimatic record. Studies from Smith et al. (1964) tested the similarity amongst the two temperature regions and showed that there exists a high degree of correlation.

Table 1. Isotopic composition of atmospheric noble gases (from Andrews, 1992).

	Vol. % in atmosphere	Mol % of element
^{3}He	6.8E–10	1.4E–04
^{4}He	5.2E–04	100.00
Total helium	*5.2E–4 (partial pressure = 5.239E–6 atm*	
^{20}Ne	1.7E–03	91.05
^{21}Ne	4.7E–07	0.01
^{22}Ne	1.6E–04	8.94
Total neon	*1.8E–3 (partial pressure = 1.818E–5 atm)*	
^{36}Ar	3.2E–03	0.33
^{38}Ar	5.9E–04	0.06
^{40}Ar	9.3E–01	99.60
Total argon	*9.3E–1 (partial pressure = 9.34E–3 atm)*	
^{78}Kr	4.0E–07	0.35
^{80}Kr	2.6E–06	2.27
^{82}Kr	1.3E–05	11.56
^{83}Kr	1.3E–05	11.55
^{84}Kr	6.5E–05	56.90
^{86}Kr	2.0E–05	17.37
Total krypton	*1.1E–4 (partial pressure = 1.139E–6 atm)*	
^{124}Xe	8.3E-09	0.1
^{126}Xe	7.7E-09	0.09
^{128}Xe	1.7E-07	1.92
^{129}Xe	2.3E-06	26.44
^{130}Xe	3.5E-07	4.08
^{131}Xe	1.8E-06	21.18
^{132}Xe	2.3E-06	26.89
^{134}Xe	9.0E-07	10.44
^{136}Xe	7.6E-07	8.89
Total Xenon	*8.6E-6 (partial pressure = 8.6E-8 atm)*	

Ideally, all five noble gases should provide similar recharge temperature estimates. However, the initial solubility of each gas can be affected by various processes, and must be accounted for:

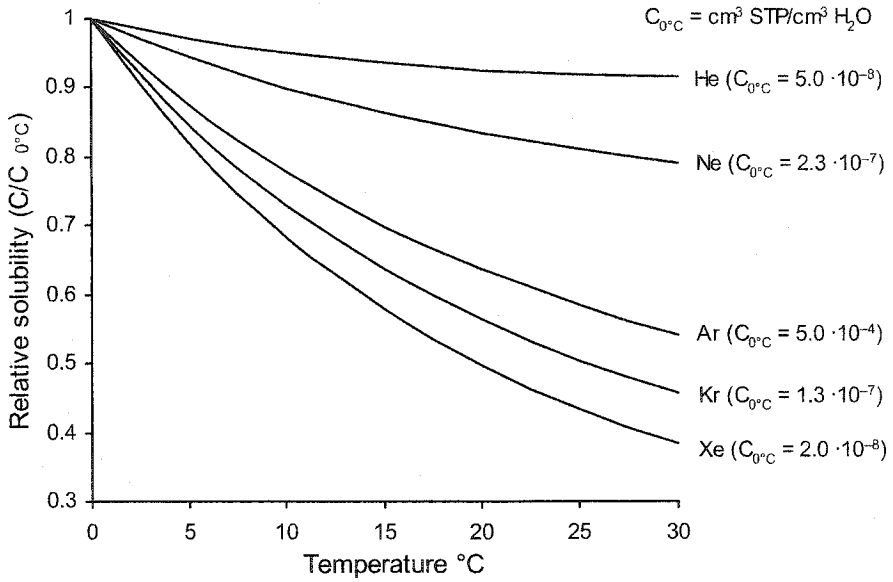

Figure 1. Relative solubilities of the noble gases as a function of temperature (Clark and Fritz, 1997; modified from Andrews, 1992).

1. 'Salting out' - An increase in the salinity of the solution will lower the solubilities of the noble gases.
2. Elevation - At higher elevations, air pressure decreases, and so does the pressure of each of the noble gases.
3. Radiogenic production - ^{4}He accumulates in the subsurface due to alpha particle production during U and Th series decay. Ingrowth of ^{40}Ar from ^{40}K decay produces overpressuring of Ar above atmospheric sources. $^{21,22}Ne$ can be produced through subsurface neutron activation reactions. $^{129,136}Xe$ are produced through spontaneous fission of U and Po in the subsurface.
4. Excess air - Entrainment of air bubbles causes relatively large volumes of noble gases to enter into solution. Table 2 indicates the effect of excess air.
5. Gas loss - High-enthalpy geothermal reservoirs (Pinti and Van Drom, 1997), which heat groundwater can cause dissolved gases to exsolve from solution into a separate gas phase. Phase separation then acts to strip the groundwater of noble gases. In a mine setting, de-saturation of fractures may also cause gas exsolution.

Table 2. The effect of air contamination on inert gas contents of air saturated water (from Youngman, 1989).

	He	Ne	Ar	Kr	Xe
A. Volume of gas in 1cm^3 fresh water Equilibrated with air at 15°C (cm^3 STP)	4.60E–08	1.95E–07	3.50E–04	7.60E–08	1.05E–08
B. Volume of gas in 0.01cm^3 air (cm^3 STP)	5.00E–08	1.82E–07	9.00E–05	1.14–8	9.00E–10
C. Volume of gas in 0.001cm^3 air (cm^3 STP)	5.00E–09	1.80E–08	1.00E–05	1.10E–09	1.00E–10
D. Volume of gas in a 1% volume air Contamination i.e. a+b (cm^3 STP)	9.60E–08	3.77E–07	4.40E–04	8.74E–08	1.14E–08
E. Volume of gas in a 0.1% volume air Contamination i.e. a+c (cm^3 STP)	5.10E–08	2.13E–07	3.60E–04	7.71E–08	1.06E–08
F. Volume % contamination of each gas in E	10%	9%	3%	1.50%	1%

The salinity, altitude and excess air effects are easily corrected for during calculation of recharge concentrations. Subsurface production from nuclear reactions poses a greater difficulty. This is particularly so for Ar and He, for which overpressuring can reach several orders of magnitude greater than atmospheric solubility.

1.3 Radiogenic Helium

Most atmospheric helium originates from radioactive decay within the crust (^{4}He) (Youngman, 1989) and to a minor extent from diffusion of primordial helium (^{3}He) from the mantle. Over time, He will migrate into groundwater flowpaths, sometimes being trapped in structures similar to those that contain petroleum and natural gas but eventually escaping into the atmosphere. The process by which ^{4}He is continuously being produced is through the alpha decay of uranium and thorium according to the following reactions (Andrews, 1992):

(1) $^{238}U \rightarrow {}^{206}Pb + 8\ {}^4He$

(2) $^{235}U \rightarrow {}^{207}Pb + 7\ {}^4He$

(3) $^{232}Th \rightarrow {}^{208}Pb + 6\ {}^4He$

Here, an alpha particle is essentially an uncharged ^4He atom. Uranium produces ^4He at the rate of $1.19x10^{-7}$ cm^3 STP/gU/yr. The present ^4He production from Th is $2.28x10^{-8}$ cm^3 STP/gTh/yr (Youngman, 1989). Because of the high geochemical abundance of these two minerals in rocks, helium production is wide-spread in the crust with enrichment resulting in concentrations 5 to 6 orders of magnitude greater (Bottomley et al., 1984; Poole et al., 1997) than the atmospheric equilibrium.

Helium concentrations have been shown to increase with depth in groundwaters contained within porous media aquifers (Andrews and Lee, 1979; Bath et al. 1979; Heaton and Vogel, 1979). Indeed, the age and radioelement content of continental basement rocks is such that they will contain 10 to 100 times the helium of most sediments. This means that diffusion of deep crustal helium into sediments is likely (Youngman, 1989), giving rise to an exponential increase in helium with depth (Figure 2).

The lighter helium isotope, ^3He, is created as a secondary reaction. Alpha particles created from the decay of uranium and thorium bombard the atomic nuclei of lighter elements. When this reaction involves lithium, ^3He is produced.

(1) $^6Li + n \rightarrow \alpha + {}^3H$

(2) $^3H \rightarrow {}^3He + \beta$

The above reaction, combined with ^7Li and gamma radiation, are equally possible but in reality produce negligible quantities of the helium isotope. However, lithium reactions involving thermal neutrons such as these listed above are responsible for virtually the entire volume of terrestrial ^3He (Youngman, 1989). Coon (1949) has determined the atmospheric ratio of $^3He/^4He$ to be $1.384x10^{-6}$. This atmospheric ratio is much smaller when compared to the deep mantle ratio. Ratios at the Mid-Atlantic Ridge are typically $3.3x10^{-5}$. Craig and Lupton (1976) calculated ratios in fumarole gas being expelled on the island of Hawaii at $2.1x10^{-5}$, and fluids from regions of high tectonic and magmatic

activity and high heat flow give values of $1.3x10^{-5}$ (O'Nions and Oxburgh, 1983), indicating that the mantle is indeed enriched in the lighter isotope.

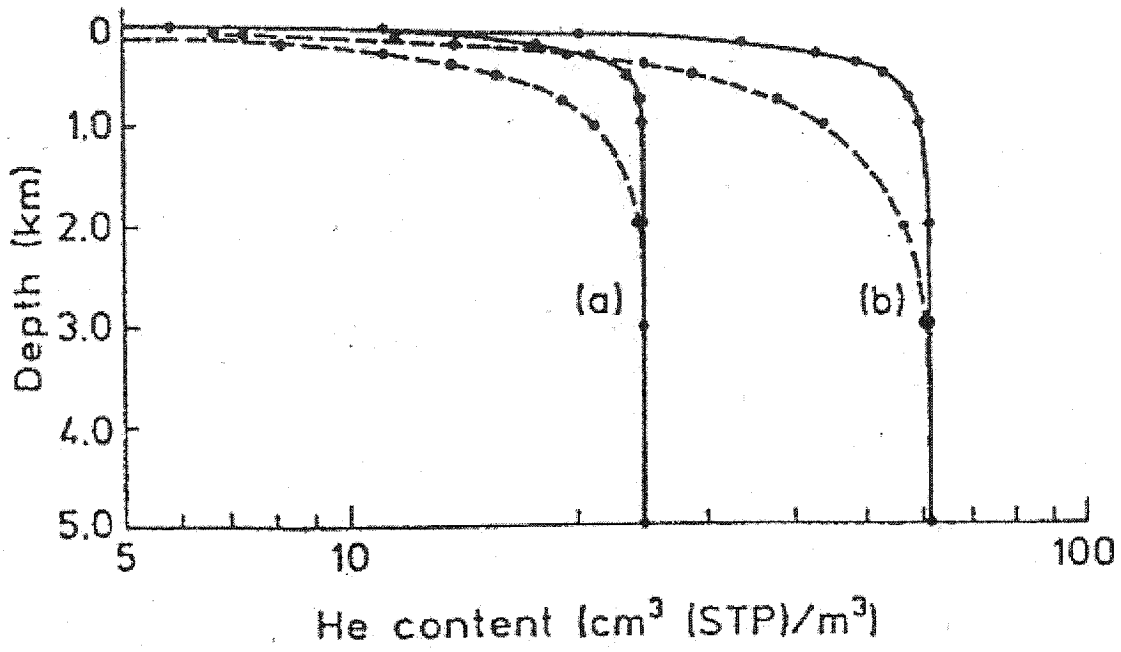

Figure 2. Diffusion profile for ^4He in sandstone with average uranium and thorium contents of 0.45 and 1.45 ppm, respectively, after: (a) 100 Ma, and (b) 250 Ma. The concentration/depth profiles are shown for diffusion coefficients of 0.00315 m^2/a (dashed line; 1/10 that for helium in 100% water) and 0.000315 m^2/a (solid line; for 1% that for He in water) (from Andrews, 1992).

With both helium isotope concentrations enhanced through radiogenic production, original estimates of recharge volumes are made impossible to calculate. For this reason, helium is not used in final paleotemperature estimations. A separate investigation was done, using multivariate statistics that proves why helium is unacceptable to use in paleothermometry. This appears in Appendix A.

1.4 Radiogenic Argon

Production of argon from potassium is responsible for generating the vast amounts of terrestrial and atmospheric argon that exists today. It also forms the foundation for the very important K/Ar dating method.

(1) $^{40}K \rightarrow {}^{40}Ar + \beta^-$

Because of the high concentration of potassium in crustal rocks, this reaction represents the primary source of new argon.

Argon can be used for recharge temperature calculations because unlike helium, the sum of the argon decay products is much more easily quantified. Because there is no significant input of radiogenic ^{36}Ar in the subsurface, this isotope can be compared to the total amount of ^{40}Ar in solution. The $^{40}Ar/^{36}Ar$ ratio for air, which is equal to 295.5, allows for the calibration for ^{40}Ar.

The sources of noble gases and their radioisotopes are summarized in Figure 3.

1.5 Canadian Shield Brines: Evaporation or Freezing of Seawater?

The Canadian Shield brines have been known to exist since early mining activities in deep crystalline settings (Lane, 1914). Canadian Shield brines are typically found in major faults and shear zones at depths greater than 650 m, and can reach total dissolved solids (TDS) up to 325 000 mg/L (Frape et al., 1984). These brines are considered to be of geological age. Theories regarding their origin have ranged from leaching of crystalline rocks over millions of years to solute enrichment through radiolysis. Frape et al. (1984), Kamineni (1987), Kamineni et al. (1992), Nordstrom et al. (1989) and Vovk (1987) have proposed that rock/water interactions is sufficient to create the necessary source of salinity . Lahermo and Lampen (1987), Nurmi et al. (1988), Kelly et al. (1986), Haynes (1988), Spencer (1987), Michelot et al. (1984), Fontes et al. (1989) as well as Guha and Kanwar (1987) argue against an in-situ source, preferring an external saline

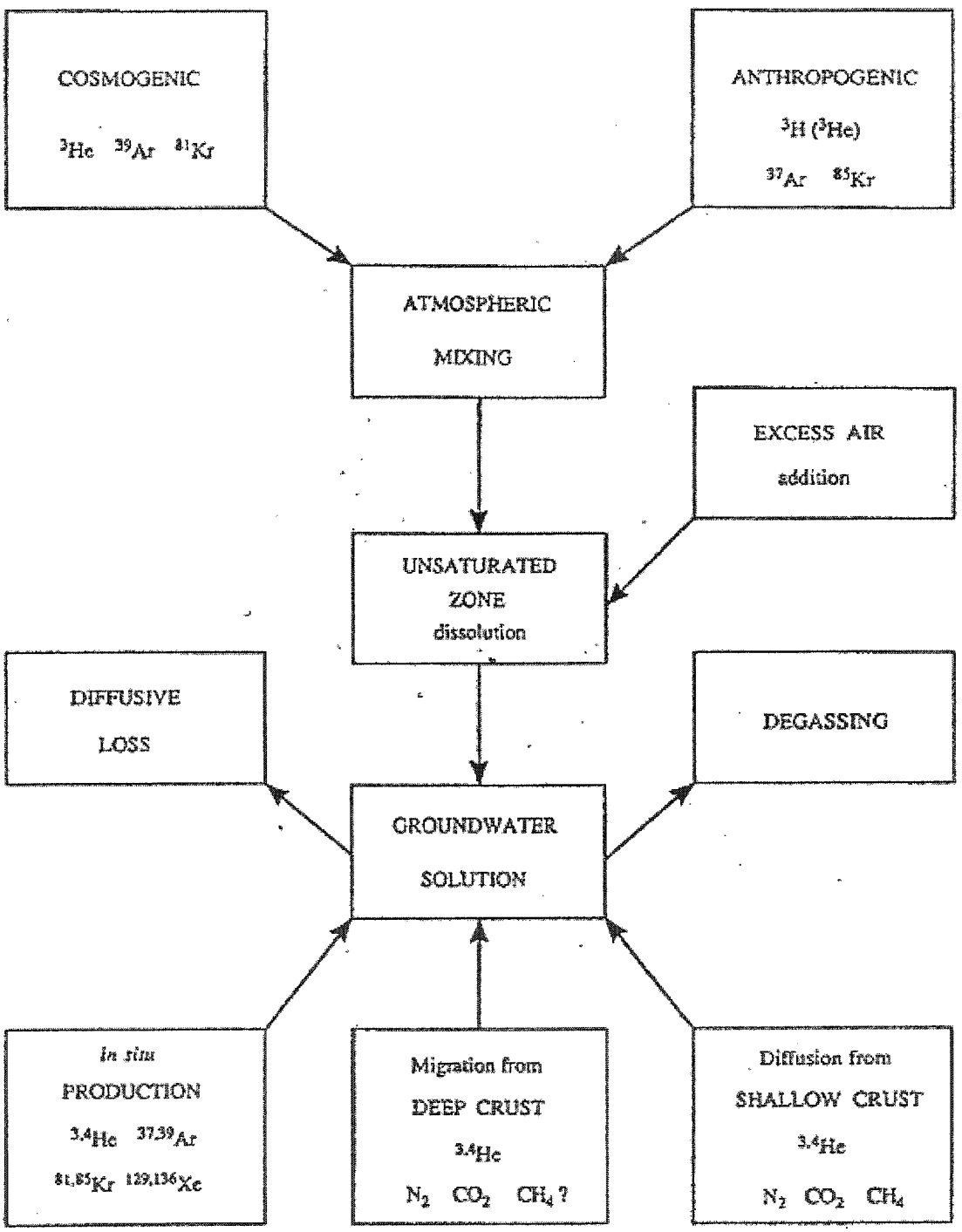

Figure 3. Sources of stable and radioactive noble gas isotopes with their sources and pathways (from Andrews, 1992).

source. That rock-water interactions have been taking place and have altered the isotopic and chemical composition of the brines has been suggested by Pearson (1987). This would indicate that the origin of these waters cannot be derived from the major ions in solution (Fontes et al., 1989). However, in-situ concentration by a factor of up to 35 times that of seawater is not supported by the minerals available within the crystalline rock of the Canadian Shield, and so other processes are likely responsible for the origin of the brines (Bottomley et al., 1994).

Bottomley et al. (1994) use geochemical evidence to support an origin by concentration of seawater. As evidence, it was pointed out that the salt deposits in the Alberta and Michigan Basins as well as the Hudson Bay region imply that much of the Canadian Shield was covered by seawater during the Lower Paleozoic. The evaporitic brines would then have migrated to the deep subsurface through existing fractures and fault zones aided by their elevated density (Stone et al., 1989; Kamineni et al., 1990), where they form isolated pockets. Further, new lithium isotope data (Bottomley et al., 1999) strongly suggest that the brines have a marine origin. Evidence includes uniformly elevated Br/Cl ratios, Li/Br ratios ranging from 0.0254 – 0.0325 and δ^6Li compositions of –32.1 to –36.3 ‰, all diagnostic marine properties.

Narrowing the source of the brines to seawater does little to end the debate, however, as it has been demonstrated that evaporation *and* freezing of seawater can produce a brine (Herut et al., 1990). In the case of subsurface brines, the concentration of seawater would have occurred during glacial periods when land-locked bodies of seawater or other restricted marine bodies such as lagoons, fjords, and bays are allowed to freeze and become blocked (Figure 4) (Herut et al., 1990). A significant portion of the H_2O would be removed as ice, with the remaining brine actually being forced into the subsurface by the hydraulic pressure of the overlying ice sheet coupled with the ambient hydrostatic pressure. Because this hydraulic pressure is not imposed upon the continental groundwater, the balance of pressure would then favour intrusion of the brines (Bein and Arad, 1992).

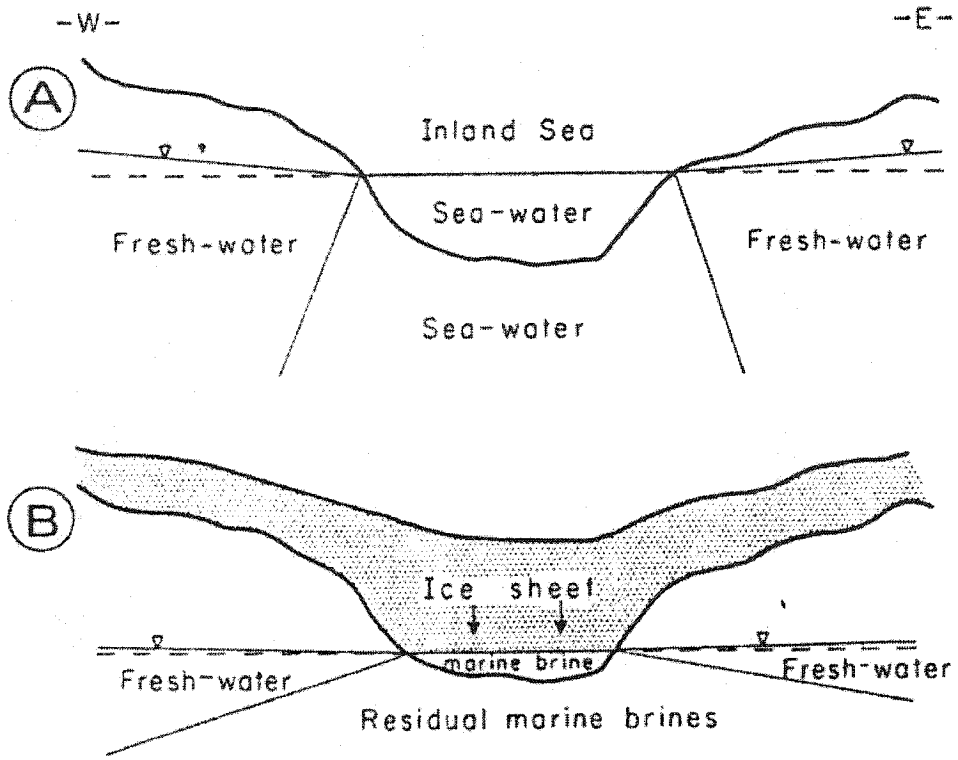

Figure 4. Hydrogeological cross-section illustrating the freezing model. (A) Freshwater-seawater relationships during the interglacial phase; (B) freshwater-brine relationships during a glacial phase (from Bein and Arad, 1992).

Even though there are distinct differences during the chemical evolution of seawater that lead to different ionic end-members and mineral precipitations (Figure 5 and Figure 6) amongst the evaporation and freezing mechanisms, environmental parameters subject them to the same physical conditions. Over time, any differences between the two would quickly be erased and the characteristic Ca-Cl brine would dominate (Herut et al., 1989). Table 3 summarizes these processes for both evaporative and freezing models. This is the 'lab-to-field discrepancy' that does not allow a final conclusion to be made one way or the other on the basis of geochemical evidence alone. While ^{129}I age data (Bottomley et al., 2002) and glacio-geomorphological evidence suggest that the brines were infiltrated prior to Pleistocene glaciations, the geochemical evidence is inconclusive. Therefore, another method to discriminate between the two is needed that is independent of chemical exchange processes. Herein lies the approach of the dissolved noble gases.

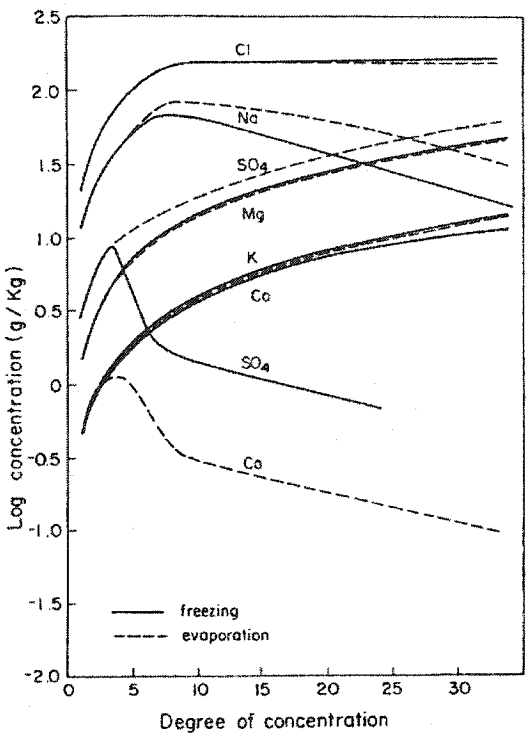

Figure 5. The chemical evolution of ions in seawater during evaporation and freezing processes (from Herut et al., 1990).

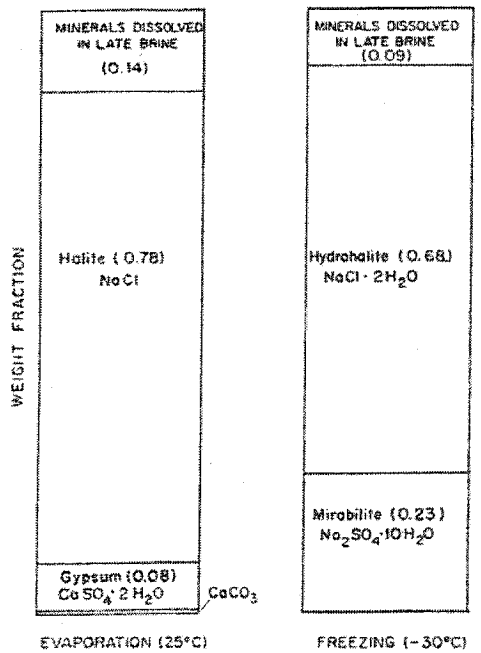

Figure 6. Quantitative comparison between the products of seawater evaporation (at 25°C) and freezing (at –30°C) (from Herut et al., 1990).

Table 3. Chemical properties of subsurface brines and their causes (from Herut et al., 1990).

I. PRIMARY MARINE ENVIRONMENT		
	Evaporitic	Glacial
Hypersalinity	Removal of H_2O by seawater evaporation	Removal of H_2O by seawater freezing
Na/Cl < 0.86	Removal of Na and Cl in halite	Removal of Na in mirabilite, and later with Cl in hydrohalite, in sediments and in ice-inclusions.
Mg/Ca <<5.2	Dolomitization of Marine carbonates.	No change
SO_4/Cl<<0.057	------Bacterial sulphate reduction----------	
	Anhydrite and/or gypsum crystallization due to dolomitization	Removal of SO_4 in mirabilite (as above).
$Ca/(SO_4+HCO_3) > 1$	Consequence of former processes	
BRINE MIGRATION INTO THE SUBSURFACE AND CONSEQUENT HEAT-UP		
II. SUBSURFACE ENVIRONMENT (brine-rock interaction)		
Temperature	Significant increase, depending on depth and on local geothermal gradient	
Salinity	Unchanged, or lowered upon dilution with fresh waters	
Na/Cl ratio	Decrease due to albitization of silicates, or increase upon dissolution of evaporite beds	
Mg/Ca ratio	Decrease upon limestone dolomitization or chloritization of silicates	
SO_4/Cl ratio	Varying, according to gypsum-anhydrite equilibrium conditions.	
$Ca/(SO_4+HCO_3)$	Increase upon dolomitization and/or chloritization.	

1.6 Project Objective

The objective of this study is to measure noble gas concentrations in Shield brines from the Con mine. Their concentrations, if atmospherically-derived, may then provide an estimate of the recharge temperatures prevailing at the time of infiltration to the subsurface. Warm temperature estimates will support an origin as evaporated seawater, whereas cold temperature results would indicate solute concentration by freezing of seawater. Subsurface production of radiogenic noble gas nuclides, if observed, would preclude paleotemperature estimates, but would provide an additional constraint on subsurface residence time that would distinguish Pleistocene (glaciogenic) brines from

Devonian (evaporitic) brines. By extension, the similarities that exist among all brines across the Canadian Shield in terms of chemical composition would indicate that they share a common geochemical history. Thus, the results obtained herein from the Con Mine subsurface waters may be applicable to other locations.

2 STUDY SITE

2.1 Location and Geologic Setting

Water samples for this project were collected from the Miramar Con Mine, which is located to the south of the town of Yellowknife. Yellowknife is situated upon the northern shores of Great Slave Lake in the Northwest Territories of Canada with coordinates 62.27°N, 114.22°W (Figure 7).

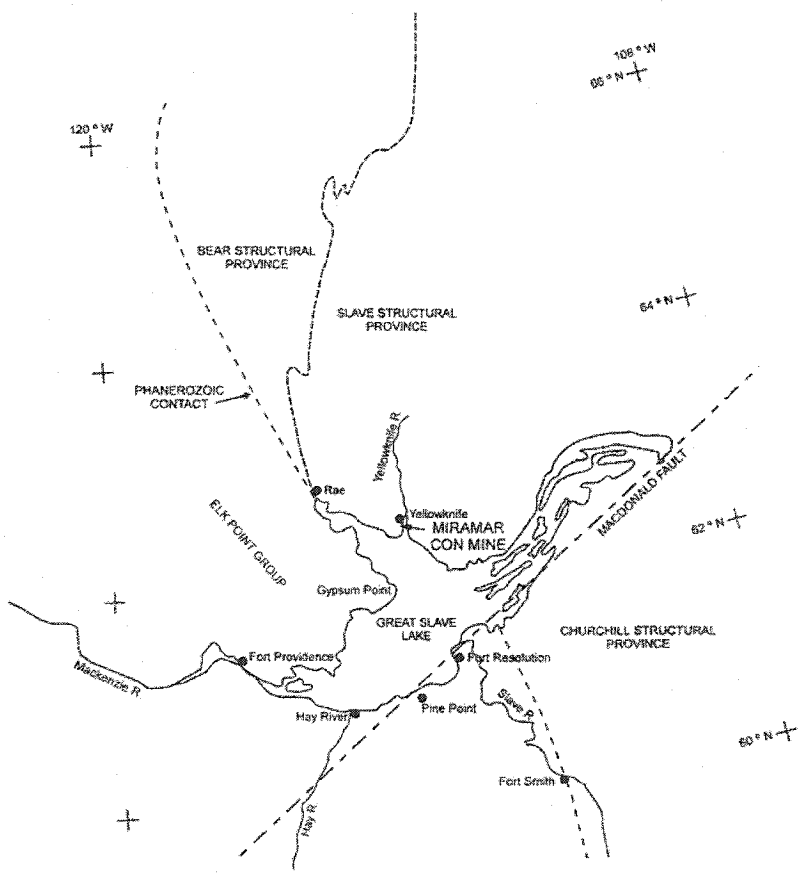

Figure 7. Con Mine location and regional geologic features (from Intera Consultants Ltd., 1997).

The geologic setting of the Con Mine places it as part of the Precambrian Shield, inside the Archean Slave Structural Province. The 2.6-2.7 Ga old rocks in the mine are volcanic in origin, consisting of mafic to intermediate tholeiitic basalts regionally metamorphosed by the proximal intrusion of the Western Plutonic Complex.

North-striking, west-dipping shear zones, created by the emplacement of the Western Plutonic Complex, play host to the gold mineralization upon which the Con Mine was founded. Of these, the Con and Campbell Shear Zones are the most economically lucrative, however, they are cut by numerous post-diabase, Proterozoic fault systems that are important in terms of groundwater movement within the mine. These fault systems, the West Bay, Pud, and Kam Faults, strike north northwesterly and intersect smaller lateral faults that include the Negus, Angel and Tibbit Faults. This geology is illustrated in Figure 8.

The surface exposure of Yellowknife includes vast expanses of scoured bedrock surfaces with little soil and vegetative covering, owing to the passage of the Laurentide Ice Sheet which covered this entire area as recently as 10 ka (Dyke and Dredge, 1989). Upon its retreat, a proglacial lake, known as Lake McConnell, formed and spread eastward and carried with it a lifespan of another thousand years (Craig, 1965). The region today is located within the zone of discontinuous permafrost (Clark et al., 2000).

2.2 Surface Geology and Surface Mine Features

The mine area is relatively flat with an average elevation of 200 masl. Several surface water bodies are located nearby, including the Pud lakes and Negus Pond that are utilized for mining operations, as well as the west coast of Yellowknife Bay and Kam Lake to the west (Figure 9). The two operating shafts, Con-1 and the Robertson are depicted as is the mine treatment plant. In addition, the traces of the West Bay, Negus and Pud Faults, which have surface expressions, are highlighted. The high northern latitude location of the mine causes surface water to freeze and remain frozen from October to May/June.

Groundwater recharge may only occur in significant quantities outside this time frame when temperatures rise above freezing during the spring thaw.

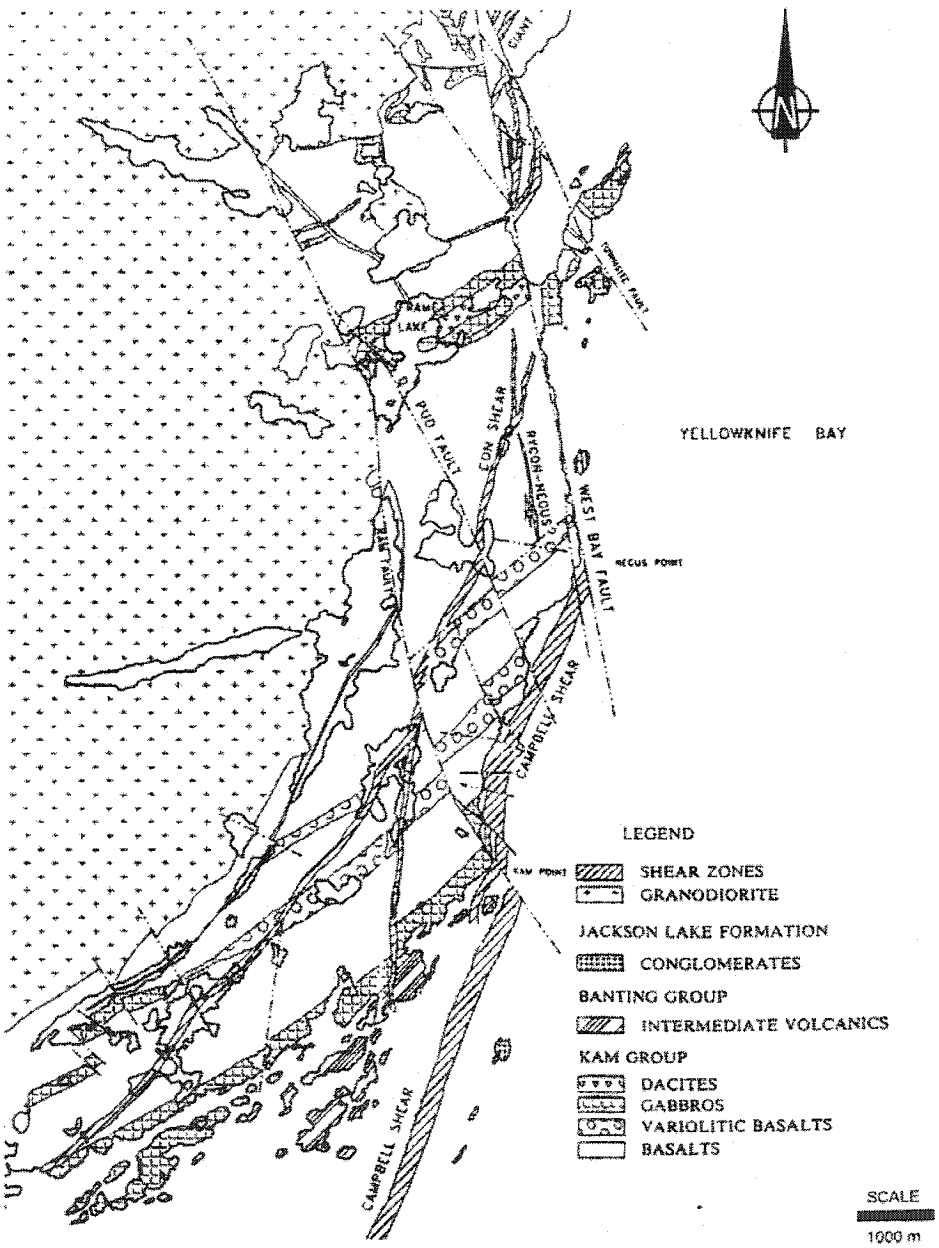

Figure 8. Geological setting surrounding the Con Mine and Yellowknife region (from Intera Consultants Ltd., 1997).

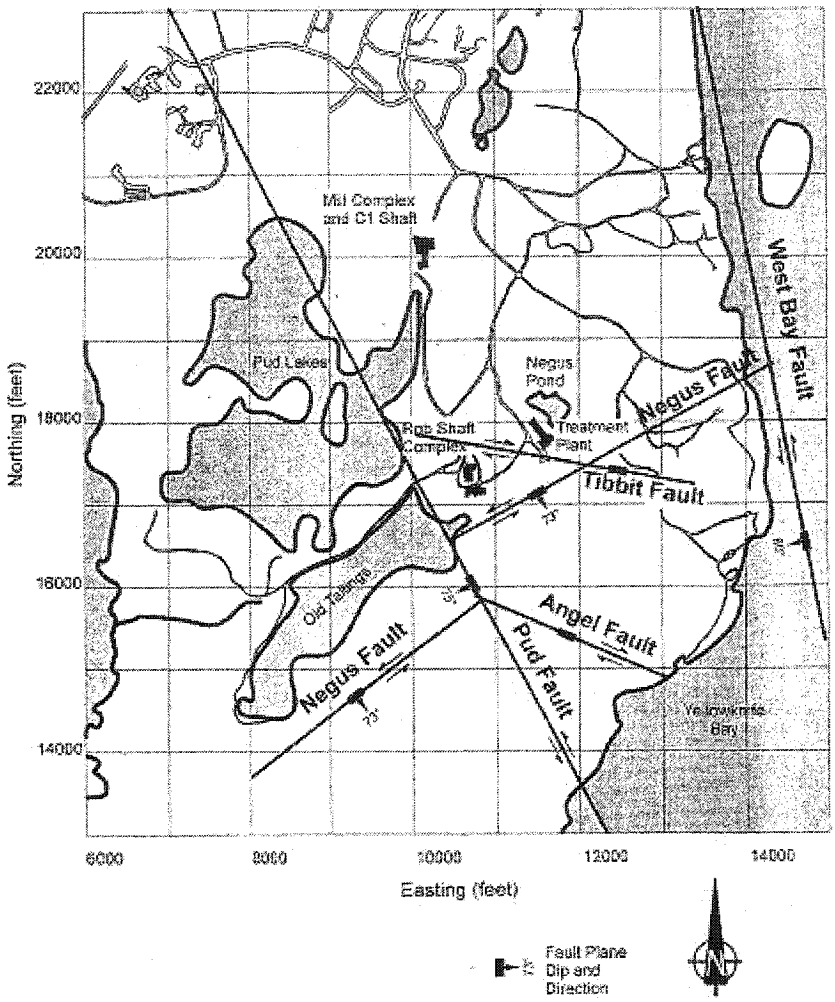

Figure 9. Map of the Con Mine site and surrounding significant features (from Intera Consulting Ltd., 1997).

2.3 Mine Geology

The Con Mine came into production in 1938 (Henderson and Brown, 1966), and continues today through the exploitation of gold deposits primarily concentrated in and around the Campbell Shear. The Campbell Shear strikes approximately north south, with a dip that is 50°W near the surface but comes about to 35°S and plunges to 70°W at the 5100' level of the mine (MacDonald et al., 1993). Located in metavolcanic rocks consisting of sequences of massive, pillowed and pillow-brecciated basalts, of the Archean Yellowknife Greenstone Belt, the entire sequence is intruded by diorite, gabbro, and diabase dykes.

Underground mining and academic studies (Henderson and Brown, 1966) have shown the existence of Precambrian age fault systems. These include the West Bay Fault, Pud Fault, Negus Fault, as well as the Angel and Tibbit Faults (classified together).

Although the West Bay Fault is not intersected by any mine openings, it represents the most significant of the faults, having a separation of more than three miles. Its orientation is nearly north south and it dips steeply to the west. It was this fault that led to the eventual discovery of Con Mine by Neil Campbell, the district geologist of the Consolidated Mining and Smelting Company of Canada Limited (Henderson and Brown, 1966).

The Pud Fault offsets the Negus by approximately 290 m through its NNW-SSE strike and SW dip. This fault plays an important role in the current research as the footwall splays of the Pud Fault have been found in the drifts of the 4500' level and below, where the water samples for this project were taken.

The Negus is the oldest of the Fault systems that carries a NE-SW trend that dips sharply to the SE. It too, plays a significant role in the hydrogeology of the mine in the vicinity of the study, appearing at the shallower 2300' - 4500' levels. The Angel and Tibbet Fault system strikes east west, and consists of numerous near vertical sets of faults that exhibit right lateral tendencies. They are present almost throughout the southern-end levels of the mine (2300' - 5300').

The Angel and Negus fault systems have the greatest hydraulic conductivity from intersecting boreholes, with inflows of up to 90L/s (Raven et al., 1997). The Pud Fault contains the lowest.

Mine workings presently extend 3.5 km in a north-south direction following the zones of mineralization. The main shaft reached a depth of 750 m in the year 1946, and continued on to reach 1890 m by 1974. Construction on the 2300' level finished in 1956, the 4900' level by 1979, and the deepest 5300' level in the year 1990 (Clark et al., 2000).

As the sampling for this study took place in the southern end of the mine, the latter three groups of faults are recognized as the most important in terms of hydrogeology and hydrochemistry. With mining activity following the Campbell Shear to the north, the southern end is relatively undisturbed such that aside from initial drift construction, no mining activity has influenced the groundwater flow regime.

2.4 Sampling locations

Samples were collected from four separate levels in the mine. The deepest was the 5300' level, followed by the 4900' level, 4500' level, and finally the 3500' level. Conditions in the drifts were poor, as the location of these sites were no longer active areas of mine operation and the working environment had been left to deteriorate. As such, floors carried thick deposits of mud and water, making the traverse on foot of approximately 500 m away from the main shaft somewhat difficult. More disconcerting was the fact that the air quality was dubious and had to be carefully monitored the entire time. In addition, safety bolts, wire mesh and large jagged pieces of rock were in the process, or had in fact already, ripped out of the ceiling and lay in heaps of rubble that created obstacles and an element of danger to the accomplishment of the field work.

The Con Mine represents a transient environment, changing year by year. Some of the previously planned sample sites, based on past published works, were discovered to have completely dried up, while others had simply had their margo plugs deteriorated beyond successful retrieval capabilities. Several changes had to be made to the schedule, but in the end, seven sites were utilized for dissolved noble gas analysis, with triplicates taken at each site. These included one at the deepest 5300' level (B-7126), one at the 4900' level (B-5310), three at the 4500' (B-3457, B-5316, B-5318), and two at the 3500' level (B-8906, B-9362). Water samples were taken from several other sites that were used for hydrogeochemical analysis. These sites are plotted on the map in Figure 10.

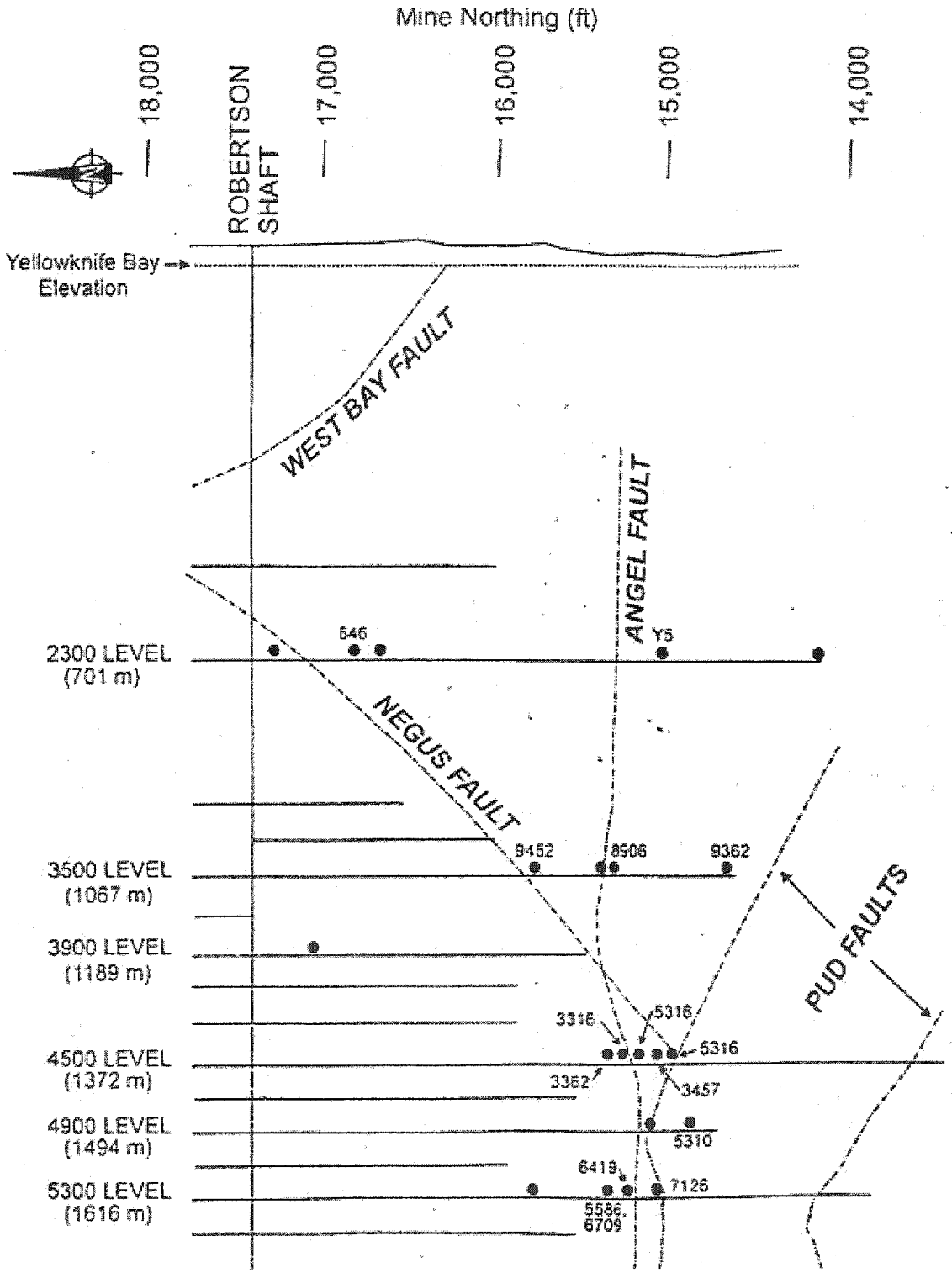

Figure 10. Profile of a cross-section through the Con Mine, showing the sample site locations along the different levels of the mine (from Bottomley et al., 1999).

3 METHODOLOGY

3.1 Field Methods - Noble gas sampling

Samples were collected in 35 cm long copper tubes, with 3/8" outer diameter, which yield approximately 16 cm^3 of water. Refrigerator clamps (Figure 11) were used to bolt directly down over the ends of the copper tubes to effectively pinch off the flow of water and create a cold weld seal.

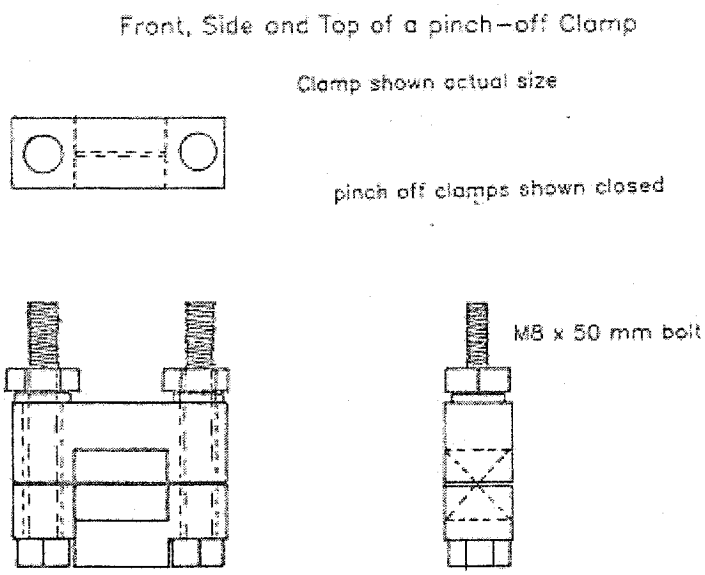

Figure 11. Schematic of a refrigerator clamp used to seal water in the copper tube (Youngman, 1989).

The apparatus for collecting water samples appears in Figure 12. One end of the copper tube apparatus (with the appropriate nut fitting), was attached directly to the margo plug in the mine wall and the control valve adjusted to give a restricted flow. Pressure gauges, one located upstream to the copper tube and the other downstream, were used to record the pressure in the well and inside the copper tube respectively. These were recorded before and after sampling the water, but observed constantly throughout the procedure to ensure that the sample remained pressurized at all times. A flow of water was allowed to proceed through the tube for two reasons: (1) to flush the copper

tube apparatus, removing the air and any impurities or solid particles which may have entered during transport, and (2), to remove a significant column of water from the borehole, which may have been degassed prior to our arrival. Once this was completed to satisfaction, the flow was completely shut off for a certain period of time (1 - 4 hours), depending upon the conditions at the respective site. Time frames were based on whether or not the margo plug was found to be in working condition, open or closed, sealed effectively, and the status of the pressure inside the borehole. The allotted amount of time was crucial in that it allowed the borehole to repressurize to its natural in-situ pressure. Otherwise, the degassed samples would not be accurate in measuring the dissolved load of noble gases as they would have originally been.

A second control valve, which originally allowed water to flow out of the distal end of the tube, was now used to cut off the flow of water entirely. After the given time frame valve 1 was closed, effectively sealing the water inside our series of copper tubes. The apparatus was then gently removed from the wall and placed inside a custom-built cradle system (Figure 13) where the refrigerator clamps were placed on the two extremities of each of the three copper tubes. When all three tubes were sealed and labeled, they were in turn separated and packed for transport out of the mine.

3.2 Field Methods - Hydrogeology and Geochemistry

At each sample site, a flow-cell was attached to the distal end of the copper tube apparatus so that flow rates and water samples could be taken and recorded. The hydrostatic pressure was sufficient enough that a pump was never required. Samples for cation and anion analysis, stable isotopes and tritium were taken in HDPE bottles directly from the borehole itself, while samples for carbon isotope analysis were taken in amber glass bottles.

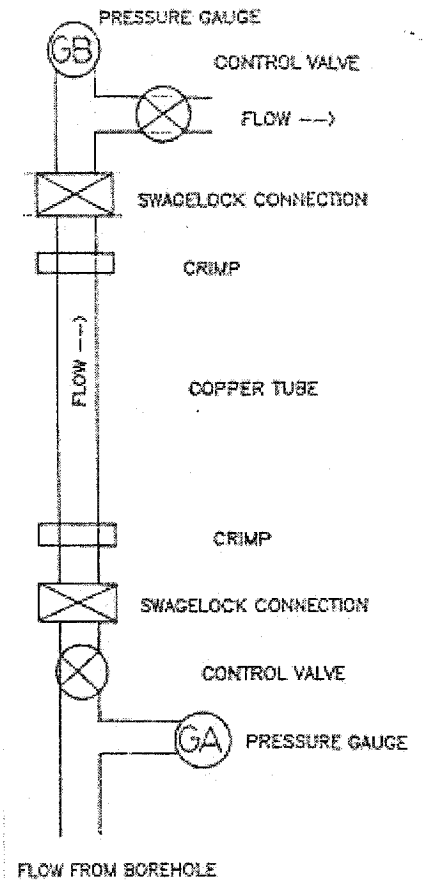

Figure 12. Apparatus for collecting pressurized water samples from the Con Mine, margo-plug outfitted boreholes (from Youngman, 1989).

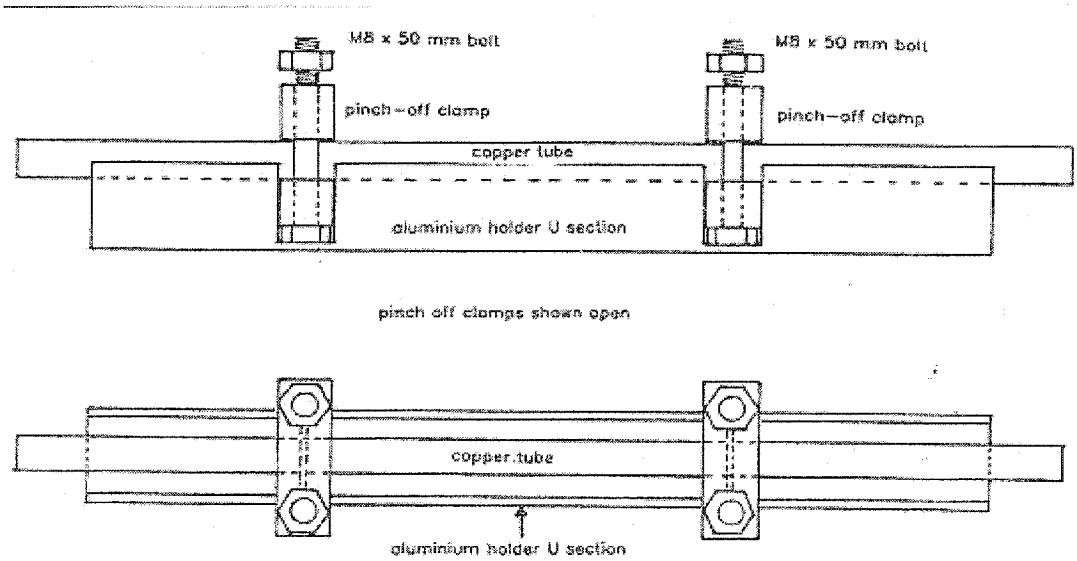

Figure 13. Cradle system for clamping refrigerator clamps on the copper tubes (from Youngman, 1989).

In situ measurements included pH, dissolved oxygen, conductivity and temperature. Precautions were taken against corrosion from the saline waters at deeper levels by covering the meters in clear plastic bags with the contacts between meters and their respective electrodes lubricated with petroleum jelly. The brines had to be diluted 10x before conductivity measurements were made owing to the high salinity of the brines. The restricted and difficult working conditions inside the mine drifts forced alkalinity titration measurements to be delayed until return arrival at the surface. At that point they were carried out using a Hach^{TM} field kit.

Accutest Laboratories carried out the major ion analyses. For cation analysis, waters underwent ICP-AES, using a Varian Liberty 220 ICP Emission Spectrometer. For anion analysis, waters were subject to a Dionex DX-100 Ion Chromatograph (HPLC) with a Dionex AS40 automated sampler. The analytical errors associated with this method are generally 10% at analyte concentrations greater than 10x the detection limit, and 100% at concentrations less than 10x the detection limit. Errors for all Br and Cl results are therefore +/– 10% of the reported value and errors for SO_4, NO_2, NO_3 and F are +/– 100% of the reported value.

Stable Isotope Analysis samples were run for ^{2}H, ^{18}O, and ^{13}C analysis. This work was conducted in the G.G. Hatch Isotope Laboratories at the University of Ottawa. Deuterium analysis involves high temperature reduction of the sample to elemental hydrogen, H_2, using 3μL of water in evacuated breakseals. The water is subsequently frozen and the breakseal re-evacuated. The analytical precision was 1.5‰ (2σ). The dissolved $\delta^{18}O$ in water was analysed by equilibration with CO_2 in a temperature-controlled bath at 25°C, with continuous shaking. The CO_2 is then extracted and analysed on a SIRA-12 gas source mass spectrometer. The fractionation factor, between CO_2 and H_2O, used by the University of Ottawa Laboratories is 1.0412 from Friedman and O'Neil (1977). Precision on these measurements amounted to 0.10% (2σ). Finally, the ^{13}C of dissolved inorganic carbon was measured by acidifying the water samples under vacuum to release CO_2. This was then cryogenically purified and analyzed on the SIRA-12 gas source mass spectrometer. Again, the analytical precision was 0.10% (2σ).

Tritium analysis was performed primarily at AECL Chalk River Laboratories using direct liquid scintillation counting techniques (MDL ~ 8 TU). Samples which were believed to contain less than 5 TU were sent to the Environmental Isotope Laboratory (EIL) at the University of Waterloo for enriched tritium analysis (MDL = 0.8 TU). Due to the complex matrix of the Con Mine water, toluene-based azeotropic distillation (Revesz and Woods, 1990) had to be performed on the samples analyzed for ^{3}H by direct liquid scintillation counting (LSC) at AECL.

3.3 Measurement of noble gas volumes by isotope dilution

According to the principles of isotope dilution, the determination of gas concentrations involves using known concentrations of both the air and spike gas. The spike gas is enriched in the minor isotopes of each of the noble gases in air (i.e ^{3}He, ^{22}Ne, ^{36}Ar, ^{78}Kr and ^{136}Xe). Both the volume and isotopic composition of the mixed spike is precisely known. This is the isotope dilution method for measuring gas concentration. By measuring the ratio of the spike gas isotopes against the abundant noble gas isotopes in air (i.e.^{4}He, ^{20}Ne, ^{40}Ar, ^{84}Kr and ^{132}Xe) the concentration of gas in the sample can be determined. The advantages of this technique are that absolute values are not measured, only ratios. This allows for accurate measurements to be made on very small samples.

A reduced formula that illustrates the isotope dilution process appears below. Using argon as an example, the problem is simply one of cross-multiplication:

$$R = \frac{^{36}V\,(t)}{^{40}V\,(at)}$$

Where R = ratio recorded from mass spectrometer readings

$^{00}V(t)$ = volume of tracer isotope

$^{00}V(at)$ = volume of atmospheric isotope

As the calibrated spike volume is known, the measured ratio is then proportional to, and yields the volume of, Ar in the sample. The same principle applies for all noble gases.

The actual formula that is used is slightly more complex, as trace amounts of both minor and major isotopes often appear in both the atmosphere and the spike aliquots. But because the isotopic concentrations of both atmosphere and tracer spike are accurately known (Table 4 and Table 1 (atmospheric concentrations)), and the volume inserted is accurately recorded, a correction can be applied to this equation (found in Youngman, 1989). Again, using argon as an example:

$$R = \frac{^{36}Ar}{^{40}Ar} = \frac{^{36}X(at)*Vat(Ar) + ^{36}X(t)*Vt(Ar)}{^{40}X(at)*Vat(Ar) + ^{40}X(t)*Vt(Ar)}$$

Where R = ratio recorded from mass spectrometer readings

$^{00}X(t)$ = mole fraction of tracer isotope

$^{00}X(at)$ = mole fraction of atmospheric isotope

Vt(Ar) = volume of tracer Ar at STP

Vat(Ar)= volume of atmospheric Ar at STP

Rearrangement of this equation for Vat(Ar) gives:

$$Vat(Ar) = \frac{Vt(Ar)*[^{36}Xt - (^{40}Xt*R)]}{[(^{40}Xat*R) - ^{36}Xat]}$$

3.4 Noble Gas Line – calibration and spike volume calculation

Following construction and leak-testing of the noble gas line, a series of preliminary tests were run. These included mass ionization runs to determine the optimum electron voltages at which to analyse the individual noble gases. This was determined to be –57 eV for all gases excluding Ne, which is measured at –37 eV as ^{20}Ne is susceptible to

artificially elevated ion intensities due to doubly charged ^{40}Ar (Ar^{+} = m/e; Ar^{2+} = 40/2 = 20). Mass calibration tests were also performed to tune the quadrupole over the mass range of interest.

Table 4. Isotopic concentrations of individual spikes from certificates of analyses.

He (99.995% pure)		Ne (99.5% pure)		Ar (99.5% pure)		Kr (99.5% pure)		Xe (100% pure)	
Isotope	%	Isotope	%	Isotope	%	Isotope	%	Isotope	%
^{3}He	99.99	^{20}Ne	<0.1	^{36}Ar	99.7	^{78}Kr	68.9	^{132}Xe	0
^{4}He	0.01	^{21}Ne	<0.1	^{38}Ar	0.3	^{80}Kr	26.3	^{136}Xe	100
		^{22}Ne	>99.9	^{40}Ar	0	^{82}Kr	3.6		
						^{83}Kr	0.6		
						^{84}Kr	0.6		
						^{86}Kr	<0.1		

Following measurement optimization, tracer gas calibration runs were undertaken. In order to calculate an accurate volume for the tracer gas aliquot an accurately measured amount of atmosphere was used as a standard. A specific quantity of air was inserted into the vacuum line, using a high-vacuum syringe, via a rubber membrane/ultra-torr attachment. Once the needle was inserted, the air was expunged into the available chamber. Two sets of valves allowed the gas to be stored and released in a controlled manner into the main line where it then mixed with the tracer spike.

Since the mole fractions of all isotopes within the air and tracer are known, as well as the volume of inserted atmospheric gas, then a further mathematical rearrangement of the equation allows for the calculation of the volume of tracer gas:

$$Vt(Ar) = \frac{Vat(Ar)*[(^{40}Xat*R) - {}^{36}Xat]}{[{}^{36}Xt - (^{40}Xt*R)]}$$

using previously defined notation.

Numerous air spikes were run and averaged together in order to get a representative value for all subsequent sample measurements.

3.5 Isolation of Noble Gases in Water

The noble gas analytical procedure began with a general cleansing of the copper tube. The exposed ends were rinsed with distilled water, followed by acetone, and dried with warm air from the heat gun. It was then weighed prior to release, which included the tube itself with associated swage-lock connectors, as well as the associated refrigerator clamps. This value would be used in conjunction with the final weight, after release, to determine the mass of the water sample analyzed in order for the noble gas content to be expressed as cm^3 gas per cm^3 water.

It was discovered early on that the size of the samples taken (35cm long), yielded a quantity of water too great for the sample inlet manifold (water vapour trap) to manage. As a solution, a third refrigerator clamp was placed in the centre of the tube, which cut the sample in two.

When ready, the copper tube sample was attached to the vacuum line inlet (refer to Figure 14 (visual representation guide only – for detailed description of actual line function, set-up, and components, see Appendix B)). After cooling the water vapor trap to approximately $-70^{\circ}C$ using a dry ice/methanol mix and evacuating the inlet manifold to pressures of approximately 10^{-5} torr, all vacuum valves were closed. The manifold was isolated for a brief moment while a mixed spike gas aliquot was admitted into the main line.

With spike ready, the manifold was again opened to the main line. The upper clamp on the copper tube sample was removed and pressure was continuously monitored on the pirani pressure guage. If no pressure jump was recorded, the cold weld was delicately opened, very slowly, until release became evident. This action was followed by heating of the copper sample tube with a heat gun for several minutes to ensure that the contained water was vaporized and all dissolved gases were released from the water into the sample inlet manifold line where they mixed with the mixed spike gas. Escaping water vapour was frozen out onto the center well of the water vapor trap. A given amount of time was

allowed to elapse so both the tracer gas and sample gas could mix and spread throughout the line. Once this expired the manifold was once again closed off, sealing the mixed gas inside the main line.

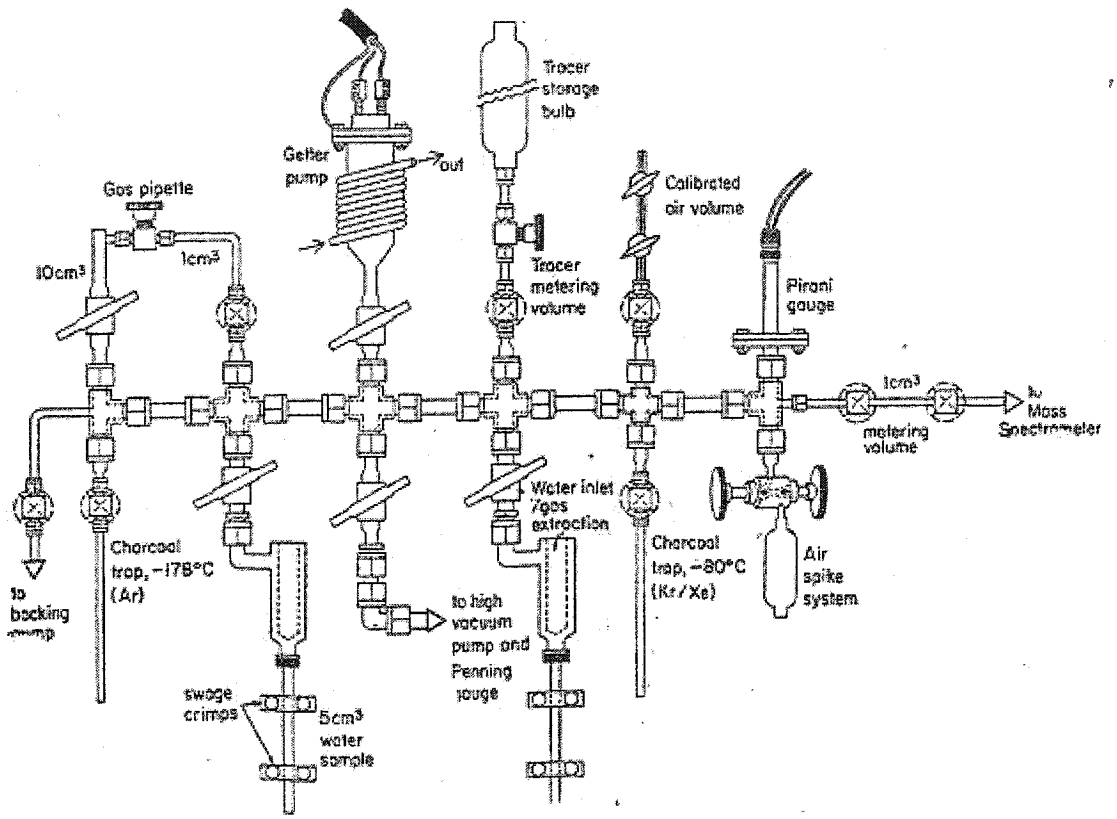

Figure 14. A typical noble gas extraction line (from Poole et al., 1997).

3.6 Methane gettering and gas trapping

A major concern, and a problem that arose, with the analysis of brine samples from the Canadian Shield was the high concentration of methane in the groundwater, which can exceed one cc per cc of solution. Any gas, or combinations thereof, existing in large quantities alongside the noble gases will have the effect of interfering with the mass spectrometer signals produced during the analysis phase and impinge upon an accurate and precise measurement. It therefore becomes crucial to get the best possible gas

separation, especially for the heavier elements of Kr and Xe that have such small quantities in air to begin with. This is accomplished through gettering and gas trapping.

The problematic methane, which has been shown by Fritz et al. (1987) and Sherwood et al. (1988) to be in high abundance amongst Canadian Shield brines, shows increasing amounts with depth (Sherwood et al., 1993(a)). Results from Sherwood et al. (1988) show that methane can achieve concentrations of up to 87.6% of the total free gas phase in the Ca,Na-Cl brines from the 4500' level of the Con Mine (Table 5). The remainder typically consists of N_2 (up to 80%), H_2 (up to 30%), He (radiogenic He - up to 20%), with only minor amounts of higher hydrocarbons, and noble gases. Although several theories have been proposed to account for the production of methane, with most evidence pointing towards an abiogenic process, the origin of this major component of shield gases remains a mystery (Sherwood et al., 1993(b)).

Table 5. Composition (in vol. %) of natural gas occurrences in the Canadian Shield (from Sherwood et al., 1988).

Locality and sample	O_2	N_2	CO_2	CH_4	C_2H_6	C_3H_8	C_4H_{10}	He	Ar	H_2
Thompson, Manitoba										
65124	0.06	30.7	<0.06	64.8	1.5	0.1	<0.01	1.8	0.35	0.76
T3-27394-84	<0.04	45	0.3	54.3	2.23	0.17	<0.01	1.59	0.54	n/a
T3-27377-84	0.3	35.6	0.46	64.3	3.05	0.39	<0.01	0.79	0.7	n/a
T3-STA 330-84	<0.04	48.8	0.26	49.1	1.85	0.14	<0.01	1.55	0.53	n/a
Sudbury, Ontario										
N3640A, Jun. 1982	n/a	79.9	<0.1	9.75	n/a	n/a	n/a	5.3	n/a	n/a
N3640B, Apr. 1983	<0.3	79.2	<0.3	8.7	0.075	<0.03	0.025	6.8	3.6	n/a
N3644B, Apr. 1983	n/a	77	<0.1	14.4	0.09	<0.02	<0.01	4.7	n/a	n/a
N3645, Apr. 1983	<.05	77.2	<0.3	12.5	0.087	0.04	0.04	6.3	3.9	n/a
N3646A, Apr. 1983	n/a	74.6	<0.1	15.6	0.09	<0.01	<0.01	6.7	n/a	n/a
CCS4000, 1985	0.17	3.28	<0.02	55.1	9.43	0.66	0.22	5.17	n/a	30.3
CCS4000, 1987	<0.04	3.51	0.04	54.9	10.8	0.81	0.29	4.22	<0.05	26.2
CCS844-1 (before)	<0.04	6.47	0.07	79.1	2.24	0.1	<0.01	5.99	<0.05	0.47
CCS844-1 (after)	<0.04	11.8	0.02	70.3	1.94	0.12	0.02	9.05	<0.05	0.88
CCS844-2	1.5	12.9	0.03	68.6	2.6	0.12	<0.01	1.74	<0.05	7.55
CCS846-1	<0.04	6.83	0.08	69.9	3.16	0.34	0.11	4.41	<0.05	0.06
CCS846-2	<0.04	10.6	0.81	74.7	1.48	0.09	0.02	5.16	<0.05	0.06
STR31178, Apr. 1983	<0.1	83.3	<0.1	0.2	n/a	n/a	n/a	10.2	2	n/a
Yellowknife (Giant and Con), Northwest Territories										
G2000 (near C-shaft floor,	<0.04	19.5	0.46	64.4	4.99	0.51	0.08	7.5	0.53	<0.01
C4301-1, N end drift	0.52	24.5	0.29	66.7	0.93	n/a	n/a	6.4	0.57	n/a
C4301-2, N drift, 1985	0.76	24.3	0.11	61.1	2.7	0.17	<0.01	6.78	0.05	<0.01
C4500-2, N drift, 1985	<0.04	50.6	0.43	40	0.63	0.03	<0.01	6.64	0.87	<0.01
C4500 (3, 1985)	2.02	73.2	0.07	15.6	0.25	0.02	<0.01	7.8	1.01	<0.01
C4500 (LAT-14650, 1985)	<0.04	8.15	0.58	87.6	1.68	0.03	<0.01	1.31	0.35	<0.01

Elliot Lake, Ontario										
JV-906	<0.07	26.7	0.11	54.3	0.11	0.02	0.03	19.3	0.75	n/a
Denison 30876, 1985	2.77	38.2	0.08	44.2	0.04	n/a	n/a	14.2	0.55	n/a
Matagami, Quebec										
2002 (90, R46)	0.72	21.4	0.22	75.9	1.55	0.12	<0.03	1.1	1.51	n/a
2000 (90, R36, 1985)	0.48	11.3	<0.02	82.1	1.81	0.14	<0.07	1.88	0.01	n/a
2000 (90, R36, 1986)	n.d.	8.26	0.02	83.2	2.27	0.13	0.03	1.22	0.13	n/a
Norita, Quebec										
N256-1985	1.59	28.6	0.46	62.3	2.1	0.26	<0.03	n/a	3.17	n/a
N18-4W-85-1985	<0.07	6.73	0.26	89.5	2.71	0.18	<0.03	1.03	0.52	n/a
UN-243 (28)-1985	<0.07	16.7	0.1	78.8	1.91	0.09	<0.03	1.11	1.5	n/a
UN398-1986	0.17	4.49	0.04	82.5	4.08	0.41	0.18	0.83	0.07	n/a
Val d'Or, Quebec										
Sigma 10680, 1985	0.07	55.1	0.27	37.8	0.66	n/a	n/a	n/a	5.61	0.51
Timmins, Ontario										
Kidd Creek 3185	0.43	12.9	0.1	76.1	3.72	0.48	0.12	1.41	0.16	n/a
Kidd Creek 3172	4.12	31.1	0.08	73.3	5.2	0.87	0.31	1.62	n/a	n/a
Red Lake, Ontario										
Dickenson 25-320	0.28	54.38	0.33	41.9	1.05	0.22	0.05	3.97	0.24	n/a
Dickenson 25-324	0.12	44	0.39	52.7	1.37	0.25	0.06	3.62	0.22	n/a
Dickenson 26-102	6.27	70.2	1.02	17.9	0.29	0.02	<0.01	1.65	0.45	n/a
Dickenson 27-119	<0.01	61.9	2.55	30.4	1.55	0.83	0.22	3.34	0.38	n/a
Campbell 2733, 1985	<0.04	34	0.02	52.5	0.63	0.12	<0.01	10.9	0.53	<0.01

This unusually high gas over-pressuring was initially found to overwhelm the original getter pump on the line, which was designed essentially for atmospheric gases (N_2, O_2 and CO_2). A second, enhanced furnace getter pump using rechargeable SEAS ST-707 zirconium-vanadium-iron getter pellets was installed to deal with this problem. The pellets have a flat circular shape (diameter ~1cm) and are 3-5mm thick. Using only three pellets, at an operational temperature of 600°C, they were found to remove virtually all the methane as well as other reactive gases including hydrogen, nitrogen, and various oxygenated compounds, to background pressures in the line. This entire process usually took less than 20 minutes, depending upon the saturation level of the pellets and the amounts of reactive gases contained within the sample.

Following the gettering of reactive gases, the spike/sample mixture of noble gases are the dominant gases in the line, with Ar typically the dominant gas (over 99%). In the deep-seated brines, however, a significant overpressuring by radiogenic ^4He exists as well, which can match, or even exceed the pressure of Ar. Nevertheless, a small portion of this gas is isolated for future Ar isotope ratio measurement inside a designated 'Ar-

bulb' container. Krypton and xenon are the first to be separated and trapped by adsorption onto a charcoal trap cooled to –78°C by a dry ice/methanol solution. Following this, the remaining argon in the line was removed by adsorption onto a second charcoal trap cooled with liquid nitrogen to temperatures of approximately –196°C. This gettering and subsequent trapping process leaves the line enriched in He and Ne, which are measured together.

3.7 Noble gas isotope ratio measurement

As the majority of gas remaining in the line is He and Ne, they become the first to undergo isotope ratio measurement on the quadrupole mass spectrometer. This is done using two valves located proximal to the mass spectrometer inlet. Small subsamples of gas can be metered in separately until a desired amount is reached. As both gases are mixed together, they are administered into the mass spectrometer at the same time, so the order of analysis is irrelevant. However, they must be measured separately as the filament current must be changed for each. $^{3}He/^{4}He$ ratios are measured using a filament current of –57 eV, while for $^{20}Ne/^{22}Ne$, it must be raised to –37 eV (to preclude doubly charged Ar contributing to mass 20).

After measuring the light noble gases, the line and mass spectrometer were evacuated to 10^{-5} . The Kr/Xe trap was heated to 350°C to release these gases for measurement of $^{78}Kr/^{84}Kr$ and $^{132}Xe/^{136}Xe$ ratios for volumetric calculations (as well as their respective additional isotopes: ^{80}Kr, ^{82}Kr, ^{83}Kr, ^{86}Kr, ^{129}Xe, ^{130}Xe, ^{131}Xe, and ^{134}Xe for select samples). These were metered into the mass spectrometer, using the two valves in the same fashion as was carried out for He and Ne.

Following the same process as outlined above, the measurement of $^{36}Ar/^{40}Ar$ was made using the original sub-sample of gas isolated immediately after gettering, inside the Ar-bulb.

A more detailed, step-by-step procedure for this process appears in Appendix C.

4 HYDROGEOCHEMISTRY – Results and Discussion

4.1 Flow Rates and Formational Pressures

Comparisons between data from this study with that collected during the year 1995 and published by Intera Consultants Ltd. (1997) are shown in Table 6 and displayed in Figure 15. The general trend shows a significant decline in the quantity of water being flushed out with depth. In addition, although the general trend remains the same from 1995 to 2000, there is a matching reduction in the quantities of water from that same time period from identical sampling sites. In the year 1995, flow rates ranged from 6000 ml/min. to 500 ml/min., whereas 5 years later these same sample sites produced an average of 3.6 times less water, with equivalent ranges of 2500 ml/min. to 0 ml/min. No information could be found on the flow rate for site B-9362 in the year 1995. For the present study, no recoverable water was found to be emanating from borehole B-6709.

Temporal trends in the formational pressures were similar to trends in flow rates when compared to 1995 measurements (Figure 16). Both sets of readings show a trend of increasing pressures with depth, with the exception of borehole B-9362 on the 3500' level. However, as with the flow rates, inferior pressure values were observed for each and every site sampled. The average decrease from the year 1995 to 2000 is on the order of 59%. Sampling equipment at borehole B-5318 did not return any pressure reading in spite of the fact that it produced a flow rate of 400ml/min. Triplicate water samples for noble gas analysis were sampled despite this setback, but with noted doubts on thereliability of the noble gas concentrations. Sample site B-6709 was discovered to contain no recoverable water, hence, no pressure measurements were possible.

Table 6. Comparison of flow rates and formational pressures from the year 1995 and 2000.

Level (ft)	Borehole	Flow Rates (ml/min.)		Formation Pressures (kPa)	
		1995	2000	1995	2000
3500	B-8906	6000	2500	750	400
3500	B-9362	-	4500	4800	3100
4500	B-3457	5000	800	1800	900
4500	B-5316	2000	700	2000	900
4500	B-5318	2000	400	2600	0
4900	B-5310	1000	1000	2600	1400
5300	B-6709	500	0	3500	-
5300	B-7126	2000	1300	3500	1500

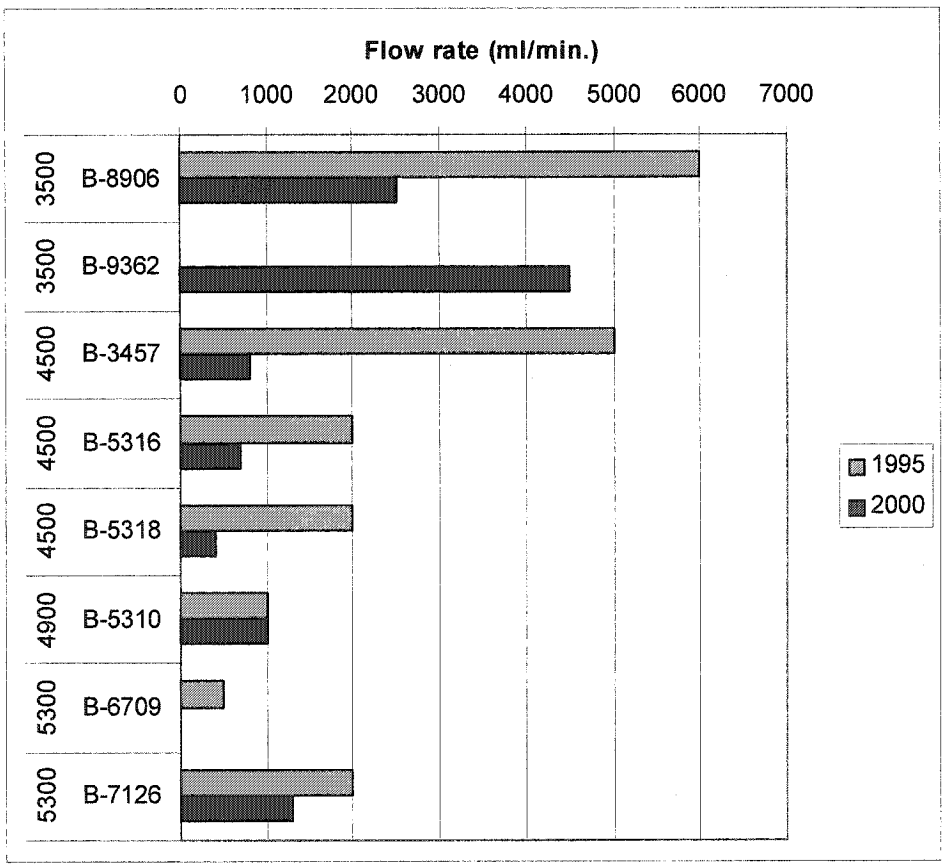

Figure 15. Comparison of flow rates in the mine during the year 1995 to those of 2000.

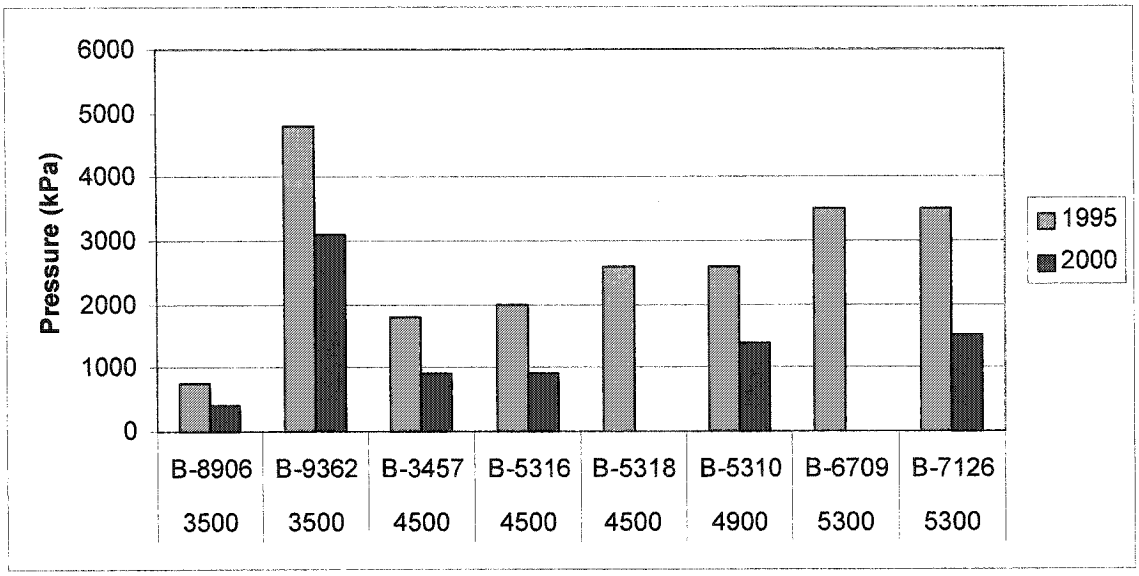

Figure 16. Comparison of formational pressures in the mine during the year 1995 to those of 2000.

4.2 Major Ions

The major ions in solution are represented primarily by calcium (Ca), sodium (Na) and chlorine (Cl), with sulfate (SO_4) and bicarbonate (HCO_3) playing a role at shallower depths (Table 7). The importance of the latter two in the upper portions of the mine can be attributed to the influx of modern meteoric surface waters and tailing pond waters, which embody the source. As the groundwater becomes more saline with depth, the concentrations of SO_4 and HCO_3 can be seen to decrease dramatically, from 638 mg/L down to 2 mg/L and from 340 mg/L to 17 mg/L, respectively. From here, the proportions of Ca, Na, and Cl increase to become the dominant concentration species (Figure 17), forming a Ca-Na/Cl brine that has been found in other areas of the Canadian Shield (Frape et al., 1984).

The brines sampled for this project during September 2000 show TDS (total dissolved solids) values ranging from 48 mg/L to 304 g/L. TDS values were calculated using the major ions of Ca, Na, Mg, K, Cl, SO_4, Br, HCO_3, and assumed to represent the overall salinity.

Table 7. Major ion concentrations for Con Mine groundwaters.

Level (ft)	Borehole	Ca	Na	Mg	K	Cl	SO4	Br	HCO3	TDS	Units
Great Slave Lake		16	5	4	<1	11	12	<0.05	-	48	mg/L
3500	B-8906	241	236	31	3	533	170	5	340.4	1559	mg/L
3500	B-9362	1780	2040	34	8	5815	580	46	39.5	10343	mg/L
3500	B-9452	1210	1110	83	7	3685	638	27	139	6899	mg/L
4500	B-3316	36800	21200	211	165	119500	15	1190	-	179081	mg/L
4500	B-3362	23900	14700	190	111	73750	27.5	683	-	113362	mg/L
4500	B-3450	18900	12400	190	83	52700	40.5	525	-	84839	mg/L
4500	B-3457	2800	2500	50	13	8190	602.5	67	39.5	14262	mg/L
4500	B-3618	13800	7910	126	55	32100	98.5	265	-	54355	mg/L
4500	B-5316	4450	3320	78	21	12250	587	112	37.8	20856	mg/L
4500	B-5318	15600	7530	148	51	33900	69.5	350	53.7	57702	mg/L
4900	B-5310	21800	11100	294	83	69900	36	-	-	103213	mg/L
5300	B-5586	81900	33000	153	308	163500	4	1600	-	280465	mg/L
5300	B-6709	82700	29800	219	318	169000	5	1650	18.8	283711	mg/L
5300	B-7126	96100	36900	486	391	168500	2	1720	17.3	304116	mg/L

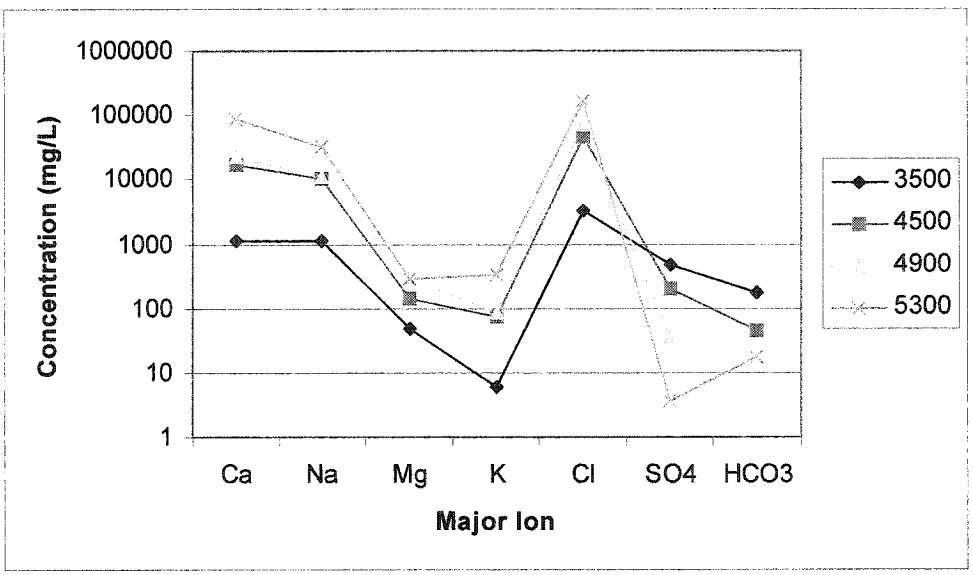

Figure 17. Concentration trends of the major ions with depth.

TDS increase logarithmically with depth (Figure 18). Borehole values that do not coincide with this general pattern can be attributed to fracture-controlled fluid flow.

The largest fraction of TDS is from the chloride ions. Although these ions can be derived from a variety of sources, its linear relationship with Br at all depths in the crust has been used by Bottomley et al. (1999) as evidence of a Paleozoic seawater source as opposed to water/rock interactions (Frape et al., 1984). A plot of Br vs. Cl was constructed from the collected data to illustrate this point, and appears in Figure 19.

A comparison of data on groundwaters sampled in 2000 with data retrieved by Clark and Douglas in the fall of 1995 (Intera Consultants Ltd.1997) show similar trends (Figure 20 (a)-(d)). The overall trends show a minor but almost unanimous decrease in the concentrations of all major ions, due to continual mixing of mine waters with surface waters enhanced by mining activities. Steep downward gradients are created by drifting, allowing the penetration of meteoric water to deeper levels where they mix and dilute the brines (Clark et al., 2000).

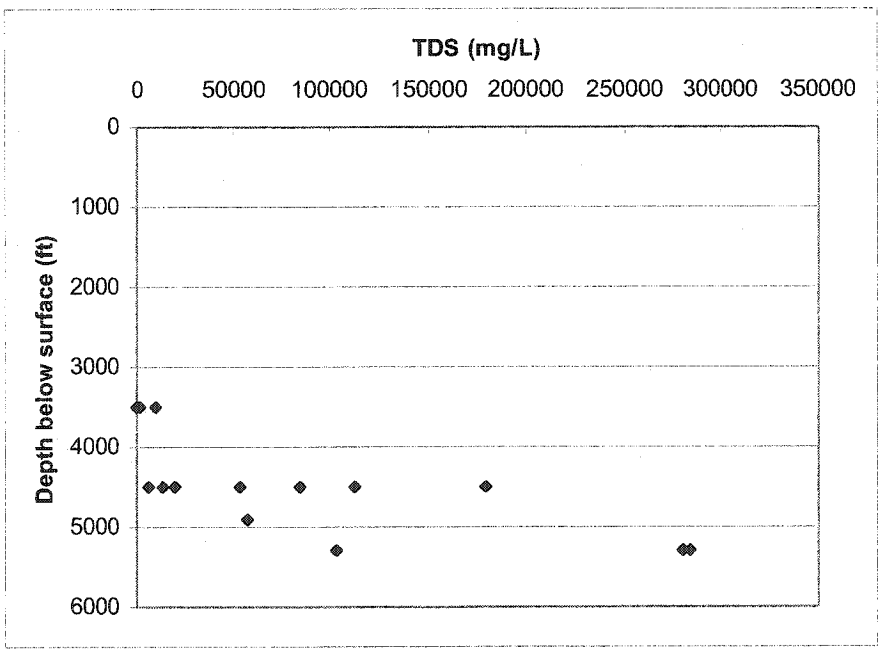

Figure 18. Representative plot of changes in total dissolved solids over the different mine levels.

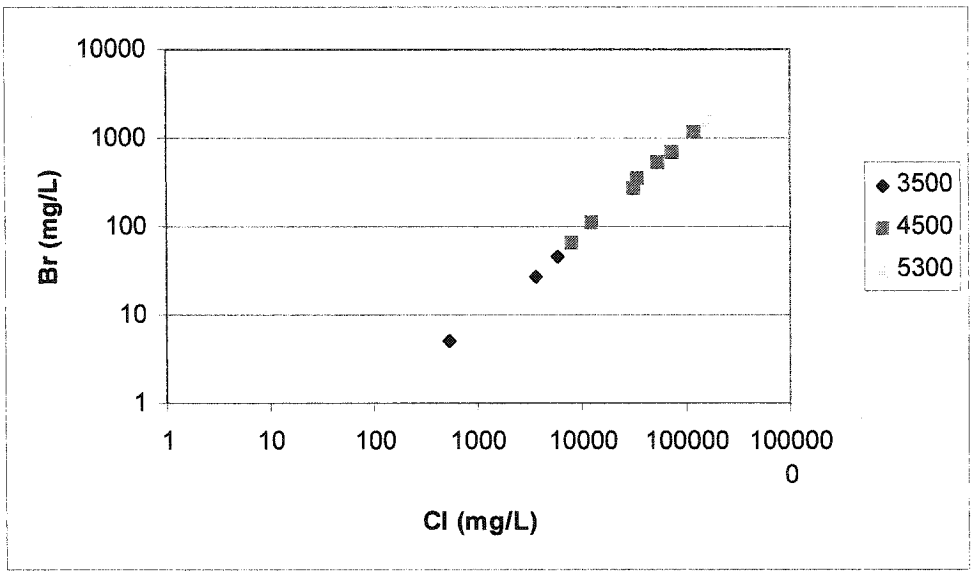

Figure 19. Br – Cl correlation in groundwater that suggests a single (marine?) source.

4.3 Stable Isotopes

Water samples were collected and analysed for stable isotopes on various levels of the mine as well as for a single sample from the Yellowknife Bay region of Great Slave Lake. It can be seen that $\delta^{18}O$ values range between –21‰ to –14‰, whereas δD values range between –162‰ and –73‰ (Table 8, Figure 21). Here, the local meteoric water line shown was that established by F.A. Michel of Carleton University, who used monthly precipitation data collected from 1989 – 1993.

The lone surface water collected in this study is seen to plot slightly below the LMWL, which agrees with other findings (Figure 22) (Frape et al, 1984; Clark et al, 2000), and represents evaporative enrichment. The isotopes from shallow level groundwaters plot along the local meteoric water line. At greater depths, a characteristic deuterium enrichment is observed, common to all Shield brines (Frape et al., 1984), with the data plotting above the LMWL.

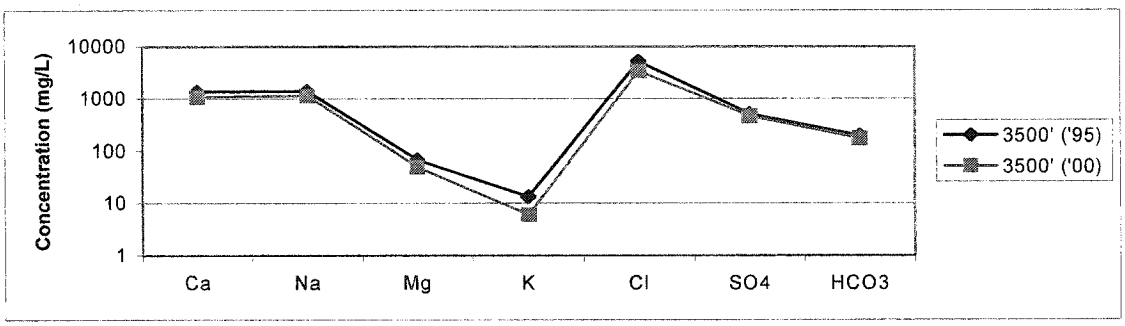

(a)

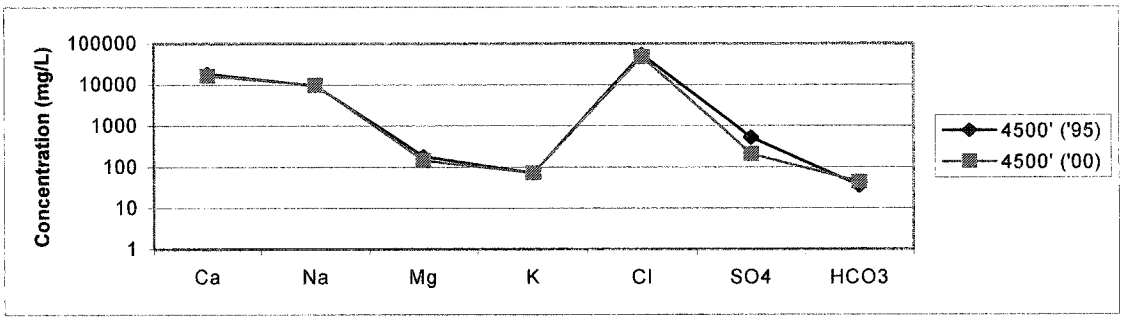

(b)

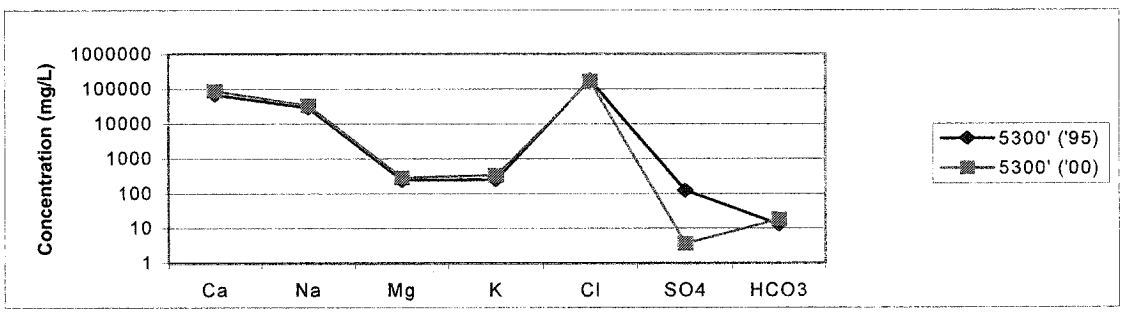

(c)

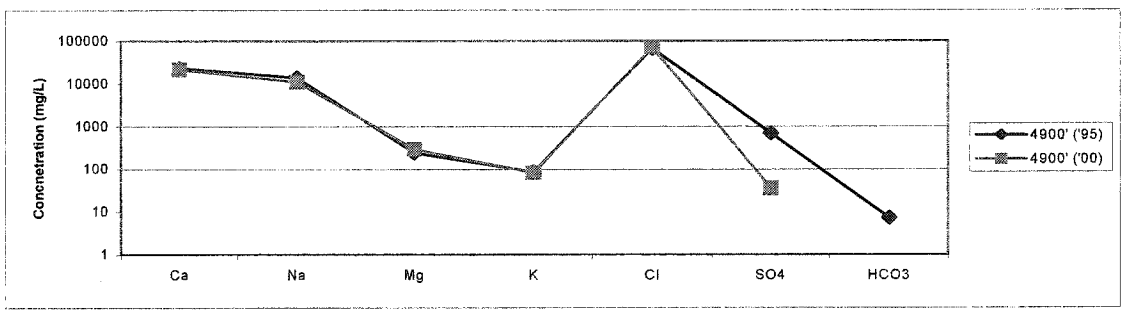

(d)

Figure 20 (a – d). Comparison of the ionic composition of groundwaters sampled during the year 1995 and 2000 for various levels in the mine.

Table 8. Stable isotopic composition of Great Slave Lake and mine waters.

Sample	Depth	δ18O	δ2H
Great Slave Lake		–16	–133
B8906	3500'	–19	–154
B9362	3500'	–21	–162
B9452	3500'	–20	–157
B3316	4500'	–17	–100
B3362	4500'	–19	–129
B3450	4500'	–19	–136
B3618	4500'	–20	–148
B3457	4500'	–20	–158
B5316	4500'	–20	–161
B5318	4500'	–19	–150
B5310	4900'	–20	–134
B5586	5300'	–16	–81
B6709	5300'	–15	–73
B7126	5300'	–15	–73

In the intermediate 4500' level, the isotopic systematics of the groundwater can be seen to fluctuate from the LMWL to the isotopically depleted brine end-member. The former has already been discussed and attributed to meteoric water influences. The latter could have been caused by recharge of precipitation from cooler climates that would have mixed with the already established in-situ waters. Clark et al., (2000) have shown that this may be a third groundwater end-member, consisting of glacial meltwater which would have infiltrated into the subsurface during the ablation of the Laurentide ice sheet around 10 000 years ago.

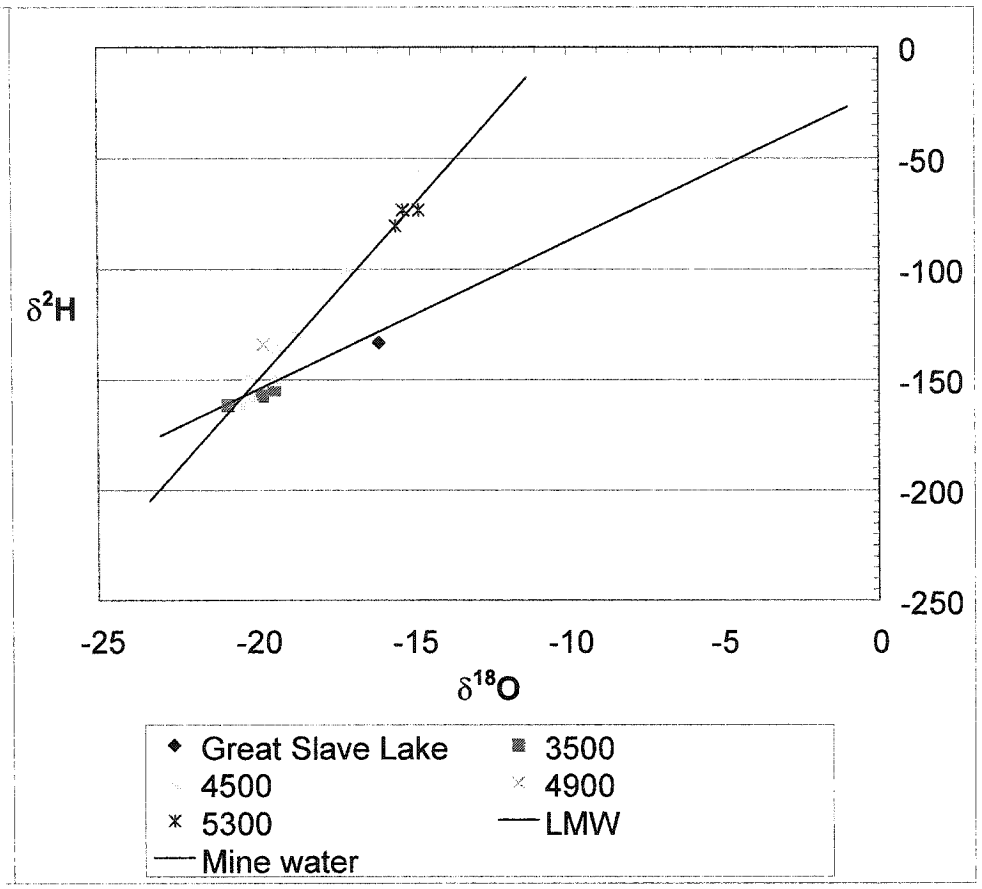

Figure 21. Relationships of $\delta^{18}O$ and $\delta^{2}H$ between modern lakes and groundwater at various depths.

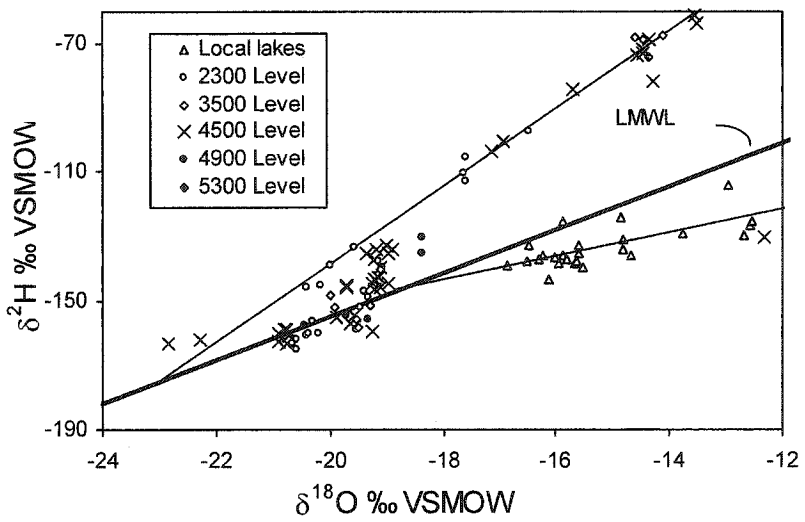

Figure 22. Isotope results from Clark et al. (2000).

4.4 Tritium

Tritium measurements can help to quantify the complex mixing dynamics that occur in the Con Mine. Tritium is a radiogenic isotope created naturally through the cosmic bombarding of solar particles with atmospheric elements. Coupled with natural decay, this results in a constant, natural, background signal. During the 1950's and 1960's, however, large amounts of ^{3}H were created through the testing of thermonuclear bombs, the concentration of which peaked in the year 1963 when the nuclear test ban treaty was implemented. Because of the large spike of tritium introduced into the hydrosphere , the presence of anthropogenic bomb-produced tritium in groundwater indicates that it has been recharged approximately 45 years prior.

Previous tritium sampling has been performed by Frape and Fritz (1981), MacDonald (1986) and Intera Consultants Ltd. (1997). Through this continual monitoring, it has been shown that the 1962-1963 weapons testing tritium bomb peak passed through the waters of the 4500' level in the mid-1980's (Intera Consultants Ltd., 1997). Initial recorded values in 1980 show tritium levels at 11.1 and 8.3 TU for sampling sites B-3457 and B-3362, respectively. In 1985, these numbers escalated to 86.4 and 70.3 TU but by 1995, they had decreased substantially again to 19.4 and 26.9 TU. The present study reveals a tritium value for sampling site B-3457 of 13 TU indicating that the anthropogenic tritium is continuing to decay and in the process, purging itself from the aquifer.

Sites sampled within the mine for tritium all came back positive (Table 9). The levels ranged from 24 TU in shallower levels to 0.9 TU in the deepest drifts of the 5300' level. The highest tritium values occur in waters proximal to the Negus Fault. Intera Consultants Ltd. (1997) has shown that this fault has higher permeability and contains a large proportion of tritium-bearing modern meteoric waters. In contrast, lower tritium values are found in waters associated with flow along the lower permeability Angel and Pud Faults, as they have a higher concentration of brine water. The presence of tritium at all sampling levels, except possibly B-7126 (within detection limits), indicates that

virtually no groundwater within the mine workings has remained isolated from modern meteoric water that has been introduced by relatively recent mining activities.

Table 9. Tritium results for Con Mine groundwaters.

Borehole	Level (ft)	Tritium (TU)
B-8906	3500'	24
B-9362	3500'	17
B-9452	3500'	26
B-3457	4500'	13
B-5316	4500'	16
B-5318	4500'	18
B-5310	4900'	3.2
B-6709	5300'	1.2
B-7126	5300'	0.9

5 NOBLE GAS FINDINGS AND INTERPRETATION

5.1 Calculation of Noble Gas Recharge Temperatures – Excess air correction

The excess air component, which is gained through the entrainment of air bubbles in the unsaturated zone during recharge, must be subtracted from the measured total concentration of each noble gas to produce estimates on the dissolved load at the time of recharge. Computer programs have been created and used by a number of authors (Youngman, 1989; Pinti and Van Drom, 1998; etc.) to correct such excess air overpressuring and then calculate the paleotemperature derived from dissolved noble gases in groundwater. All such programs first calculate the noble gas solubilities in atmospherically equilibrated water for a certain temperature range. For each of the four heavier noble gases, Ne, Ar, Kr, Xe, the program will then compare the sample concentrations with the solubility data to determine a set of potential recharge temperatures. Increments of air are then iteratively subtracted from the noble gas concentrations in proportions equivalent to that of neon's composition in air. With each subtraction, new temperatures are calculated and compared. This process proceeds until

a pre-selected limit for neon is reached, whereby the program selects the group of values with the closest agreement. The average of these temperatures is then taken to represent the ambient temperature of the surface water at the time of recharge (i.e. the temperature at which air/water equilibration took place).

Neon (91.05% ^{20}Ne) is used as the lead element in the iterative routine as it is relatively insensitive to changes in recharge water temperature. Also, its relatively high concentration in air makes neon highly sensitive to small additions of excess air (Youngman, 1989). Furthermore, unlike radiogenic ^{4}He and ^{40}Ar, ^{20}Ne is not produced in-situ, and so can only be gained from the atmosphere. Subsurface production of ^{21}Ne and ^{22}Ne, created through nuclear interactions amongst U-Th generated α-particles with oxygen and fluorine [$^{18}O(\alpha, n)^{21}Ne$ and $^{19}F(\alpha, n + \beta^{+})^{22}Ne$] are referred to as nucleogenic in origin (Hiyagon and Kennedy, 1992), and do not contribute significantly to Ne concentrations in waters (Kennedy et al., 1990; Bottomley et al., 1984).

The accuracy given by these calculation programs should be such that the resultant temperatures of the four noble gases used are within $\pm$ 1°C for samples recharged at 10°C (Youngman, 1989). Subsequent analyses on the same sample are expected to fall within these parameters as well.

These computer programs, however, cannot be used for the Con mine groundwaters because they are no longer single-sourced. Over time, these groundwaters have become a composite of 3 end-members consisting of brine, glacial and meteoric waters. The noble gas content must therefore be calculated for each component individually. Only in the case where fresh waters (3500' level samples) were sampled could the Pinti and Van Drom (1998) model be used. For all other samples located at greater depths, an arbitrary recharge temperature of 0°C was assumed since the dominant component is glacial meltwater. The secondary freshwater component is modern meteoric water, which is estimated to recharge with a temperature close to 5°C. This is believed to be acceptable based on two findings: (1) mean annual ground temperature (MAGT) climatic data for the Yellowknife region exists between 0° and 5°C (Yoon, 2002), and (2), a sample run

from the 3500' level (B-8906), containing no brine, resulted in a calculated recharge temperature of 5°C. Based on the inability of using pre-constructed computer programs, the excess air-correction described above was slightly modified. An iterative calculation subtracted air aliquots from the measured amount of Ne in the sample until the concentration equaled that for Ne solubility at 0°C (apportioned according to the fraction of both modern and glacial components) and in the fraction of brine (determined as discussed in the following section).

The following table (Table 10) and equations represent an actual sample calculation based on the Yellowknife B-7126, 5300' level sample:

Table 10. Example of sample calculations taken from worksheet.

Con Mine, Yellowknife B-7126, 5300' level		
time		**$^{20}Ne/^{22}Ne$**
1		0.0173
2		0.0158
3		0.0152
4		0.0150
5		0.0150
6		0.0150
7		0.0148
8		0.0150
9		0.0151
10		0.0148
11		0.0150
12		0.0148
13		0.0148
14		0.0149
15		0.0148
average ratio		**0.0149**
cc gas[1]		1.12E-05
cc water[2]		12.63
cc gas/cc water =		*8.90E-07*
Glacial+Modern+Excess		8.67E-07
Brine cc/cc		3.38E-08
Water @ 0°[3]		2.29E-07
Brine @ 0°[4]		3.38E-08
Overpressuring[5]	0.0443	1
Corrected volume		9.30E-08
Excess gas		7.97E-07

[1] **cc gas** is determined using Youngman's equation (as outlined above), with the average ratio measured from mass spectrometer analysis.

[2] **cc water** was calculated using the mass difference between the tube before and after release, density corrected to give volume.

[3] **water @ 0°** is taken from the Ne solubility vs. temperature graph, freshwater curve.

[4] **brine @ 0°** is taken from the Ne solubility vs. temperature graph, brine curve.

[5] **overpressuring**=(brine cc/cc)/(brine@0°C) corrected using the mathematical iterative goal seek function to give excess air (0.0443) in cc's.

Fraction composition dry air		Component	
He	5.20E-06	% brine	69.73%
Ne	1.80E-05	% glacial	22.71%
Ar	9.30E-03	% modern	7.56%
Kr	1.10E-06		
Xe	8.60E-08		

$$\text{Glacial+Modern+Excess} = (\text{water @ } 0°C)*(\%\text{Glacial} + \%\text{Modern}) + (\text{Excess}*[Ne_{air}])$$

$$\text{Brine cc/cc} = [(cc_{gas}/cc_{water}) - (\text{Glacial+Modern+Excess})] / \%\text{Brine}$$

$$\text{Overpressuring} = (\text{Brine cc/cc}) / (\text{Brine @ } 0°C)$$

$$\text{Corrected vol.} = (cc_{gas}/cc_{water}) - (\text{Excess}*[Ne_{air}])$$

$$\text{Excess Ne} = \text{Excess}*[Ne_{air}]$$

The volume of excess air calculated with excess Ne (in this case 0.0443cc's), gained during fresh water recharge (either modern recharge through soils or glacial recharge through the ice sheet and basal sediments) was used to correct measured concentrations of Ar, Kr and Xe. In most samples He could not be measured due to it's enhanced presence from radiogenic production in the subsurface, which placed it beyond safe mass spectrometer operating levels. Corrections were applied to the other noble gases using the volume of excess air retrieved from the Ne calculation, multiplied by the atmospheric abundance of Ar, Kr and Xe determined from the measured concentration of each gas in the sample:

$$\text{Excess (Ar, Kr, Xe)} = \text{Excess}*[Ar_{air}, Kr_{air}, Xe_{air}]$$

Mixing fractions were calculated according to the method used by Douglas et al. (2000). This consisted of a running a statistical principal component analysis (PCA), based on ten geochemical components. On the basis of this test, Cl^- and $\delta^{18}O$ values were determined to represent the dominant factors characterizing groundwater end-

members in the Con Mine. The Cl^- and $\delta^{18}O$ values measured in this study (above) were used to update these mixing fractions.

5.2 Noble gas equilibrium concentrations in brine

The concentrations of noble gases in brines can be calculated from the first order relationship between chloride salinity and the ratio of Bunsen coefficients for fresh water and brine.

$$M = \frac{S\ (ppm)}{35.5} \quad \text{(Youngman, 1989)}$$

Where M = molarity of the saline fluid

S = salinity (related to the chlorinity)

and the value of 35.5 represents the atomic weight of chlorine

The temperature-dependent salting coefficients have been determined by Smith and Kennedy (1983) and have been used to determine the solubility of the noble gases in brines with a chloride salinity of 4.75 M (from B-7126).

$$B = \frac{Bo}{e^{M*Ks}} * [X_{air}]$$

Where Bo = freshwater Bunsen coefficient for temperature of interest

M = molarity of the saline fluid

Ks = salting coefficient

$[X_{air}]$ = partial pressure of individual noble gas element in air

Calculations are made for fresh water, seawater and brine, and are graphically presented in Figure 23, below.

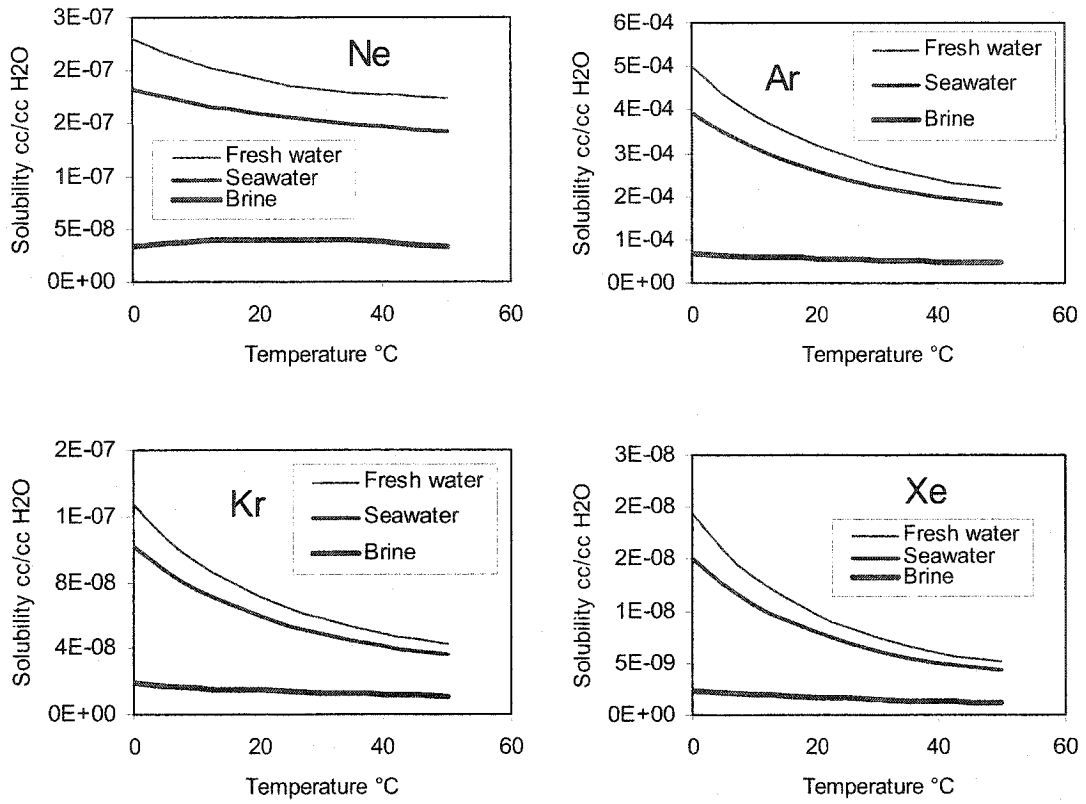

Figure 23. Noble gas solubility in brine solutions (calculated for chloride salinity of 4.61 M)

5.3 Noble gas results

The results of noble gas analysis of samples collected from the Con Mine, Yellowknife in 2000, as well as two unused samples salvaged from Intera Consultants Ltd. et al. (1997), are summarized in Table 11. It was discovered that clamping the tubes around their mid-section in order to reduce the volume of water travelling through the sample inlet manifold resulted in unequal distributions of gas content. In order to receive justifiable results, two separate runs per single sample became necessary, with the results being summed together. This was accomplished by simply reversing the sample after the initial run to engage the second half. Generally, the pattern observed was one high-pressured end followed by one low-pressured end. Highlighted rows in Table 11 represent combined samples.

The reported volumes of Ne, Ar, Kr and Xe were corrected for excess air by the iterative (goal seek) method described earlier. He concentrations were unable to be measured in most samples because forced reduction of the ^{4}He peak to safe operating levels for the mass spectrometer usually coincided with the lowering of the ^{3}He peak below detection limits. With the exception of the entirely freshwater sample (B-8906, 3500' level), Ar was found to be moderately to highly overpressured, signifying large subsurface contributions of radiogenic ^{40}Ar. As the calculation of gas volume in the sample by isotope dilution requires the isotope ratio in the sample as input, this presented a serious impediment for calculating Ar volumes in the samples. This was overcome by a second iterative calculation, for which the excess Ar was assumed to be entirely due to accumulation of ^{40}Ar. An initial atmospheric $^{40}Ar/^{36}Ar$ ratio was assumed to determine volume Ar in the sample according to the isotope dilution equation. The result was then compared with a calculated volume of Ar based on atmospheric equilibrium at 0°C for each of the brine, glacial and modern components. The excess measured Ar was assumed to be due to ^{40}Ar, and the $^{40}Ar/^{36}Ar$ ratio used then modified to recalculate Ar volume. This was repeated until the modified input ratio matched with the iteratively calculated Ar overpressuring. The so-calculated $^{40}Ar/^{36}Ar$ ratio is given in Table 11.

5.3.1 Temperature measurements

The sample collected from B-8906, discharging largely modern water with no brine component, provided a temperature estimate of 5°C. Temperature estimates for the freshwater component at other sites was not possible due to the high overpressuring of He and Ar that precluded the degree of gas separation and analytical precision necessary to discriminate between the reduced solubility-temperature variations existing for brines (Figure 23). Although this ruled out the possibility of gathering any further paleotemperature data, the high overpressuring observed for these gases provided another means of solving the mystery that would exclude a Pleistocene age for the Canadian Shield brines.

Table 11. Gas concentrations in Con Mine groundwaters

Borehole	Depth	Brine	glacial	modern	Excess Air	He	Ne total	Ar total	Kr total	Xe total	$^{40}Ar/^{36}Ar$
					cc/cc water						
B-9362.1.1	3500'	0.02	0.23	0.75	0.010		2.17E-07	5.34E-04	1.80E-07	5.71E-08	355
B-9362.1.2	3500'	0.02	0.23	0.75	0.052		2.17E-07	6.87E-04	1.77E-07	2.06E-08	380
B-9362.1	3500'	0.02	0.23	0.75	0.023		2.17E-07	5.89E-04	1.49E-07	3.21E-08	363
B-8906.1.1	3500'	0.00	0.05	0.95	0.014	1.72E-4	2.17E-07	4.48E-04	1.05E-07	(pre Xe)	302
B-5318.1.1	4500'	0.14	0.18	0.68			ND	2.28E-03	1.25E-06	ND	408
B-5310.1.1	4900'	0.28	0.37	0.35			1.18E-07	1.34E-03	1.09E-07	ND	
B-5310.3.1	4900'	0.28	0.37	0.35	0.007		3.58E-07	2.13E-03	1.78E-07	3.09E-08	1118
B-5310.2	4900'	0.28	0.37	0.35	0.116	2.91E-3	2.29E-07	1.34E-04	7.98E-08	3.73E-08	850
B-7126.2	5300'	0.70	0.23	0.08	0.045		3.38E-08	9.04E-03	9.11E-08	4.05E-08	3499
B-6709-1996 (1)	5300'	0.77	0.16	0.07				ratio only			3106
B-6709-1996 (2)	5300'	0.77	0.16	0.07				ratio only			2941
B-7126.3	5300'	0.70	0.23	0.08				ratio only			2065

Note: samples B-5318.1.1 and B-5310.1.1 were run with a chopped spike during earlier testing, which was found to preclude measurement of Ne and Xe.

5.3.2 Over-pressuring of noble gases in brine component

The interpretation and discussion that follows of noble gas concentrations in the brine component are focused on samples run from the 4900' level (B-5310) and the 5300' level (B-7126). These two samples carry the largest component of brine of all the levels sampled. The 5300' level is today comprised of 70% brine, 23% glacial meltwater and 8% modern water (calculated according to the ternary mixing model of Douglas et al., 2000). The 4900' level is comprised of 28% brine, 37% glacial meltwater and 35% modern water. Both of these samples were run in split pairs in order to handle the large quantities of water and gas released from the copper tubes. Following analysis of noble gas concentrations, the results for each of the two were combined.

Calculated volumes of gases for each of these two sites were normalized to cc_{gas}/cc_{brine} by factoring-in the amount of gas dissolved by each of the freshwater components (modern and glacial) at the appropriate temperature under equilibrium conditions. The resulting brine-volume determinations of each noble gas was then compared with the solubility value for brine equilibrated with air at 0°C to give the relative over-pressuring of that gas. Improvements made over time in gas separation and analysis procedures allowed for the measurement of He in the 4900' level sample, although the attempt failed during analysis of the 5300' level sample. These values appear in Table 12 and Table 13 for the two sites. Note that both samples show no over-pressuring in Ne. This is because Ne was used to calculate the excess air component during recharge of fresh (modern and glacial) water, as discussed above.

These calculations indicate that there is an extreme over-pressuring for both He and Ar in the brines. Both of these gases are candidates for daughter product enrichment through radiogenic reactions, and their over-pressuring above atmospheric equilibrium levels reflects accumulation from this during their residence time in the subsurface. This is discussed more fully in the following section.

The near-equilibrium pressures for Kr (4x in B-7126 and -2x in B-5310) indicates that within the uncertainties of the measurements, there is no observable subsurface production of Kr. This is consistent with the low production rates for Kr in the subsurface (Hiyagon and Kennedy, 1992), and in particular for the isotope measured (^{84}Kr).

Xenon concentrations in both samples show an over-pressuring that would suggest a subsurface contribution. However, as discussed further in the following section, the isotopic ratios for Xe in the deep sample are consistent with atmospheric proportions. This excess may be related to mineral degassing, or to noble gas fractionation during the entrainment of excess air.

Although not able to wholly address the sheer volume of Xe overpressuring observed, it was brought to attention that Xe tends to be strongly enriched relative to water

solubility (132Xe/36Ar is about 50x air). Based on this fact, and an assumption that the Xe/Ne ratio of the "excess air" component is fractionated relative to air by as much as twice the atmospheric ratio, consistent with partial dissolution of gas bubbles, a correction can be applied which helps to give a more accurate account of the Xe present (Hudson, 2002). This correction was applied, but determined to be negligible (overpressuring for sample B-7126 dropped from 17x to 14x) considering the analytical limits of detection on the quadrupole mass spectrometer.

Table 12. Calculated concentrations of noble gases in the brine component of 53-A (B-7126).

Sample 53-A (B-7126)	Ne	Ar	Kr	Xe
cc gas/cc H_2O	8.9E–07	6.8E–03	1.4E–07	3.7E–08
Glacial plus modern components	6.9E–08	1.5E–04	3.8E–08	5.9E–09
Excess Air (0.045 cc)	**8.0E-07**	**4.1E-04**	**4.9E-08**	**3.8E-09**
Volume corrected for excess air (cc/cc)	**7.6E-08**	**6.42E-03**	**9.2E-08**	**3.3E-08**
Brine (corrected) (cc/cc)	**3.4E–08**	**9.0E–03**	**9.1E–08**	**4.0E–08**
Overpressuring (brine/brine @ 0°C)	1	141	4	17

Table 13. Calculated concentrations of noble gases in the brine component of 49-A (B-5310).

Sample 49-A (B-5310)	He	Ne	Ar	Kr	Xe
cc gas/cc H_2O	2.9E-03	2.3E-06	2.5E-03	2.1E-07	4.7E-08
Glacial plus modern components	3.9E-08	1.7E-07	3.5E-04	8.7E-08	1.4E-08
Excess Air (0.119 cc)	**6.2E-07**	**2.1E-06**	**1.1E-03**	**1.3E-07**	**1.0E-08**
Corrected volume cc	**2.9E-03**	**1.7E-07**	**1.4E-03**	**7.6E-08**	**3.7E-08**
Brine cc/cc	**1.0E-02**	**3.4E-08**	**3.8E-03**	**-2.7E-08**	**8.1E-08**
Overpressuring (brine/brine @ 0°C)	851,000	1	57	-2	55

5.3.3 Noble gas isotope ratio measurements

In an attempt to assess whether subsurface contributions were being added to the different gases, one of the samples from the 5300' level, as well as both of the 1996 samples from the same depth (Intera Consultants Ltd. et al., 1997), were analyzed without the addition of the mixed spike. While this eliminated any artificial inclusions of

isotopes, it also removed the possibility of recording any volumetric measurements. Results are given in Table 14, Table 15, and Table 16.

Note that the percent composition of sample and air are modified to exclude isotopes that were below detection on the quadrupole analyzer (in particular, ^{128}Xe and ^{130}Xe, and ^{78}Kr present as a trace background from the spike). Also, for the B-6709-1996 samples, low concentrations coupled with inferior gas separation trials, lead to the inability of capturing any accurate measurements for Xe.

The light isotope enrichment occurring for Xe, Kr, and Ne (higher elemental percentages for low isotopes, lower percentages for higher isotopes) is an observed phenomenon characterized by mass dependent linear fractionation relative to either air or

Table 14. Relative abundance of noble gas isotopes for B-7126, compared with atmospheric values.

	^{129}Xe	^{131}Xe	^{132}Xe	^{134}Xe	^{136}Xe
Air	27.6	22.1	30.1	10.9	9.3
Sample	30.8	23.7	31.5	7.6	6.4

	^{80}Kr	^{82}Kr	^{83}Kr	^{84}Kr	^{86}Kr
Air	2.27	11.56	11.55	56.90	17.37
Sample	6.10	12.25	13.86	53.00	14.79

	^{36}Ar	^{40}Ar
Air	0.34	99.66
Sample	0.05	99.95

	^{20}Ne	^{22}Ne
Air	91.05	8.94
Sample	91.81	8.19

Table 15. Relative abundance of noble gas isotopes for B-6709-1996 (1), compared with atmospheric values.

	^{80}Kr	^{82}Kr	^{83}Kr	^{84}Kr	^{86}Kr
Air	2.27	11.56	11.55	56.90	17.37
Sample	9.59	10.55	10.11	56.63	12.77

	^{36}Ar	^{40}Ar
Air	0.34	99.66
Sample	0.03	99.97

	^{20}Ne	^{22}Ne
Air	91.05	8.94
Sample	91.57	8.43

Table 16. Relative abundance of noble gas isotopes for B-6709-1996 (2), compared with atmospheric values.

	^{80}Kr	^{82}Kr	^{83}Kr	^{84}Kr	^{86}Kr
Air	2.27	11.56	11.55	56.90	17.37
Sample	14.88	13.00	12.67	50.00	9.10

	^{36}Ar	^{40}Ar
Air	0.34	99.66
Sample	0.03	99.97

	^{20}Ne	^{22}Ne
Air	91.05	8.94
Sample	95.62	4.38

air-saturated water (Hiyagon and Kennedy, 1992). It is currently unknown whether the cause of this fractionation is experimental or indigenous.

5.3.4 He subsurface residence times

The excessive over-pressuring characteristic of He at depth provides an indication of subsurface residence time due to the radiogenic production of ^{4}He through alpha particle reactions during the natural $^{238, 235}U$ and ^{232}Th decay series. Similarly, Ar over-pressuring is a direct result of the accumulation of ^{40}Ar from ^{40}K decay and also provides a measure of subsurface residence time.

He concentrations, expressed as cm^3 He (STP) g^{-1} water, can exceed atmospheric saturation by several orders of magnitude in some crustal fluids. Andrews (1989) measured over 0.003 cm^3 g^{-1} in groundwaters from 800 to 1000 m below surface in the Stripa Mine, Sweden, Zaikowski and Kosanke (1987) found He concentrations up to 0.006 cm^3 g^{-1} in sedimentary basin brines in the Palo Dura basin, Texas, and Clark and Phillips (2000) show up to $1.8 \cdot 10^{-5}$ total He in hot springs from British Columbia.

Measurements of He concentrations in the Con Mine brines by isotope dilution was only possible if both peaks could be made to appear simultaneously inside the safe operational zones imposed by the mass spectrometer. Usually, one peak was too high and the other too low. However, in sample B-5310, in which the brine fraction was 28%, a measurement was successfully made. From Table 13, the measured He content of this water, corrected for the minor contribution from excess air, was 0.0029 $cm^3\ g^{-1}$. This radiogenic He is believed to have accumulated in the brine before the start of an ongoing process of dilution caused by the mixing of downward travelling glacial meltwater and modern meteoric water components. Correction for this dilution increases the concentration of He in the brine to 0.01 $cm^3\ g^{-1}$. In comparison to published values for He in brines, this value approaches the upper limit of He in crustal fluids (Bottomley et al., 1984).

An equation developed by Andrews (1983) shows a linear relationship between He accumulation and time, based on rock properties including porosity, density and the U and Th concentrations therein:

$$[He] = \rho\ \phi^{-1}\ t\ (1.19 \cdot 10^{-13}\ [U] + 2.88 \cdot 10^{-14}\ [Th])$$

Where ρ = is the rock density

ϕ = fractional porosity

[X] = concentrations in ppm

In modeling calculations describing meltwater infiltration at the Con mine, Clark et al. (2000) used a rock density of 3 g cm^{-3} and a porosity of 0.01. The average of 4 U measurements in the metavolcanics from the Con mine is calculated to be 0.725 ppm, and based on its relative abundance with respect to U, as well as literature values for mafic rocks, a concentration for Th of 2 ppm was used. Using the above information, a result of 230 Ma was obtained, indicating that these brines are Paleozoic in age. However, this calculation is fraught with uncertainty, as changing the magnitude of certain values can affect the outcome of this calculation considerably. For example, a reasonable range of

porosity values exists between 0.005 and 0.02. Using these alternatives for porosity gives lower and upper age estimates of 120 and 460 Ma.

Furthermore, in this calculation only in-situ production and accumulation of He is considered. It is possible that a portion of the He is being produced from U and Th decay in other rock types (i.e. the Yellowknife Supergroup), and traveling through the fault systems to this current location. It has been assumed that an equilibrium between the rock and surrounding fluid in terms of dissolution of radiogenic He has been achieved, based on a high dilatency of microfractures created through exposure of long term crustal strain patterns (Honda et al., 1982). Such is the mechanism whereby trapped He at grain boundaries is released into the surrounding fluid. Further, He loss by diffusion towards the atmosphere through fractures has not been accounted for. Andrews (1989) determined that for the Stripa mine waters, diffusion from 1000 m depth was a significant process which can limit He accumulation through development of a steady-state He profile. Both these factors would reduce the apparent age of the brines, making the age estimates calculated above minimum values.

5.3.5 Ar over-pressuring and residence time

Subsurface production of ^{40}Ar from decay of ^{40}K has increased both the Ar concentration ([Ar] up to 9.0E–3 $cm^3\ g^{-1}$) and $^{40}Ar/^{36}Ar$ ratio (>2000) to values well above atmospheric equilibrium values ($^{40}Ar/^{36}Ar$ = 295 and [Ar] = 6.7E–5 $cm^3\ g^{-1}$ at 0°C). Furthermore, the $^{40}Ar/^{36}Ar$ for the Con mine samples is shown to increase in a roughly linear fashion with increased fraction of brine in the sample Figure 24.

Diffusion of Ar from K-bearing minerals at temperatures below about 200°C is negligible (Andrews, 1989). In order to achieve ^{40}Ar levels in the host rock that exceed the atmospherically-equilibrated levels in water (that would then produce a diffusional gradient into the fracture fluid) requires rocks of Precambrian age and K concentrations on the order of a few weight percent. The accumulation of radiogenic argon in groundwaters from crystalline rocks, such as those present in the Canadian Shield, can be

attributed largely to the release of ^{40}Ar during alteration of K-bearing minerals. In the case of the Con mine brines, this has been attributed to the alteration of plagioclase feldspars with minor K content during the process of albitization. This process allows for the uptake of Na, coupled with the release of Ca, which also functions as the mechanism for the evolution of a marine-based evaporitic brine towards the Ca-Cl brine now existing in the Canadian Shield (Bottomley et al., 1994 and references therein).

However, the strong over-pressuring of Ar observed in the Con mine brines is unlikely to be caused entirely by this method. The potassium feldspar dissolution rate was an inadequate means to produce even the $^{36}Ar/^{40}Ar$ ratios prevalent in the GAB (Torgersen et al., 1989). Hiyagon and Kennedy (1992), suggest that a more likely source of radiogenic Ar is the Precambrian basement. Their studies of noble gas concentrations in methane-rich gas fields in southern Alberta (taken from Cretaceous and Devonian reservoirs), reveal radiogenic and nucleogenic isotopic compositions (for their Group B data) strikingly similar to those of the Con Mine. As evidence for their theory they point to the remarkably uniform geochemical compositions of all their samples, helium isotopic compositions equivalent to those of the Precambrian basement rocks, and nucleogenic neon ratios identical to those found in a host of other geographical locations across North America, indicating a vast, single source. The most compelling evidence, they believe, is simply the close proximity of all of their Group B reservoirs to the underlying basement and the similarity of noble gas concentrations in the brines produced from adjacent Precambrian rocks.

Since it is currently impossible to quantify the volume of degassing which occurs from the Precambrian basement into the overlying layers, any attempt at an age calculation would be futile. However, for groundwater to accumulate the amount of Ar necessary to reach the levels witnessed in the brines is in itself an indication of relative residence time, regardless of the source. Waters collected close to the surface are mostly glacial in composition and carry but a fraction of the radiogenic Ar that is present at depth. Being glacial in origin implies a minimum age of 10 000 years. This would imply that the ^{40}Ar-saturated brines underlying these must be much, much older.

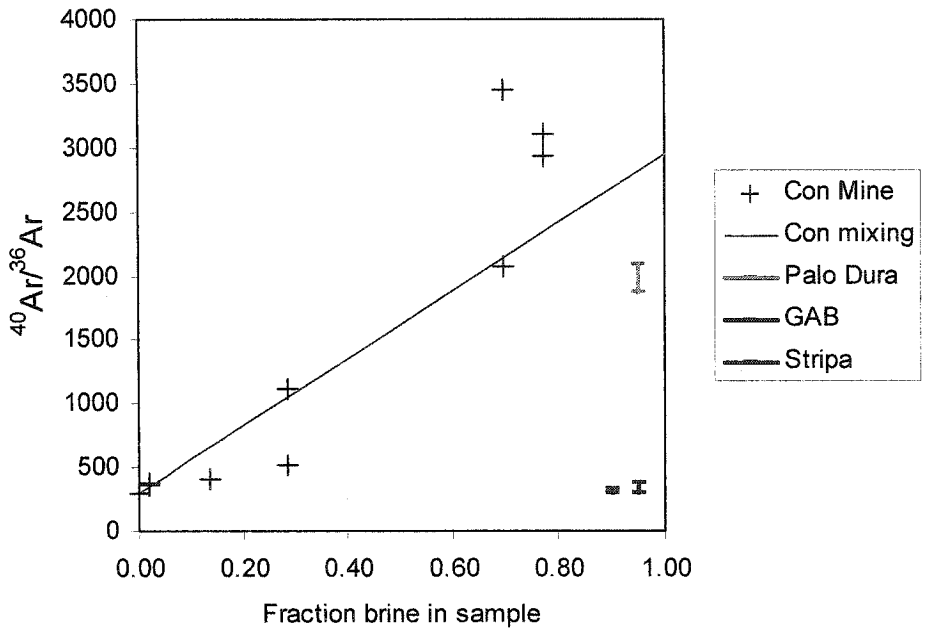

Figure 24. Variation in the $^{40}Ar/^{36}Ar$ with increased fraction of brine in Con Mine groundwaters. Line follows mixing between atmospherically equilibrated fresh waters and brine with $^{40}Ar/^{36}Ar$ = 3000 (from 53-A measured value normalized to 100% brine). Comparison data are ratio only (plotted at high fraction brine for convenience) from Zaikowski et al., 1987 (Palo Dura basin), Torgersen et al., 1989 (Great Artesian Basin) and Andrews et al., 1989 (Stripa mine).

The $^{4}He/^{40}Ar^{*}$ ratio for the brine in sample B-5310 is 2.7, calculated from the [He] value in Table 13 and the [Ar] value corrected for atmospherically-derived Ar. This compares with values obtained by Sherwood Lollar et al. (1993) of 3.7-8.5 at the same level. Additional values from other locations include 4.71 in granite sediments of the Palo Dura basin (Zaikowski et al., 1987), 4.0 from the Great Artesian Basin (Torgersen et al., 1989), and 6.68 for the highest [He] groundwaters in the Stripa granite (Andrews et al., 1989). The value obtained from this study is contained within the limits of analytical detection for the average of these three, as well as the accepted production ratio of the Earth's crust ($^{4}He/^{40}Ar^{*}$ = 7). The lower value obtained herein from the Con mine sample reflects the increased contributions of radiogenic Ar derived from the present-day mass flux from the Precambrian basement into the overlying material as well as some minor input from K-bearing mineral alterations. $^{4}He/^{40}Ar^{*}$ results tend to be depth-

dependent (Figure 25), which explains the differing results of the Palo Dura basin, GAB, and Stripa granite groundwaters.

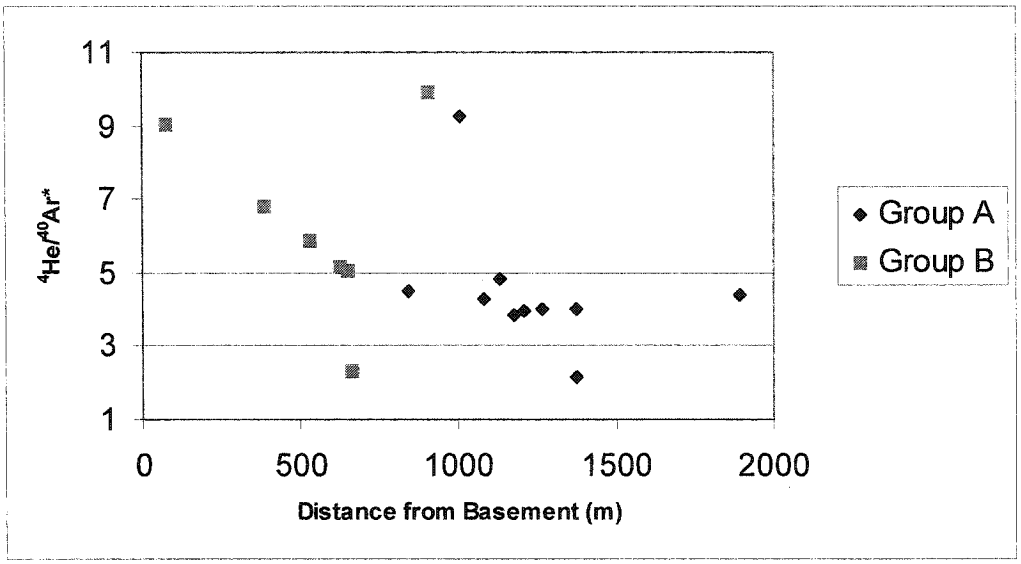

Figure 25. $^4He/^{40}Ar^*$ results vs. depth (from Hiyagon and Kennnedy, 1992). Note the almost linear decrease in ratio values with increasing distance from the basement before leveling off at approximately 800m.

6 SUMMARY

The design and construction of a noble gas extraction line with quadrupole mass spectrometer analyser was completed based on the premise of using isotope dilution as the measurement technique. Leak testing, calibration of mass peaks and ionization intensity preceded air-sample calibration runs. These tests ensured proper functionality of the line before beginning the actual sample analysis.

Only one paleotemperature calculation was possible due to the complex mixing dynamics of the Con Mine groundwater. The lone sample from the 3500' level showed concentrations of Ne, Ar, Kr and Xe corresponding to a recharge temperature of 5°C.

Deeper groundwaters in the mine indicate that additions of He, Ar and Xe are taking place. In particular, the results for B-7126 and B-5310 show a considerable noble gas over-pressuring above that which would be expected from atmospherically-equilibrated components only. Measured gas volumes have been corrected for the excess air component and are expressed as concentrations relative to those for an air-saturated brine. The 5300' level brine sample, which represents 70% of the discharging water, is over-pressured in Kr by a factor of 4, in Xe by a factor of 17 and in Ar by a factor of 141. The reduced brine component on the 4900' level (28% brine) enabled a measurement of He to be made. Over-pressuring of 851 000x above the atmospheric equilibrium was recorded, giving a concentration for He of 0.01 $cm^3\ g^{-1}$.

This large quotient of dissolved He places it at the upper limit of the range of published values for crustal fluids. The measured value normalized to 100% brine provides an estimated subsurface residence time for the brine of 230 million years ± 50% for a porosity range of 0.01 (0.005 to 0.02). This suggests recharge of these brines during the Paleozoic, consistent with the findings of Bottomley et al. (1994; 2002).

The lower He concentrations found in sample B-8906 at the 3500' level (1.72E–4 $cm^3\ g^{-1}$, with <1% brine) is nonetheless over-pressured by over 3000x, evidence of He diffusion into fresh groundwaters in the upper zone from the enriched regions of the lower crust as well as from the surrounding rock matrix.

The largest $^{40}Ar/^{36}Ar$ ratios observed in this study, normalized for the brine component (up to 3450), are some of the highest ratios ever measured in crustal fluids. The ratio of He to radiogenic Ar ($^{4}He/^{40}Ar^{*}$) was found to be 2.7, a low value in comparison to brines in other geological settings. This is a direct function of the over-pressuring attributed to the diffusion of radiogenic ^{40}Ar from the deeper basement.

Additional measurements of both gas concentration and isotopic ratios at other mines in the Canadian Shield are required to better define the unexpected enrichment observed for some noble gas elements. While excess He was anticipated, the high degree of Ar

over-pressuring was not adequately foreseen. In addition, the over-pressuring of Xe was unexpected and warrants further research. Improved analytical precision is a required asset for these advances and revelations to take place, which would allow for better age determination leading into a better understanding of their origin and importance in establishing a nuclear waste repository in the Canadian Shield.

REFERENCES

Aitken, J.D. (1991). Two Late Proterozoic glaciations, Mackenzie Mountains, northwestern Canada. Geology 19, 445-448.

Andrews, J.N. (1992). Mechanisms for noble gas dissolution by groundwaters. Isotopes of Noble Gases as Tracers in Environmental Studies. International Atomic Energy Agency, Vienna, 87-109.

Andrews, J.N. (1983). The isotopic composition of helium and its use to study groundwater movement. Proc. 4th Intl. Symp. Water-Rock Interaction, Misasa, Japan, 17-21.

Andrews, J.N., R.J. Drimmie, H.H. Loosli, M.J. Hendry, (1991). Dissolved gases in the Milk River aquifer, Alberta, Canada. Applied Geochemistry 6, 393-403.

Andrews, J.N, and Lee, D.J. (1979). Inert gases in groundwater from the Bunter Sandstone of England as indicators of age and paleoclimatic trends. J. Hydrology 41, 233-252.

Andrews, J.N., N. Hussain, and M.J. Youngman (1989). Atmospheric and radiogenic gases in groundwaters from the Stripa granite. Geochimica et Cosmochimica Acta 53, 1831-1841.

Bath, A.H., Edmunds, W.M., Andrews, J.N. (1979). Paleoclimatic trends deduced from the hydrochemistry of a Triassic Sandstone aquifer, United Kingdom. Isotope Hydrology 2, 545-568.

Bein, Amos, and Arnon Arad (1992). Formation of saline groundwaters in the Baltic region through freezing of seawater during glacial periods. Journal of Hydrology 140, 75-87.

Bottomley, D.J., Ross, J.D. and Clarke, W.B., 1984. Helium and neon isotope geochemistry of some ground waters from the Canadian Precambrian Shield. Geochimica Cosmochimica Acta, 48: 1973-1985.

Bottomley, D.J., Renaud, R., Kotzer, T. and Clark, I.D., 2002. Iodine-129 constraints on residence times of deep marine brines in the Canadian Shield. Geology, 30: 587-590.

Bottomley, D.J., D. Conrad Gregoire, and Kenneth G. Raven (1994). Saline groundwater and brines in the Canadian Shield: Geochemical and isotopic evidence for a residual evaporite brine component. Geochimica et Cosmochimica Acta, 58 (5), 1483-1489.

Bottomley, D.J., A. Katz, L.H. Chan, A. Starinsky, M. Douglas, I.D. Clark, and K.G. Raven (1999). The origin and evolution of Canadian Shield brines: evaporation or freezing of seawater? New lithium isotope and geochemical evidence from the Slave craton. Chemical Geology 155, 295-320.

Clark, I.D. and Phillips, R.J., 2000. Geochemical and $^{3}He/^{4}He$ evidence for mantle and crustal contributions to geothermal fluids in the western Canadian continental margin. Journal of Volcanology and Geothermal Research, 104: 261-276.

Clark, Ian D., Malcolm Douglas, Kenneth Raven, and Dennis Bottomley (2000). Recharge and Preservation of Laurentide Glacial Melt Water in the Canadian Shield. Ground Water 38 (5), 735-742.

Coon, J.H. (1949). 3He isotopic abundance. Phys. Rev. 75, 1355-1357.

Craig, B.G. (1965). Glacial Lake McConnell, and the surficial geology of parts of Slave River and Redstone River map-areas, District of Mackenzie. Geological Survey of Canada Bulletin122.

Craig, H., Lupton, J.E. (1976). Primordial neon, helium and hydrogen in oceanic basalts. Earth Planet Sci. Lett. 31, 369-385.

Douglas, M., I.D. Clark, K. Raven, and D. Bottomley (2000). Groundwater mixing dynamics at a Canadian Shield mine. Journal of Hydrology 235: 88-103.

Dyke, A.S. and L.A. Dredge (1989). Quaternary geology of the North-western Canadian Shield. Fulton, R.J. (Ed.), Quaternary Geology of Canada and Greenland. Geological Survey of Canada, Geology of Canada, No. 1: 189-214.

Fontes, J.C., D. Louvat, and J.L. Michelot (1989). Some constraints on geochemistry and environmental isotopes for the study of low fracture flows in crystalline rocks. In *Isotope Techniques in the Study of the Hydrology of Fractured and Fissured Rocks*, pp29-67. International Atomic Energy Agency, Vienna.

Frape, S.K., and Fritz, P. (1981). The occurrence and chemistry of groundwaters in the Canadian Shield. University of Waterloo, Waterloo Research Institute, Project No. 002-08-18 for Atomic Energy of Canada Ltd., 74 p.

Frape, S.K., P. Fritz, and R.H. McNutt (1984). Water-rock interaction and chemistry of groundwaters from the Canadian Shield. Geochimica et Cosmochimica Acta 48: 1617-1627.

Gascoyne, M., C.C. Davison, J.D. Ross, and R. Pearson (1987). Saline Groudwaters and Brines in Plutons in the Canadian Shield. Geological Association of Canada Special Paper 33: 53-68.

Guha, J. and R. Kanwar (1987). Vug brines-fluid inclusions: A key to the understanding of secondary gold enrichment processes and the evolution of deep brines in the Canadian Shield. In: Fritz, P., Frape, S.K. (Eds.), Saline Water and Gases in Crystalline Rocks. Geological Association of Canada Special Paper, 33, p. 95-103.

Haynes, F.M. (1988). Fluid inclusion evidence of basinal brines in Archean basement, Thunder Bay Pb-Zn-Ba district, Ontario, Canada. Canadian J. Earth Science 25, 1884-1894.

Heaton, T.H.E., and Vogel, J.C. (1979). Gas concentrations and ages of groundwaters in Beaufort Group sediments, South Africa. Water SA 5, 160-170.

Helmstaedt, H., and W.A. Padgham (1986). A new look at the stratigraohy of the Yellowknife Supergroup at Yellowknife, N.W.T. – implications for the age of gold-bearing shear zones and Archean basin evolution. Canadian Journal of Earth Sciences 23: 454-475.

Henderson, J.F., and Brown, O.C. (1966). Geology and structure of the Yellowknife Greenstone Belt, District of Mackenzie. Bulletin 141. Ottawa, Canada: Geological Survey of Canada.

Herut, Barak, Avraham Starinsky, Amitai Katz, and Amos Bein (1990). The role of seawater freezing in the formation of subsurface brines. Geochimica et Cosmochimica Acta 54, 13-21.

Hiyagon, H., and Kennedy, B.M. (1992). Noble gases in CH_4-rich gas fields, Alberta Canada. Geochimica et Cosmochimica Acta 56, 1569-1589.

Honda, M., Kurita, K., Hamano, Y., Ozima, M. (1982). Experimental studies of He and Ar degassing during rock fracturing. Earth and Planetary Science Letters 59, 429-436.

Hudson, G. Bryant (2002). Physicist in Chemistry and Material Science Directorate, Lawrence Livermore Laboratories, Berkeley, California. Personal communication.

Intera Consultants Ltd., I.D. Clark, and M.C. Douglas (1997). Hydrological and Hydrogeochemical Study of the Miramar Con Mine – Yellowknife, NWT. Prepared by Intera Consultants Ltd., and I.D. Clark and M.C. Douglas, Ottawa, 128 p.

Johnson, L.H., R. Burgess, G. Turner, H.J. Milledge, and J.W. Harris (2000). Noble gas and halogen geochemistry of mantle fluids: Comparison of African and Canadian diamonds. Geochimica et Cosmochimica Acta 64 (4), 717-732.

Kaminemi, D.C. (1987). Halogen-bearing minerals in plutonic rocks: a possible source of chlorine in saline groundwater in the Canadian Shield. In: Fritz, P., Frape, S.K. (Eds.), Saline Water and Gases in Crystalline Rocks. Geological Association of Canada Special Paper, 33, p. 69-79.

Kaminemi, D.C., M. Gascoyne, T.W. Melnyk, S.K. Frape, and R. Blomqvist (1992). Cl and Br in mafic and ultramafic rocks: significance for the origin of salinity in groundwater. In: Kharaka, Y.K., Maest, A.S. (Eds), Water-Rock Interaction. Proceedings of the 7th International Symposium on Water-Rock Interaction, Park City, UT, July13-18, 1992, Vol.1, 801-804. Balkema.

Kaminemi, D.C., Stone, D., and Peterman, Z.E. (1990). Early Proterozoic deformation in the western Superior province, Canadian Shield. GSA Bulletin 102, 1623-1634.

Kelly, W.C., Rye, R.O., Livnat, A. (1986). Saline minewaters of the Keweena Peninsula, Northern Michigan: Their natural origin and relation to similar deep waters in the Precambrian rocks of the Canadian Shield. American J. Science 286, 281-308.

Kennedy, B.M., Hiyagon, H. and Reynolds, J.H., 1990. Crustal neon: a striking uniformity. Earth and Planetary Science Letters, 98: 277-286.

Lahermo, P.W. and Lampen, P.H. (1987). Brackish and saline groundwaters in Finland. In: Saline waters and gases in crystalline rocks, Editors: Fritz, P. and Frape, S.K.; *Geological Association of Canada Special Paper 33,* 103-109.

Lane, A.C. (1914). Mine water composition, and index to the course of ore bearing currents. Economic Geology 9, 239-262.

MacDonald, I.M. (1986). Water-rock interactions in felsic rocks of the Canadian Shield. M.Sc. project, University of Waterloo, Canada.

MacDonald, D.W., Duke, N.A., Hauser, R.L. (1993). Geological setting of the NERCO Con Mine and the relationship of gold mineralisation to metamorphism, Yellowknife, NWT. Exploration Mining Geology 2, 139-154.

Michelot, J.L., Bentley, H.W., Brissaud, I., Elmore, D., and Fontes, J. (1984). Progress in environmental isotope studies (36Cl, 34S, 18O) at the Stripa site. Isotope Hydrology 1983, 207-229. IAEA.

Nordstrom, D.K., Ball, J.W., Donahoe, R.J., and Whittemore, D. (1989). Groundwater chemistry and water-rock interactions at Stripa. Geochimica et Cosmochimica Acta 53, 1727-1740.

Nurmi, P.A., Kokkonen, I.T., and Lahermo, P.W. (1988). Geochemistry and origin of saline groundwaters in the Fennoscandian Shield. Applied Geochemistry 3, 185-203.

O'Nions, R.K., and Oxburgh, E.R. (1983). Heat and helium in the earth. Nature 306, 429-431.

Osenbruck, Karsten, Johanna Lippmann, and Christian Sonntag (1998). Dating very old pore waters in impermeable rocks by noble gas isotopes. Geochimica et Cosmochimica Acta 62 (18), 3041-3045.

Pearson, F.J., Jr, 1987. Models of mineral controls on the composition of saline groundwaters in the Canadian Shield. In: Saline waters and gases in crystalline rocks, Editors: Fritz, P. and Frape, S.K.; *Geological Association of Canada Special Paper 33,* 39-51.

Pinti, Daniel L., Bernard Marty, and John N. Andrews (1997). Atmosphere-derived noble gas evidence for the preservation of ancient waters in sedimentary basins. Geology 25 (2), 111-114.

Pinti, Daniele L., and Eddy Van Drom (1998). PALEOTEMP: A Mathematica® program for evaluating paleotemperatures from the concentration of atmosphere-derived noble gases in ground water. Computers and Geosciences 24 (1), 33-41.

Poole, Jason C., Gavin McNeill, Stephen R. Langman, and Frank Dennis (1997). Analysis of noble gas in water using a quadrupole mass spectrometer in static mode. Applied Geochemistry 12, 707-714.

Raven, K.G., Bottomley, D.J., Sweezey, R.A., Smedley, J.A., and Ruttan T.J. (1987). Hydrogeological characterization of the East Bull Lake Research Area; Inland Waters Directorate Scientific Series No. 160, Environment Canada. National Hydrology Research Institute.

Sherwood, B., Fritz, P., Frape, S.K., Macko, S.A., Weise, S.M., Welhan, J.A. (1988). Methane occurrences in the Canadian Shield. Chemical Geology 71, 223-236.

Sherwood Lollar, B., Frape, S.K., Fritz, P., Macko, S.M., Welhan, J.A., Blomqvist, R., Lahermo, P.W. (1993a). Evidence for bacterially generated hydrocarbon gas in Canadian Shield and Fennoscandian Shield rocks. Geochimica et Cosmochimica Acta 57, 4567-4574.

Sherwood Lollar, B., Frape, S.K., Weise, S.M., Fritz, P., Macko, S.A., Welhan, J.A. (1993b). Abiogenic methanogenesis in crystalline rocks. Geochimica et Cosmochimica Acta 57, 5087-5097.

Smith, G.D., Newhall, F., Robinson, L.H., Swanson, D. (1964). Soil temperature regime – their characteristics and predictability. US Dept. Agricul., Soil Conservation Service, Rep. SCS-TP-144, 14 p.

Smith, S.P. and Kennedy,B.M., . 1983 The solubility of noble gases in water and in NaCl brine. Geochimica et Cosmochimica Acta 47: 503-515.

Spencer, R.J. (1987). Origin of Ca-Cl brines in Devonian formations, Western Canada Sedimentary Basin. Applied Geochemistry 2, 373-384.

Stone, D., Kaminemi, D.C., Brown, A., Everitt, R. (1989). A comparison of fracture styles in two granite bodies of the Superior Province. Canadian J. Earth Sci. 26, 387-403.

Stute, M., and P. Schlosser (1992). Principles and applications of the noble gas paleothermometer in: Geophysical Monograph 78: Climate change in continental isotopic records, 89-102.

Torgersen, T., Kennedy, B.M., Hiyagon, H., Chiou, K.Y., Reynolds, J.H., and Clarke, W.B. (1989). Argon accumulation and the crustal degassing flux of 40Ar in the Great Artesian Basin, Australia. Earth and Planetary Science Letters, 92, 43-56.

Vovk, I.F. (1987). Radiolytic salt enrichment and brines in the crystalline basement of the East European Platform. In: Saline waters and gases in crystalline rocks, Editors: Fritz, P. and Frape, S.K.; *Geological Association of Canada Special Paper 33,* 197-210.

Welhan, J. (1987). Characteristics of abiotic methane in rocks. In: Saline waters and gases in crystalline rocks, Editors: Fritz, P. and Frape, S.K.; *Geological Association of Canada Special Paper 33,* 225-233.

Yoon, Peter (2002). Cryosphere System in Canada. University of Waterloo website, URL: http://www.crysys.uwaterloo.ca/education/permafrost/permafrost_edu.cfm.

Youngman, Michael J. (1989). Dissolved Gases and Radioelements in Groundwaters. The British Library, West Yorkshire, 422p.

APPENDIX A: Statistical Helium Analysis

The following multivariable statistical analysis chronicles the path of the noble gases through the mathematical procedures necessary to derive paleotmeperatures. Helium values are then compared to the others in order to determine whether or not they are significantly different, and based on the results, whether or not it should be used in paleotemperature estimation.

A computer program for paleotemperature estimation of atmospheric-derived noble gases in groundwater had to be created for the purposes of this paper, but followed the same mathematical principles as previously described in section 5.1: *Calculation of Noble Gas Recharge Temperatures – Excess air correction.* The program, entitled BOULTYE, was created and used to determine the recharge temperature values for dissolved helium concentrations as well as for the other nobles found in groundwaters from the Molasse Basin in Upper Austria (Figure A-1), based on a dataset provided in

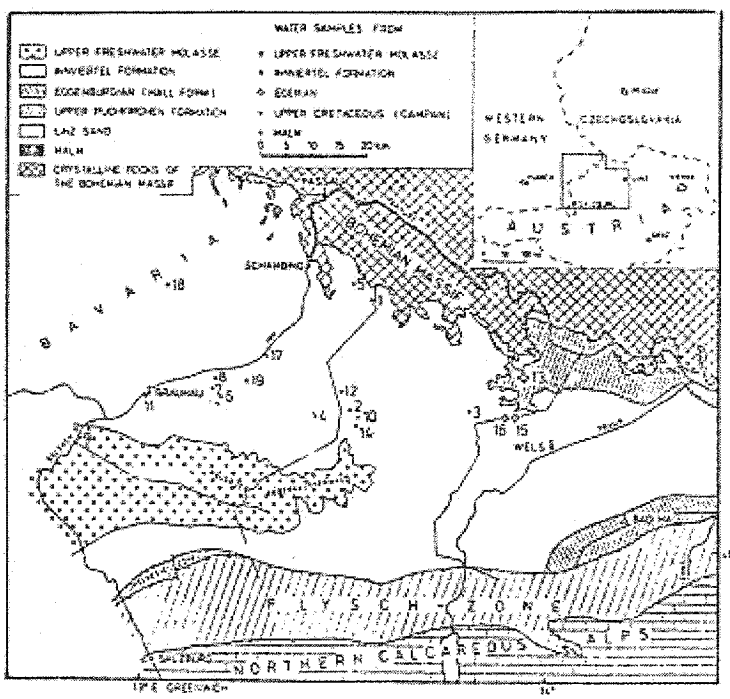

Figure A-1. Map of the Molasse Basin, Upper Austria (from Youngman, 1989).

Youngman (1989). Helium values are typically left blank in published works (Table A-1), reporting only the numbers for the latter four noble gas elements. By comparison, the values obtained for both programs are extremely similar, only deviating an average of +/- 0.2°C in most cases (Table A-2). The reason for the slight offset is most

Table A-1. Molasse Basin Shallow Groundwaters - calculated from program RECHARGE™

No.	Location	Depth	He R.T.	Ne R.T.	Ar R.T.	Kr R.T.	Xe R.T.	Average R.T.
1a	Sigharting 2	30		10.1	9.5	10	11.5	10.3
1b	Sigharting 2			10.5	9.7	11	10.4	10.4
2a	Ried 3	20		9.2	9.7	8.3	9.1	9.1
2b	Ried 3			9.5	11	8.4	9.5	9.6
3a	St. Georgen	30		7.6	7.3	7.2	7.9	7.5
3b	St. Georgen			7.9	7	8.6	7.9	7.8
4a	Mehrnbach 15	85		10.2	9.7	10.3	10.9	10.3
4b	Mehrnbach 15			11.2	13	10.9	10.1	11.3
5a	Rainbach 2	75		9.9	9.3	9.4	10.4	9.7
5b	Rainbach 2			9.7	8.7	9.6	9.7	9.4
6a	Altheim 6	142		6.1	6.2	5.4	5.8	5.9
6b	Altheim 6			7	7	7.8	6.6	7.1
7a	Weng 3	209		5.6	5.9	5.5	5.5	5.6
7b	Weng 3			5.6	5.3	5.4	6	5.6
8a	Mining 7	150		6.1	6.3	6.1	6.2	6.2
8b	Mining 7			5.6	5.5	5.5	5.6	5.5
9a	Aufhaussen	345		6.4	5.9	6.1	7.2	6.4
9b	Aufhaussen			6.7	5.9	6.6	7.5	6.7
10a	Ried 7	330		6.4	7.3	6.4	6	6.5
10b	Ried 7			5.9	3.9	5.6	6.5	5.5
11a	Braunau 1	138		4.2	3	3.8	5.6	4.2
11b	Braunau 1			4.8	4.1	4.6	5.9	4.9
12a	Aurolmunster	370		6.4	6.6	7.2	5.2	6.4
12b	Aurolmunster			8.6	9.9	7.3	9.1	8.7
13a	St. Marienkirchen	105		6.1	5.3	5.5	6.4	5.8
13b	St. Marienkirchen			5	3.7	5.3	5.3	4.8
14a	Ried 18/D 1	542		6.7	6.5	5.6	8	6.7
14b	Ried 18/D 1			5	5.7	4.3	5.3	5.1
15a	Schallerbach 1	460		6.1	5.3	5.7	6.7	5.9
15b	Schallerbach 1			6.1	8.3	5.6	5.7	6.4
16a	Schallerbach 2	670		3.4	3.2	-0.1	6.8	3.3
16b	Schallerbach 2			5.9	7.6	4.6	5.4	5.9

17a	Obernberg	1080						
17b	Obernberg							
18a	Birnbach 3	1618						
18b	Birnbach 3							
19	Geinberg	2180		1.9	-0.9	1	3.8	1.4

Table A-2. Molasse Basin Shallow Groundwaters - Calculated from program BOULTYE

No.	Location	Depth	He R.T.	Ne R.T.	Ar R.T.	Kr R.T.	Xe R.T.	Average R.T.
1a	Sigharting 2	30	-53.7	10.3	9.5	10	11.5	10.3
1b	Sigharting 2		-61.6	10.6	9.8	11	10.5	10.4
2a	Ried 3	20	-58.8	9.1	9.7	8.3	9.1	9.1
2b	Ried 3		-50.3	9.5	11	8.5	9.5	9.6
3a	St. Georgen	30	-37.6	7.7	7.4	7.3	7.9	7.6
3b	St. Georgen		-59.3	7.9	7.2	8.7	8	7.9
4a	Mehrnbach 15	85	-55.2	10.2	9.7	10.3	10.8	10.2
4b	Mehrnbach 15		-50.1	11.5	13.1	10.9	10.2	11.3
5a	Rainbach 2	75	-58.3	9.8	9.3	9.5	10.4	9.8
5b	Rainbach 2		-56.9	9.3	8.7	9.6	9.7	9.4
6a	Altheim 6	142	-67.5	6	6.4	5.5	6	6
6b	Altheim 6		-70.2	7.1	7.1	7.9	6.7	7.2
7a	Weng 3	209	-81.1	5.7	6.1	5.7	5.7	5.8
7b	Weng 3		-80.6	5.8	5.5	5.6	6.2	5.8
8a	Mining 7	150	-76.3	6.2	6.4	6.2	6.3	6.3
8b	Mining 7		-76.4	5.7	5.7	5.7	5.7	5.7
9a	Aufhaussen	345	-92	6.6	6.1	6.3	7.3	6.6
9b	Aufhaussen		-93.1	6.9	6.1	6.7	7.5	6.8
10a	Ried 7	330	-78.6	6.7	7.5	6.5	6.2	6.7
10b	Ried 7		-78.6	5.7	4.1	5.8	6.6	5.5
11a	Braunau 1	138	-96.8	4.6	3.3	4.1	5.8	4.4
11b	Braunau 1		-95.1	5.3	4.3	4.8	6.1	5.1
12a	Aurolmunster	370	-103	6.5	6.8	7.3	5.4	6.5
12b	Aurolmunster		-102.5	8.7	9.9	7.4	9.2	8.8
13a	St. Marienkirchen	105	-98.6	6	5.4	5.7	6.6	5.9
13b	St. Marienkirchen		-95.4	5.2	3.9	5.5	5.5	5
14a	Ried 18/D 1	542	-84.7	6.8	6.6	5.8	8.1	6.8
14b	Ried 18/D 1		-89.3	5.3	5.9	4.6	5.5	5.3
15a	Schallerbach 1	460	-107.8	6.4	5.5	5.8	6.8	6.1
15b	Schallerbach 1		-106.2	6.5	8.4	5.7	6	6.7
16a	Schallerbach 2	670	-115.7	3.5	3.4	0	6.9	3.4
16b	Schallerbach 2		-114	5.8	7.7	4.8	5.6	6
17a	Obernberg	1080						

17b	Obernberg							
18a	Birnbach 3	1618						
18b	Birnbach 3							
19	Geinberg	2180	-121.9	1.8	-1	1.2	4.2	1.6

likely due to the fact that the corrections described in the introduction could not be carried out on Youngman's dataset because of a lack of the necessary details provided in his paper. Nevertheless, as it turns out in this circumstance, the corrections account for only a minor difference in the recharge temperature estimate. Even the additional input of radiogenic argon had very little effect on its overall individual concentrations.

The radiogenic input of helium, however, turns out to be quite significant. Judging by the relative coherence of the latter four noble gas elements, helium is in all cases, much lower than its counterparts, registering highly negative values in all cases. This is a direct cause of the increased subsurface production of helium, manufactured through the decay of uranium and thorium. This input of radiogenic helium completely destroys the surface recharge-temperature signal, used for scientific study, by adding to the dissolved atmospheric input. This process is inversely proportional; by increasing the dissolved concentration in groundwater, the temperature value subsequently derived through calculation is decreased. The blatant differences in temperature values between helium and the others underscore the reasons why helium has, and always will be, discarded in recharge temperature calculations.

This contrast is further illustrated by examining the Pearson correlation matrix and subsequent diagram (Figure A-2), through which it is readily apparent that for a given noble gas element, the lowest correlation always exists with helium, although the correlation can be low between other nobles as well. The highest correlation exists with neon. This has its roots in the original calculations, whereby, the small excess air corrections that were made to each of the noble gases were subtractions based on relative percentages of neon.

	HELIUM	NEON	ARGON	KRYPTON	XENON
HELIUM	1.000				
NEON	0.758	1.000			
ARGON	0.652	0.931	1.000		
KRYPTON	0.777	0.952	0.845	1.000	
XENON	0.686	0.913	0.775	0.802	1.000

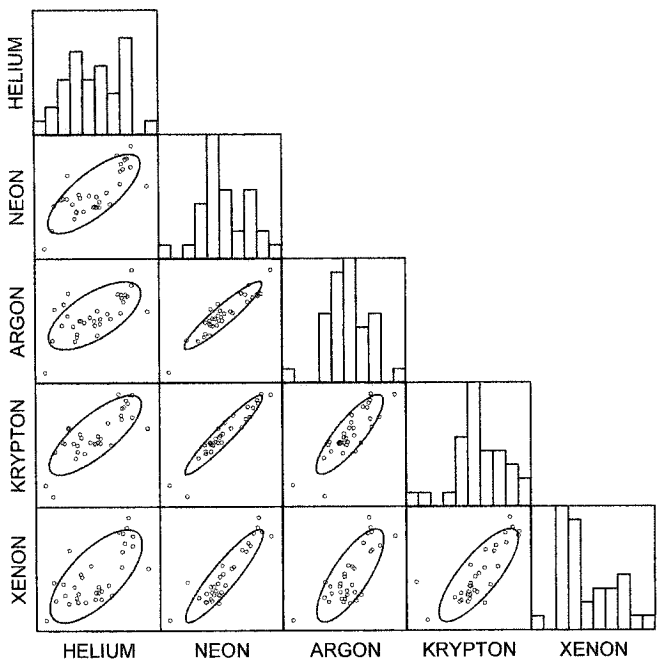

Figure A-2. Pearson correlation matrix and plot.

A statistical analysis observing the effect of depth and noble gas type on the recharge temperature can test the accuracy of helium estimates as samples are taken closer to the source of its radiogenic input. To this end, a Principal Component Analysis was run on the noble gases, excluding helium, to be used in comparison with the helium recharge temperature estimates; the results appear below.

```
Latent Roots (Eigenvalues)

          1          2          3          4

     19.469      1.147      0.878      0.009
```

Component loadings

	1	2
NEON	2.146	0.127
ARGON	2.549	-0.809
KRYPTON	2.337	0.317
XENON	1.705	0.613

Variance Explained by Components

1	2
19.469	1.147

Percent of Total Variance Explained

1	2
90.543	5.334

Following the Kaiser Rule, these results indicate only two principal components are present (based on eigen values greater than 1). However, because the reliability of the second is poor (it lacks at least four loadings with absolute values greater than 0.6, or at least three loadings with absolute values greater than 0.8), and it only contains approximately 5% of the total variance, it should be dismissed. Factor 1, on the other hand, accounted for an overwhelming 90.5% of the total variance.

Before moving directly into the General Linear Model (GLM), the data was analyzed for linearity between the X and Y variables, a main assumption for the full model. As shown in Figure A-3 (a & b), the relationship between helium estimates and OTHERS versus LOGABSDEPTH, can be considered to be fairly linear based on these high-tension lowess curves.

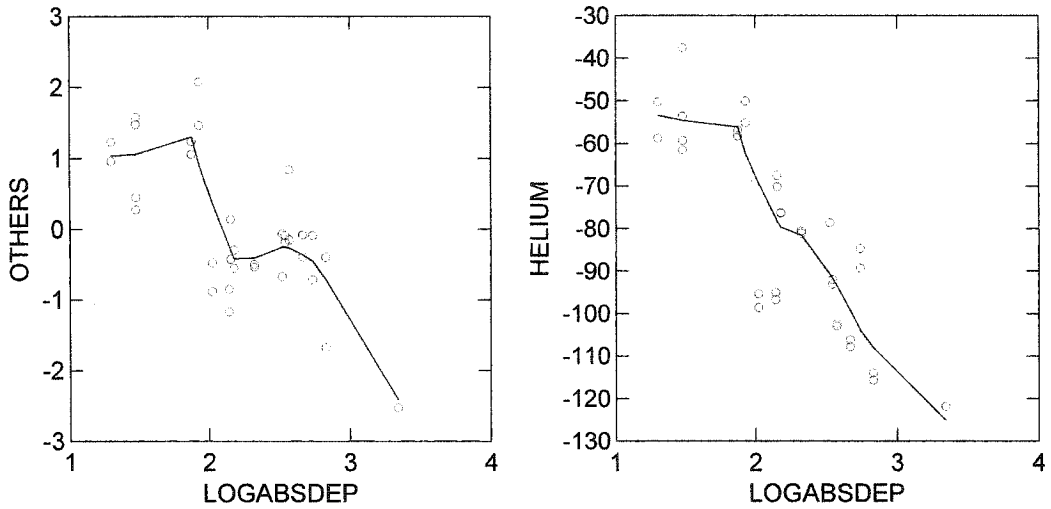

(a) (b)

Figure A-3 (a & b). Test of linearity on the data.

A general linear model was created using helium recharge temperature estimates as well as the Factor 1 scores for the other nobles, as the combined dependent variables. This created a 2-level categorical variable consisting of Helium and Others. LOGABSDEPTH (the log of the absolute depth) was the independent variable. To determine whether or not helium estimates become increasingly unreliable with depth, it needed to be determined if the slopes of the two regression lines were significantly different ($H_0$2: B1 = B2). Running the full model we get:

Dep Var: VALUE N: 66 Multiple R: 0.981 Squared multiple R: 0.962

Analysis of Variance

Source	Sum-of-Squares	df	Mean-Square	F-ratio	P
LOGABSDEP	5870.871	1	5870.871	77.95	0
NOBLETYPE$	3.759	1	3.759	0.05	0.824
NOBLETYPE$*LOGABSDEP	5053.342	1	5053.342	67.096	0
Error	4669.568		62		75.316

Durbin-Watson D Statistic 1.109
First Order Autocorrelation 0.446

We can therefore reject the null hypothesis based on these findings and say that the slope of regression of recharge temperature estimates on depth is different for the different

noble types since p(NOBLETYPE$*LOGABSDEPTH) = 0.000 < 0.05. Helium estimates of recharge temperature can therefore be expected to become increasingly inaccurate with depth, as they approach higher levels of radioactive decay at deeper levels. This decay represents the source of new helium that enters into the water column, increasing the dissolved concentrations, which further enhances the negative recharge temperature estimate.

The next step was to model individual regressions by computer, in an effort to determine whether or not recharge temperature could be predicted given an arbitrary depth. Different data transformations were tested for this procedure to achieve optimum results.

Dep Var: HELIUM N: 33 Multiple R: 0.837 Squared multiple R: 0.701

Adjusted squared multiple R: 0.691 Standard error of estimate: 12.251

Effect	Coefficient	Std Error	Std Coef	Tolerance	t	P(2 Tail)
CONSTANT	0.864	9.816	0		0.088	0.93
LOGABSDEP	-37.043	4.345	-0.837	1	-8.525	0

Analysis of Variance

Source	Sum-of-Squares	df	Mean-Square	F-ratio	P
Regression	10908.895	1	10908.895	72.681	0
Residual	4652.885	31	150.093		

Durbin-Watson D Statistic 1.107
First Order Autocorrelation 0.446

Dep Var: SQRABSHE N: 33 Multiple R: 0.837 Squared multiple R: 0.700

Adjusted squared multiple R: 0.690 Standard error of estimate: 0.699

Effect	Coefficient	Std Error	Std Coef	Tolerance	t	P(2 Tail)
CONSTANT	4.256	0.56	0		7.601	0
LOGABSDEP	2.108	0.248	0.837	1	8.505	0

Analysis of Variance

Source	Sum-of-Squares	df	Mean-Square	F-ratio	P
Regression	35.328	1	35.328	72.336	0
Residual	15.14	31	0.488		

Durbin-Watson D Statistic 1.190
First Order Autocorrelation 0.478

Dep Var: LOGABSHE N: 33 Multiple R: 0.831 Squared multiple R: 0.691

Adjusted squared multiple R: 0.681 Standard error of estimate: 0.072

Effect	Coefficient	Std Error	Std Coef	Tolerance	t	P(2 Tail)
CONSTANT	1.424	0.057	0		24.827	0
LOGABSDEP	0.211	0.025	0.831	1	8.322	0

Analysis of Variance

Source	Sum-of-Squares	df	Mean-Square	F-ratio	P
Regression	0.355	1	0.355	69.264	0
Residual	0.159	31	0.005		

Durbin-Watson D Statistic 1.284
First Order Autocorrelation 0.352

Dep Var: OTHERS N: 33 Multiple R: 0.692 Squared multiple R: 0.479

Adjusted squared multiple R: 0.462 Standard error of estimate: 0.734

Effect	Coefficient	Std Error	Std Coef	Tolerance	t	P(2 Tail)
CONSTANT	3.061	0.588	0		5.207	0
LOGABSDEP	-1.388	0.26	-0.692	1	-5.335	0

Analysis of Variance

Source	Sum-of-Squares	df	Mean-Square	F-ratio	P
Regression	15.317	1	15.317	28.461	0
Residual	16.683	31	0.538		

Durbin-Watson D Statistic 1.542
First Order Autocorrelation 0.195

Dep Var: SQRABSOTHERS N: 33 Multiple R: 0.223 Squared multiple R: 0.050

Adjusted squared multiple R: 0.019 Standard error of estimate: 0.352

Effect	Coefficient	Std Error	Std Coef	Tolerance	t	P(2 Tail)
CONSTANT	1.158	0.282	0		4.11	0
LOGABSDEP	-0.159	0.125	-0.223	1	-1.275	0.212

Analysis of Variance

Source	Sum-of-Squares	df	Mean-Square	F-ratio	P
Regression	0.201	1	0.201	1.626	0.212
Residual	3.832	31	0.124		

*** WARNING ***
Case 43 is an outlier (Studentized Residual = 3.586)
Durbin-Watson D Statistic 1.523
First Order Autocorrelation 0.106

Dep Var: LOGABSOTHERS N: 33 Multiple R: 0.294 Squared multiple R: 0.086

Adjusted squared multiple R: 0.057 Standard error of estimate: 0.421

Effect	Coefficient	Std Error	Std Coef	Tolerance	t	P(2 Tail)
CONSTANT	0.282	0.337	0		0.836	0.409
LOGABSDEP	-0.255	0.149	-0.294	1	-1.71	0.097

Analysis of Variance

Source	Sum-of-Squares	df	Mean-Square	F-ratio	P
Regression	0.518	1	0.518	2.923	0.097
Residual	5.496	31	0.177		

Durbin-Watson D Statistic 1.697
First Order Autocorrelation 0.059

All three helium runs placed very closely in terms of measure of fit (R^2). However, there was significant improvement in independence assumptions for the log transformed helium data for a negligible decrease in R^2 (0.701 → 0.691). For the modeling of regression slope for helium, this provides the best result with the following equation (Figure A-4):

$$LOGABSHE = 1.424 + 0.211*LOGABSDEPTH$$

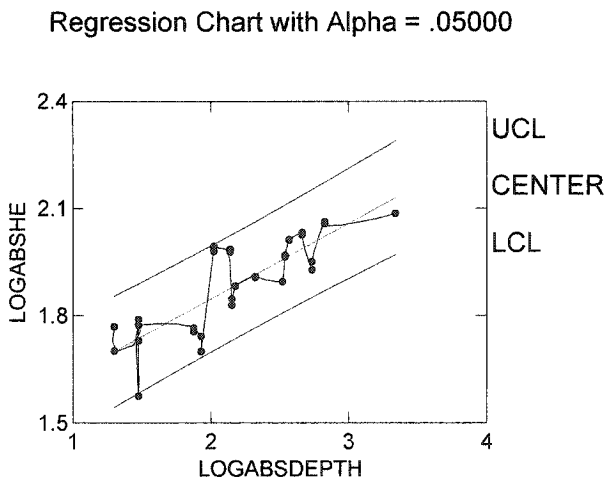

Figure A-4. Graph of LOGABSHE vs. LOGABSDEPTH with regression line and 95% confidence intervals.

The same transformations were conducted on the OTHERS dataset. As expected, the measure of fit is poor in the best case (OTHERS), and unusable in both transformations ($R^2 < 0.10$). For lack of a better alternative, the untransformed data must be utilized in this case, and yields a regression equation of (Figure A-5):

FACTOR 1 = 3.061 – 1.388*LOGABSDEPTH

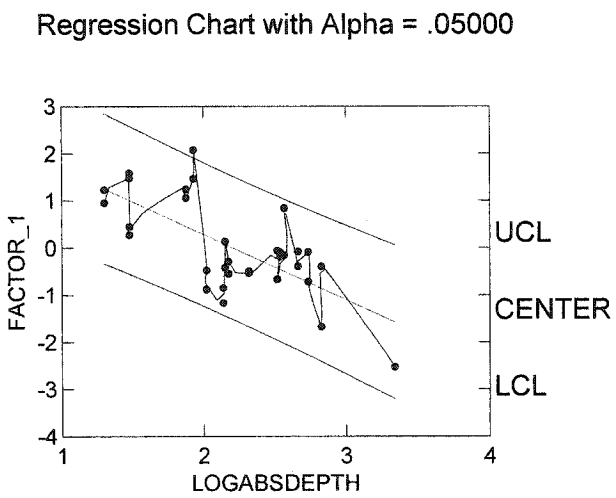

Figure A-5. Graph of FACTOR 1 vs. LOGABSDEPTH with regression line and 95% confidence intervals.

Simple linear regression makes four assumptions. First, that depth is measured without error. Although it cannot be assumed that this is the case, the fact that the error in the depth variables can be considered small, relative to the range of depths taken, then the associated error is negligible and therefore, unlikely to influence the outcome measurably. Second, that the relationship between Y and X is linear. This has already been determined not to be the case, which gives rise to the possibility that any predictions made from the regression equations could give false results. Third, for any value of X, the Y's are independently and normally distributed. This can be tested by means of a normal probability plot of residuals as well as plotting studentized residuals versus predicted values. Plots for the prime datasets (log transformed helium and factor 1 scores for OTHERS) appear below (Figure A-6 (a – d)).

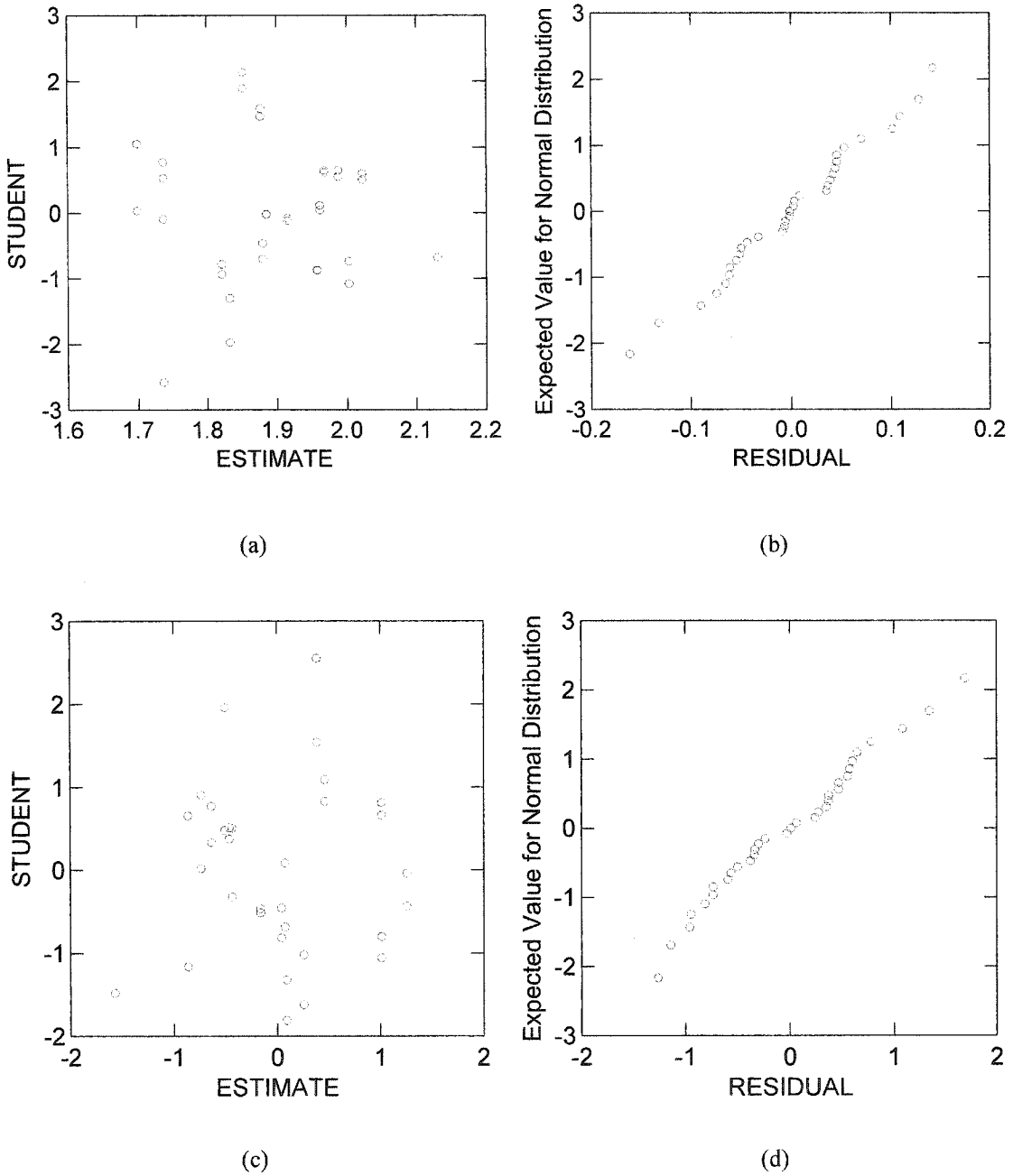

Figure A-6 (a – d). Top two graphs represent proof of assumptions for LOGABSHE values and bottom two graphs are proof of assumptions for Others values.

Both normal probability plots of residuals reveal approximately linear lines with no distinct outliers. In addition, the studentized residuals vs. estimates reveal no apparent pattern, giving no evidence of increasing or decreasing variability with the estimate, indicating that the third assumption has been met. The fourth and final assumption is that

the variance in Y for fixed X is independent of X. Recalling the Durbin-Watson Statistics from the simple linear regression, we had values of 1.284 and 1.542 for the log transformation of helium and Factor 1 scores (OTHERS). This suggests that there is a slight positive correlation at lag 1. This makes sense as adjacent data points in the dataset represent duplicates from the same site, and was expected. Autocorrelation plots were generated to test this assumption for lags greater than 1, and appear below (Figure A-7 (a-b)).

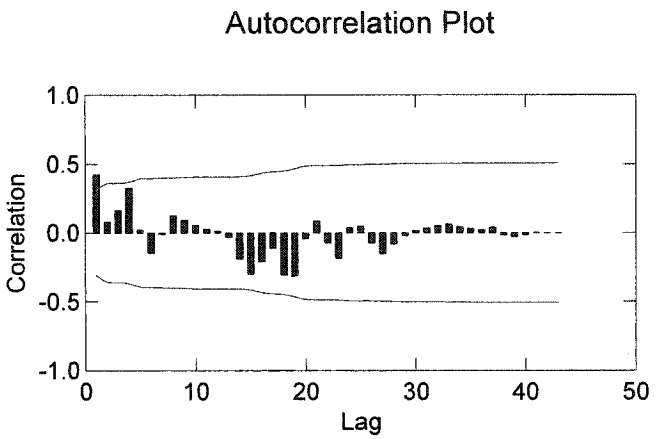

(a)

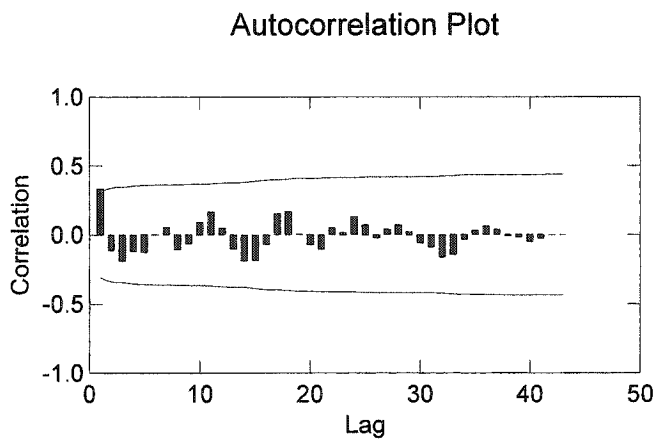

(b)

Figure A-7 (a-b). Upper ACF plot for LOGABSHE, lower ACF plot for OTHERS.

As shown, only at lag 1 for both series does the correlation exceed the 95% confidence interval, indicating that aside from the duplicates, the assumption of independence is met.

The probabilities associated with the two null hypotheses (H_{01}: constant = 0; H_{02}: coefficient for LOGABSDEPTH = 0) for both regression lines are 0.000. This means that we can reject these null hypotheses and conclude that there is indeed a relationship between the estimates of recharge temperature for all nobles, with depth. However, due to the autocorrelation of residuals, the degrees of freedom are inflated for the hypothesis testing which results in answers that are unfortunately, too good to be true.

APPENDIX B: Layout of Noble Gas Line and Extraction Principles

This appendix consists of a glossary succinctly describing all the major components associated with the noble gas extraction line and quadrupole mass spectrometer.

Tracer spike apparatus

The tracer spike apparatus is a series of compartmentalized tube sections with valve bulkheads designed to prevent the accidental release and loss of the expensive tracer noble gases. As the gas travels from one compartment into another, the valves directly behind the new section are immediately closed. This ensures that no gas can enter or leave, and guards against mishaps. It also serves as a partitioning divider to measure out and mix precise volumes of each individual noble gas isotope. The following sections describe key features in the apparatus:

Isotope spike containers

The isotope spike containers are all constructed of stainless steel in the form of elongated cylinders and include the following noble gases: helium, neon, argon, krypton, and xenon. The volumes of the cylinders change with the isotopes as do the volume of gases therein.

Isotope aliquots

The aliquots are custom-built stainless steel precision measuring devices, each of which is attached in series to a specific noble gas isotope container. Each aliquot has a stainless steel rod, of which the volume is accurately known, inserted into the main chamber that cuts the original enlarged volume down to a desired level. Through the aliquots, only a precise amount of each noble gas isotope is allowed to pass through, and continue on.

Mixing tree

The four aliquots of gas mentioned in the previous section then pass into the mixing tree where they are allowed intermingle for the first time. An appropriate amount of time should be given at this stage to ensure adequate mixing.

Mixed spike tank

The mixed spike tank is a 500 cc reservoir tank that houses the mixture of isotope tracer spikes created in the preceding stage. This tank is kept open, but sealed off from the mixing tree and remainder of the line by appropriately positioned valves.

Spike aliquot

Directly below the mixed spike tank is another custom-built aliquot that allows a precise amount of the mixed spike to be inserted directly into the main line. This will be combined with the sample to be analysed and inserted into the mass spectrometer, forming the basis of isotope dilution analysis.

All tubing and valves throughout the tracer spike apparatus have been meticulously measured so as all volumes along the path of the travelling gas are accounted for. Everytime a valve is shut, the gas volumes are chopped, and a residual portion is left behind. Only with these calculated volume measurements can information on the remaining gas be determined. In such a fashion, the volume of gas for each tracer isotope is tracked from beginning to end.

Air Spike

The air spike system is used to calibrate the tracer spike volume. A desired amount of atmospheric air is captured in a high-vacuum syringe and inserted into a specific section of the vacuum line via a rubber membrane/ultra-torr attachment. Once the needle is inserted, the air is released and is expanded into the available chamber. Two sets of valves allow the gas to be stored and released in a controlled manner into the main line where it mixes with the tracer spike.

Since the mole fractions of all isotopes within the air and tracer are known, then a mathematical rearrangement of Youngman's equation given in section *3.4: Noble Gas Line – Calibration and spike volume calculation* allows for the calculation of volumes of the tracer isotopes.

Numerous air spikes were run and averaged in order to get a representative value for the tracer spike isotope volumes.

Main Line

The term 'main line' is referenced numerous times throughout this paper and as such will be defined here. The main line is taken to be the horizontal stainless steel piping, to which all components are attached, and runs from the sideways T-joint on the far left down to V3.

Gauges

Two gauges are used to monitor gas pressure and vacuum in the main line: the Pirani and the Cold Cathode gauges.

Pirani

The pirani guage operates only at lower vacuums, functional between atmosphere (760 torr) to 10^{-3} torr, read-out on the MKS Gauge Controller display (A1). It operates on the physical principle of the ability of a gas to conduct heat and the resultant pressure dependency. Within the guage head and exposed to the region of pressure to be measured, lies a fine-wire filament which is heated by passing an electric current through it. When the pressure is high, frequent collisions between the gas molecules and the filament will result in the transfer of heat from the filament to the walls of the guage head. When the pressure is low, fewer molecules of gas will be available to collide with the filament, and less heat will be removed. Constant pressure will enable the filament to settle at a certain temperature. These changes in temperature alter the resistance of the wire filament, which represents one side of a Wheatstone bridge. As it fluctuates up or down, the bridge becomes unbalanced and it is from the changing current that a measure

of the gas pressure is calculated. Below 10^{-4} torr, however, the thermal conductivity principal becomes insensitive, and other gauges must be used to calculate the pressure.

Cold Cathode (CC)

The cold cathode guage operates at higher vacuums, accurate between 10^{-4} torr and 10^{-7} torr, and read-out on the MKS Guage Controller display (CC). The CC gauge consists of a straight-wire rod anode running through the centre of a cylindrical cathode, and a magnet that produces a magnetic field that runs parallel to the anode. This set-up causes the magnetic field to be perpendicular to the electric field in all places. Applying voltage to the anode rod begins the probability of ionizing a particle. The ions and electrons are accelerated towards the cathode and anode respectively, and may ionize other molecules by collision as well. Further free electrons are produced when the ions bombard the cathode. These ions and electrons then produce other ions until a steady state is reached whereby the rate of production of ions is equal to the rate of loss (from arrival at the cathode or from recombination with electrons). The ion current formed is displayed on a meter and is proportional to the pressure in the guage head.

A third guage is used to monitor the vacuum in the mass spectrometer. This is done with an ion gauge attached directly on the StarCell ion pump. The gauge head reads from a location on the pump, down stream from the mass spectrometer. It is capable of monitoring pressures well below the lower range of the CC, which is limited by the low level of electron production for ionization at low vacuum. The ion guage overcomes this problem through the installation of a filament in the guage head. When heated, this fine tungsten wire provides a steady stream of free electrons at a controlled rate, ensuring that ionization proceeds regardless of the pressure inside the system.

Getter Pumps

Unlike mechanical pumps, the getter relies solely upon chemical sorption processes for trapping gases. Gettering is a term used to define the chemisorption of gas molecules on a reactive surface. These active materials provide a bondable substrate allowing for the creation of stable compounds with unwanted gases located in the

vacuum line. Common substances used for this purpose are typically titanium metal or, in the case of the GP50, an aluminum-zirconium alloy.

Gettering results when an electrical current of 1.5A (which heats the unit to a running temperature of 300°C) is passed through two protruding leadthroughs located on the top surface of the flange. This causes sublimation of the titanium source that collects onto a condenser surface, creating an active layer capable of gettering gas molecules.

Enhanced performance is achieved if the titanium can be deposited onto a cooled surface. To this end, the GP 50 has been outfitted with a water-cooled cooling jacket. A length of tubing originating from a nearby tap feeds water into the lower input port of the getter which fills it until the point where it exits a second outflow port located at the top. Here, firmly attached is a second length of tubing returning the heated water back to the sink.

These titanium cartridge getter pumps are capable of removing such gases as nitrogen, oxygen, hydrogen, carbon dioxide, water vapour and carbon monoxide by creating titanium hydride, titanium oxide, titanium nitride, etc. At pressures exceeding 10^{-5} torr, the consumable titanium will be overwhelmed by the amount of reactive gas present. In this situation, the pumping speed is dependent upon the rate of production of sublimated titanium. Only at pressures below 10^{-6} torr is it possible to deposit titanium faster than it can be consumed. Limitation on pumping speed then becomes a matter of gas flow conductance, i.e., the amount of gas that is able to enter the gettering chamber. For the purposes of this experiment, the getter is always forced to deal with pressures in excess of 10^{-5} torr, whereby it is initially overwhelmed by the unwanted gases present in the main line. Time periods consisting of half an hour to a full hour must be allotted for partial gettering of the sample in order to reduce somewhat the pressure existing in the main line. Only through this exercise can pressures be reduced to levels that will enable a portion of the sample to be passed through to the mass spectrometer. Waiting for time periods greater than those mentioned are futile, as the titanium source will quickly become saturated and will no longer chemically absorb the reactive gases present in a feasible amount of time.

Successive use of the getter will therefore reduce its sorption capacity. Fortunately, applying a greater current through the leads can reactivate the titanium

source. The amount is unique to each individual getter pump, but for the GP 50, the reactivation current is set for 2.5 A for 1hour, which amounts to a temperature of 400°C. The degree and periodicity of use will dictate how often the getter pump will need to be reactivated, however, because the demands of the current experiment saturate it each and every time, it is advisable to reactivate after every run.

Vacuum pumps

The vacuum within the system is maintained through the use of three separate and unique pumps that function in sequence, similar to the gauges that monitor their performance.

Air pump

There are many designs of air pumps, so only an elementary description of their function will be given here. The rotary-vane pump consists of a housing (strator) with a cylindrical bore. Inset is a cylindrical rotor, smaller than the bore and positioned proximally in one location. The rotor contains two spring-loaded blades which slide in diametrically opposed slots in constant contact with the walls of the strator, such that two compartments are created which are as air-tight as possible. In order to create air tight compartments, the space between the blade tips and the inside wall of the strator must be minimized. Generally, 0.025 mm is an acceptable distance. To complete the seal, a thin oil film is maintained around the inside of the housing compartment, drawn in from an oil reservoir in the pump interior. This oil circulates through the housing compartment and is ejected back into the reservoir through the exhaust valve along with the pumped gas.

The functional steps of these blades consist of four stages during operation. The first stage, induction, draws air into the void space of the housing compartment. During the second stage, further rotation of the blades isolate the package of air in the lower compartment. The third stage compresses the air against a one-way valve in the top of the strator opposite of the inlet valve. The fourth stage, exhaust, sees the air, under increased pressure, released through the exhaust valve. This cycle continues again and again.

Depending on the type of pump, lubricating oils and components used, different ranges of low pressure can be realized. For the current application, once a reading of $3\text{-}4 \cdot 10^{-1}$ is achieved by the air pump (observed by the pirani guage), a switch to the diffusion pump becomes acceptable.

Diffusion pump with Edwards roughing pump

The diffusion pump is the most common pump for achieving high vacuum, and it is here that the chain of separate pumps stops for the system to the west of V27. Diffusion pumps are capable of reducing the pressure inside a system to 10^{-10} torr, but cannot be started from atmospheric pressures. An air pump is therefore used to begin the evacuation process. In addition, an Edwards roughing pump is attached in series which takes the load at higher pressures.

The diffusion pump consists of an electric heater on the underside of the pump that boils low-vapour pressure oil situated in a reservoir in the base of the interior. The whole apparatus is air-cooled through the use of a small fan mounted and directed towards the fixed fins along one side of the pump. When the heater is turned on, the oil in the reservoir begins to boil. Hot oil vapour rises up though the vapour chimney to the jet stage and escapes through the jet nozzle. In traversing from a region of high pressure inside the chimney to an area of low pressure outside, an annular vapour jet is formed which moves at a velocity that is supersonic, thus impinging on the interior of the air-cooled walls. The vapour condenses back to liquid form and runs down the walls, recycling back into the reservoir from which it came. The gas molecules entering the chamber collide easily with the heavier oil vapour particles and take up a velocity vector component directed towards the exhaust side of the pump, where they are subsequently removed from the diffusion pump by the roughing pump. A pressure gradient becomes established across the continuously flowing vapour jet.

A methanol cold trap (cooled using a Cryocool machine to –50°C) is situated upstream to the diffusion pump. Its function is to capture, by condensing, any back-streaming vapour originating from the pump, or from the vacuum chamber caused from outgassing.

An important term to remember if pumping by diffusion is the Critical Backing Pressure (CBP). This is the maximum permissible pressure allowable in the pumping line between the diffusion pump and the rotary pump. If this pressure is exceeded, the normal pumping action of the jets in the diffusion pump ceases and the pump 'stalls'. The reason behind this event is that the final vapour jet in series becomes unable to sustain the pressure in the backing line. This in turn disrupts the operation of the remaining jets and causes the oil vapour to be redirected towards the vacuum chamber, ultimately resulting in the cessation of pumping by the diffusion pump. The CBP can be reached if a significant volume of water gains access to the line, which can occur through improper or omission of freezing-out practices during sample inletting. In such a case, the diffusion pump should be isolated from the vacuum line and the methanol cold trap removed. The trap should then be heated with a heat gun to vaporize the water vapour (in the form of ice at this point).

Luckily, all diffusion pumps have a certain degree of self-purification. Thus, when heating the cold trap, the diffusion pump should be left pumping even if it has stalled. The volatiles in the trap will be vaporized and travel into the pump where they will condense on the cooled inner walls. This condensate will run down the cooled walls until it reaches an increased temperature area caused by the thermal conductivity of the electric base heater. The more volatile constituents and permanent gases are released at this point and removed by the roughing pump. The remaining elements will enter the reservoir, be re-evaporated and will be purged from the system over time.

StarCell Ion pump

Ion pumps provide long term ultra-high vacuums. They should not be used in situations where they would undergo frequent oscillations to atmosphere. For this reason, the StarCell Ion pump is located on the eastern portion of the line (to the right of V27), and is responsible for keeping ultra-high vacuum in the mass spectrometer chamber space only.

A typical ion pump consists of two flat rectangular cathodes with a stainless steel anode between them made up of a large number of open-ended tubes. This assembly is

surrounded by a permanent magnet. The anode is operated at a potential of approximately 7 kV, while the cathodes operate at ground potential.

The pump uses ions to sputter (knock off) a getter film. Initiation is started when electrons are created, by cosmic rays or by the emission of electrons from one of the cathodes, and make their way towards the anode. Ionizing collisions will occur between the electrons and the available gas molecules resulting in positively charged gas ions that bombard the cathodes. Cathode material (titanium) is sputtered by these high velocity ions creating a reactive titanium film similar to that used in getter pumps. The ion pump, however, is more advanced as it can remove the inert gases as well. These non-reactive gases are ionized in the same manner as the reactive gases and are subsequently buried on the cathode by the sputtered titanium. Light gases, such as hydrogen and helium, follow the same process but continue the burial process by diffusion into the cathode.

Sample inlet

The function of the sample inlet apparatus is to allow the dissolved gases to pass through into the main line while holding back the unwanted water vapour. This is accomplished through the use of a dry ice/methanol well. A swagelock screw fitting at the lower extremity of the inlet piece allows a solid connection to the copper tube. As the sample is vapourized, it rises up though the inlet line and encounters the enlarged area of the well; the interior of which, being cooled to approximately -70°C, instantly freezes any incoming water vapour as ice directly on the interior walls of the well. Only the accompanying gases remain free, and are therefore able to continue up the sample inlet apparatus through an adjoining pipe located on the upper area of the well, leading into the main line.

The outer dimensions of the well are 4.2cm in depth, with a diameter of 2.2cm. A modified funnel-like top is added when running samples to contain the boiling dry ice/methanol concoction.

Argon bulb

After the arrival of all gases from the sample inlet line and subsequent gettering, the primary gases remaining are the nobles. A small sample subset is taken at this point, in

what is referred to as the argon bulb. This sample is retained for argon isotope analysis only, justified because of the overwhelming supply of argon that is released per sample. Therefore the size of the bulb need not be great, and is contained within a stainless steel cylinder with an internal area of 10cc's.

Argon and Krypton/Xenon traps

These traps are simply cylinders of stainless steel filled with activated charcoal designed to capture specific noble gases. The argon trap is 23cm in length with an inner diameter of 1.21cm while the krypton/xenon trap is 12cm in length, with an inner diameter of 0.95cm. Both are completely filled. The argon trap's greater area is a reflection of its abundance in air, much larger than any other noble gas.

Kr and Xe are removed by absorption onto the charcoal, cooled to roughly -78°C. This gas will later be released and used for isotope analysis. Ar is captured in the same way, onto its own charcoal trap cooled to -196°C. This concentration of argon is of no further use and will eventually be pumped away; isotope analysis will be run on the argon bulb sample. This leaves only Ne and He in the line, which can be analysed together.

Spike chop tank

A second chop of the mixed spike became necessary as problems developed with the use of krypton. The isotope concentrations for the krypton tracer spike are listed in Table 4. The isotope of importance therein is ^{78}Kr with a majority 68.9% of the total concentration. Various other minor isotopes constitute the remainder, of which, only ^{84}Kr is of any importance, as this is the main Kr isotope in air. Despite having only a 0.6% ^{84}Kr concentration within the krypton tracer spike, it was found that this signal was completely overwriting any signal being produced by the ^{84}Kr within the samples. It was therefore necessary to chop the spike concentration further in an attempt to reduce the ^{84}Kr signal originating there.

This was accomplished by admitting the mixed spike into the main line, with all accessory valves closed. Allowing an expansion into a second stainless steel 500cc tank and then shutting it in, chops the spike by approximately $4/5^{ths}$. The remainder of the spike in the main line was then used for the isotope dilution analysis.

ST 707 furnace getter

The ST 707 furnace getter was a late addition to the line after problems arose with the extreme amount of methane gas that was found to be dissolved within the deep-seated brine samples.

An extension was made to the main line, protected by a high-vacuum valve, on the left side that in turn connected to an ultra-torr fitting securing a clear glass tube, over which, the furnace was situated. From the underside of the glass tube, a second ultra-torr fitting transformed back into swagelock where the line continued to include a high-vacuum valve, a pirani guage, and a second roughing pump. This underside ultra-torr fitting is undone to provide access into the glass tube where three ST 707 pellets are placed on top of an elongated stainless steel rod and slid up the glass tube such that the pellets themselves sit directly in the centre of the furnace. With the upper valve closed and lower valve open, the roughing pump can be used to reduce the pressure (read out on the pirani), before being opened to the main line.

The ST 707 pellets themselves are concentrated zirconium/aluminum in a flat circular shape, 3-5mm thick. When heated to ~500°C, they are capable of removing the problematic methane, as well as other reactive gases including hydrogen, nitrogen, and various oxygenated compounds.

Quadruple mass spectrometer

The VGQ Residual Gas Analyser is used to (Poole). It can be broken down into two main components: the Analyser, and the VGQ.

The Analyser

The mass spectrometer can only be operated at low pressures (less than $1x10^{-4}$ Torr). To do otherwise is to risk electrode contamination, filament deterioration and ultimately, burning-out the filament completely.

Higher pressures are delineated by an increase in volume of gas molecules, which move continuously and collide with other molecules. The distance that molecules must

travel before they collide with another molecule is known as the 'mean free path'. As pressure is increased, the MFP will be reduced. In order for the mass spectrometer to function, the probability of collisions between ions and molecules within the analyser must be low.

The VGQ analyser is a quadrupole mass spectrometer. All the components within use ultra-high vacuum compatible materials that ensure vacuum integrity is maintained. The analyser can be sub-categorized to include the ion source, mass filter, and the detector.

The Ion Source

The purpose of the ion source is to ionize the atoms and molecules of the sample gas as they enter into the mass spectrometer chamber. This is accomplished by running a current through the filament. As it becomes hot, it emits highly excited electrons that collide with the incoming atoms and molecules from the sample gas causing the removal of the outer shell electrons. The result is a positively charged atom or molecule, which is said to be 'ionized'. Outfitted with a charge imbalance, the particles can then be maneuvered down the mass filter by electrostatic fields.

The Mass Filter

The mass filter of a quadrupole mass spectrometer consists of four precision ground stainless steel rods, which are aligned to fine tolerances in alumina ceramic collars. The rods that are diagonally opposite one another are electrically connected and imbued with a combination of RF and DC voltage potentials that are opposite in phase and sign.

The electric fields created cause any ion that enters the region to undertake a spiral trajectory governed by the level of RF and DC voltages applied to the rods. As they travel down the length of the mass filter, the radii of the trajectory is dependent upon the magnitude of RF to DC fields being applied at any given instant in time and on the energy of the ions. This gives rise to the mass to charge ratio (m/e), upon which the residual gas observations are made. Unfortunately,

this method of identification can cause some confusion, as the mass to charge ration is identical for both Ar^{2+} and Ne^{+}.

For a fixed RF/DC ratio, only one m/e will strike the detector. Ions with higher or lower m/e will collide with either the rods or the walls of the vacuum chamber before reaching the detector and are consequently 'filtered out'. On the other hand, scanning through the RF and DC fields alters the RF/DC ratio and enables a complete mass spectrum of species to be displayed at any particular instant in time.

The Detector

Once the ions have traveled the length of the mass filter, they are collected by the detector, which can be either the Faraday or the Multiplier.

The Faraday is a cup-like receptor that produces a positive ion current based on the accepted positively charged ions. The magnitude of this current is proportional to the quantity of ions arriving from the mass filter and therefore, the quantity of sample gas present. The signal created is amplified and digitally converted into a value that can be read from the GasWorks software. The Faraday detector is limited to pressures in excess of $1x10^{-10}$. Pressures below this detection limit must be observed using the Multiplier detector.

The multiplier is a curved glass tube coated with a special material with electrical contacts at either end. A negative voltage is applied to the mouth of the multiplier that draws the positive ions in. A single ion colliding with the curved, coated-glass surface causes a cascade of electrons to be released. These electrons are repelled away from the negatively charged mouth towards the Faraday cup, which is grounded. Each electron released from the initial ion collision in turn causes a cascade effect when they come into contact with the walls of the multiplier. By the time the electrons reach the Collector, the signal has typically increased about 10 000 times. A signal current is again created and amplified, albeit negative this time, and is translated into a pressure reading using the GasWorks software. By this method, not only can smaller values be detected, but improved response times leading to faster scans are possible. However, where the

Faraday is robust and enduring, the reactive coating on the Multiplier limits its lifetime. High output current, created by high intensity signals can quickly degrade the coating. As such, the Multiplier should never be used to monitor pressures exceeding $1x10^{-6}$ Torr.

The VGQ

The VGQ is a self-contained, microprocessor-controlled unit that contains all the necessary power supplies and intelligence required to operate the mass spectrometer system. This section of the mass spectrometer connects directly to the analyser flange and communicates with the GasWorks software running on the PC. Operating through the software, the VGQ can perform a variety of functions, including:

- Self-test and instrument status monitoring
- Autotuning
- Monitoring of pressure gauges
- Monitoring turbomolecular pump speed
- Operation of filament protection interlock
- Operation of external relays
- Gas alarm monitoring

APPENDIX C: Procedure for the Analysis of Noble Gases in Water

A-1 Sample Preparation

Samples for analysis are contained within 3/8" (outer diameter) copper tubes measuring 26 cm in length. This gives a sample volume of approximately 26 cc's.

Rinse ends of copper tubes with distilled water, followed by acetone, and dry with warm air.

Weigh sample with its swagelock connectors and refrigerator clamps.

A-2 Preparation of Samples and Gas Extraction Line

2.1 Turn on mass spectrometer and allow to equilibrate (30 minutes).

2.2 Pump down system and all components (charcoal traps, aliquots, getter pump, etc.). Heat charcoal in furnace/heat gun to 350°C between samples and the getter pump to 450°C (2.5 A) for 45 minutes, every 30 samples (otherwise, run at 280°C (1.5 A).

2.3 Close down all valves attached to the main line.

2.4 Prepare necessary cold trap concoctions (i.e. dry ice/methanol for Kr and the sample water vapour trap (-78°C to -80°C), liquid nitrogen for Ar (-178°C to -196°C)). Cool down sample inlet trap with liquid nitrogen first.

2.5 Attach copper tube at section 7.

2.6 Take background measurements by opening up the entire main line to the mass spectrometer. Close V26 when done and pump out with ion pump.

A-3 Analytical Procedure

3.1 Open V7, turn on air pump and open V27 evacuating atmospheric air down to the top clamp on the copper tube. Close V27. Open V3, V2, V1 and cold cathode, to pump away remaining air in line. Close off V7 & V5 afterwards.

3.2 Retrieve tracer aliquot by opening V13, followed by V11. Then, close V11. Aliquot is contained between V10 and V11. Release the aliquot into the line by opening V10, then close.

3.3 Dilute the spike by opening SB3 and allowing the pressure to equalize. Close SB3.

3.4 Open V7. Remove upper clamp and un-pinch the copper tube. Warm tube with heat gun for 10 minutes. Wait 5 minutes for gases to mix, then close V7.

3.5 Open V6 (getter pump) and V4 (pirani) to monitor the pressure changes. When the pressure has equilibrated, continue with procedure (V6 remains open as well as V4).

3.6 Open V9 (Kr charcoal trap) and leave open for 10 minutes for adsorption to take place. After allotted time, close V9.

3.7 Open V8 (Ar charcoal trap) and leave open for 5 minutes for adsorption to take place. Leave V8 open.

3.8 Open V9 again for 5 minutes. Any Ar stuck in Kr charcoal trap will be transferred over. Close just V9.

3.9 Evacuate to the right of V3 before analyzing sample in the mass spec using the diffusion pump for one to two minutes. Be sure to close off diffusion pump.

3.10 Meter successive aliquots of gas into the mass spectrometer using V3 and V2. Record the tracer and sample peak for both He and Ne. Make sure the ion pump is off.

***The ion source is set at a default value of –57.99 eV, where the ionization efficiency has been determined to return satisfactory numbers for He and Kr. For Ne and Ar analysis, however, the electron acceleration voltage must be reduced to –37.99 eV to prevent the double ionization of ^{40}Ar to $^{40}Ar^{2+}$, which has m/e=20, and interferes with $^{20}Ne^{+}$.